Geological Survey of Japan Cruise Report No. 18, p. 138–223, 1982

VII. VARIABILITY OF MANGANESE NODULE DEPOSITS: THE WAKE TO TAHITI TRANSECT

Akira Usui

Introduction

Manganese nodules and associated bottom materials were collected from 59 stations spaced over a distance of 100 or 180 kilometers along two traverses from the Mid-Pacific Mountains area to the Penrhyn Basin crossing the equator. The traverses, Lines A and B, are located in the direction of NW–SE about 200 kilometers apart nearly parallel to the Line Islands chain. The lines cross the Hakurei-Maru GH76–1, GH77–1, GH78–1, and GH79–1 survey areas between 5° and 13°N. They cross four characteristic geological provinces of the Mid-Pacific Mountains area, the Central Pacific Basin, the Manihiki Plateau, and the Penrhyn Basin and two troughs in the Central Pacific Basin.

The primary objective of the GH80–1 cruise is to outline the variety of manganese nodule deposits in the Central to South Pacific and to get foundamental geological and geophysical data related to these nodule provinces. This article describes the geological occurrence and some physical properties of manganese nodules along the traverses and discusses the relationship between the regional variety of nodule deposits and the regional characteristics of bathymetry and geology. The intervals between stations are not short enough to trace the local variability of nodule properties. More detailed and systematic surveys are scheduled in some selected areas along the traverses in succeeding years. Onboard observation of nodules was assisted by N. MASUDA and Y. BABA, the Metal Mining Agency of Japan.

Sample collection

Successful bottom sampling was conducted at 59 stations with two types of box corer (bottom area: 40 × 40 cm and 50 × 50 cm), freefall grab (bottom area: 34 × 34 cm), piston corer (8 cm dia.), and large dredge. One-shot 16 mm deep-sea camera was installed with the freefall grab and box corer for the bottom photographing. The box core sampling accompanied by a bottom photographing was proved to be most favorable for the in-situ observation of manganese nodules and the estimation of nodule abundance. Freefall sampling, however, seems to be less reliable for estimation of nodule abundance. At St. 1589(FG191–2) and St. 1616(FG218–1) no nodule was collected, even though the bottom photographs show the presence of many nodules on the sea floor. It suggests that in some cases the freefall grab does not collect all nodules when the nodule coverage is very large. Thus the nodule abundance at each site shown in Appendix VII-1 is approximate data affected by sampling and measurement conditions such as sampling equipments, weight and size of nodule nuclei, wetness etc.

Figure VII-1 shows the procedure of sampling and observation of manganese nodules. Immediately after the box corer was recovered on deck, nodules and sediments were

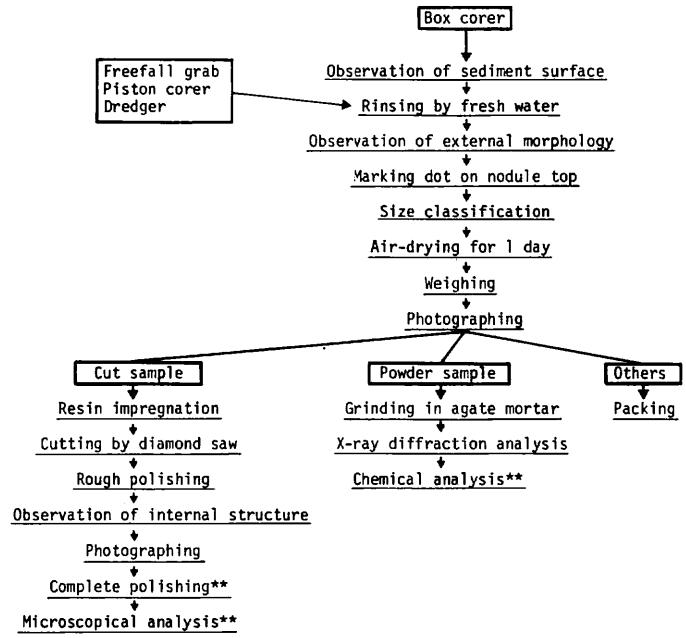

Fig. VII-1 Procedures of analysis and investigation of manganese nodules.
**Shore-based laboratory work.

photographed and described. All nodules picked up and washed were observed and classified on the basis of size and morphological type. Selected nodules were split with a diamond saw and polished for observation of internal structure. The results are summarized in Appendix VII-2.

Manganese nodules were collected from 47 out of 59 stations or 120 out of 162 samplers. The nodule abundance exceeds 10 kg/m^2 in one sixth of all stations and exceed 5 kg/m^2 in one third or one fourth of them. No nodule was collected in one fifth of all stations. Micronodules and encrustations were also collected from several stations.

Morphological classification

The external shape of nodule is primarily controlled by the shape and the number of nuclei. Nodules with small nuclei such as a rock particle are mostly of spherical shape, while nodules with irregular nuclei such as shark's teeth or tabular rock fragments are of elongated or tabular shape. However, in some cases the primary shape is closely related to the growth history of nodules, as observed characteristically in the nodules from the southern part of the Central Pacific Basin (USUI, 1979) and some parts of the Northeastern Pacific (HEYE, 1975).

During our previous cruises, the scheme of MORITANI *et al.* (1977) which was modified from MEYLAN's schema (1974) has been applied for the onboard description and proved to be valid in the limited survey area of the Central Pacific Basin (GH76–1, GH77–1, GH78–1 and GH79–1). In the present cruise, the precise understanding of all nodules of variable shape and surface texture was not always capable with their scheme. Here

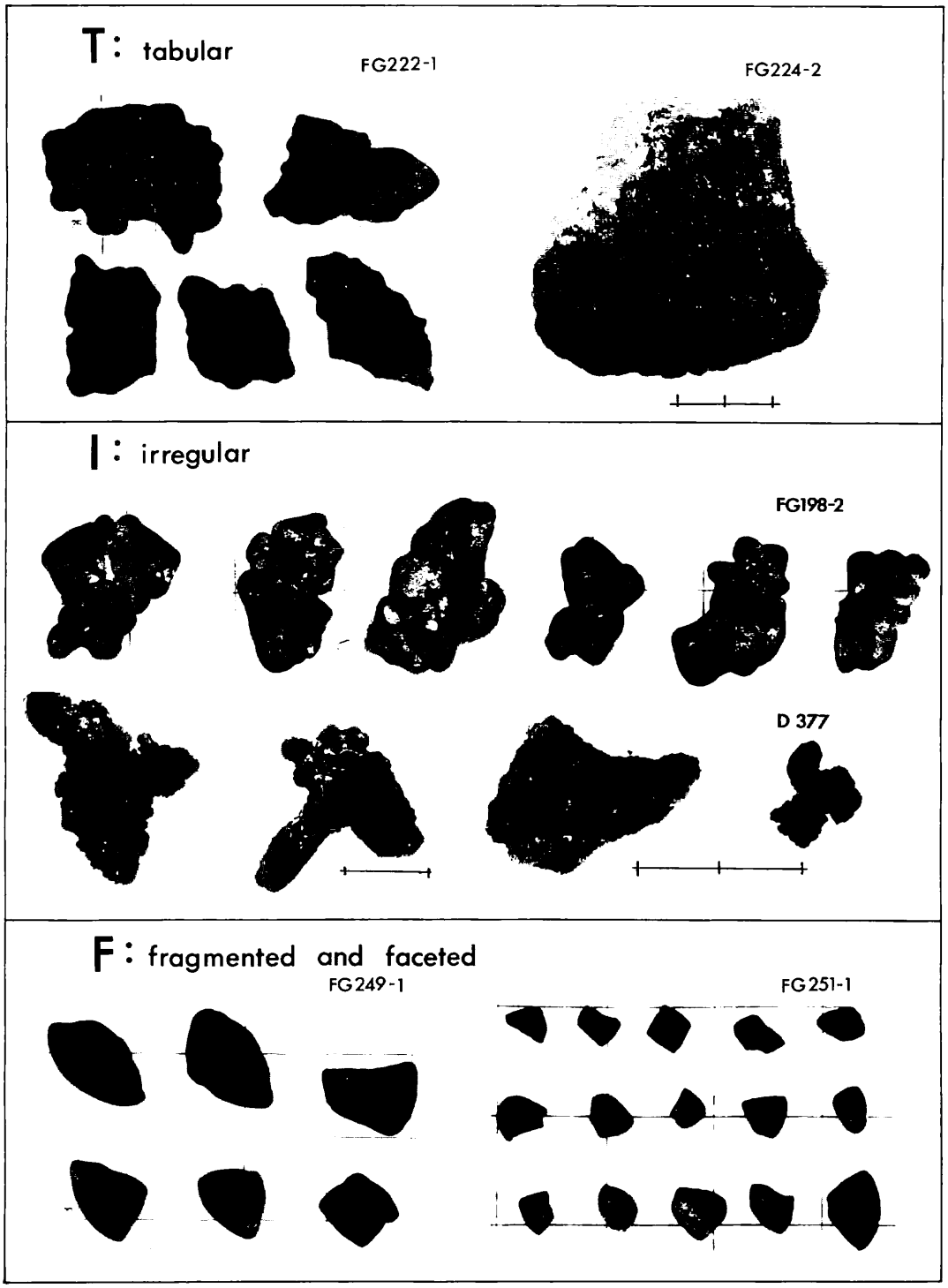

Fig. VII-2 Types of nodule shape newly defined. Scale mesh: 25 mm.

we adopt their scheme with some modification and enlargement.

Nodules of unfamiliar type to the Central Pacific Basin were found from the Mid-Pacific Mountains area and the Penrhyn Basin. Additional terms for shape are "F" (faceted and/or fragmented) and "T" (tabular) after MEYLAN's scheme and "I". The term "I" means the irregular shape of nodules, mainly composed of manganese oxide cementation and impregnation with various clastic rocks, shark's teeth etc. Figures VII-2 and 3 demonstrate external and internal morphology of these three types.

Various types of surface texture have been reported on Pacific nodules by MEYER (1973), MEYLAN (1974), HALBACH *et al.* (1975), MORITANI *et al.* (1977), USUI (1979), and others. The surface structure is generally grouped into two types, i.e., rough "r" including botryoidal, and smooth "s" including microbotryoidal. Regional distribution of the two types is generally exclusive to each other, although the both textures occur in an individual nodule from the northern region of the transect (type s+r as described later).

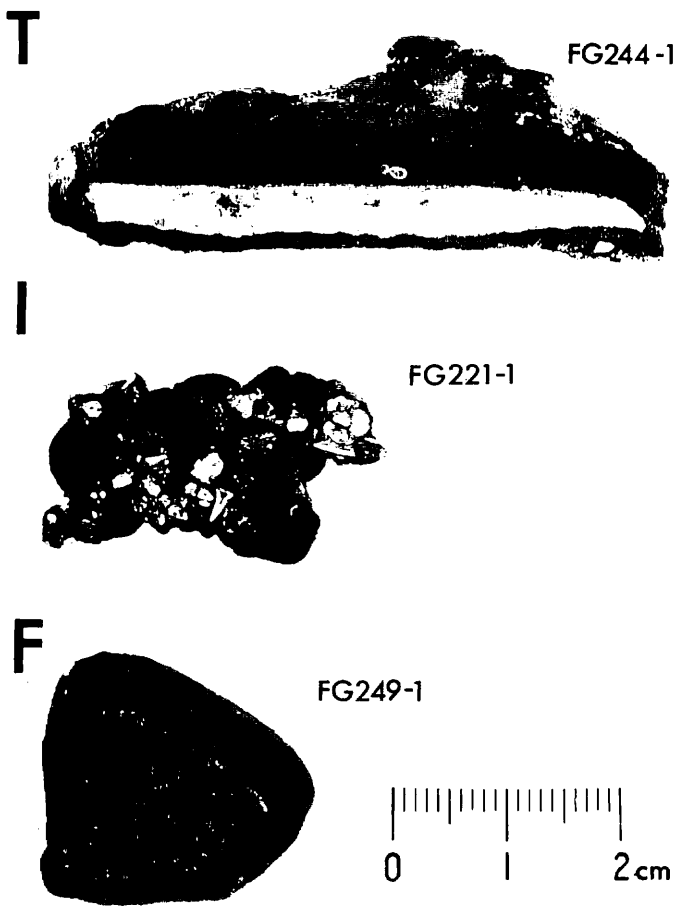

Fig. VII-3 Cross sections of typical nodules listed in Fig. VII-2.

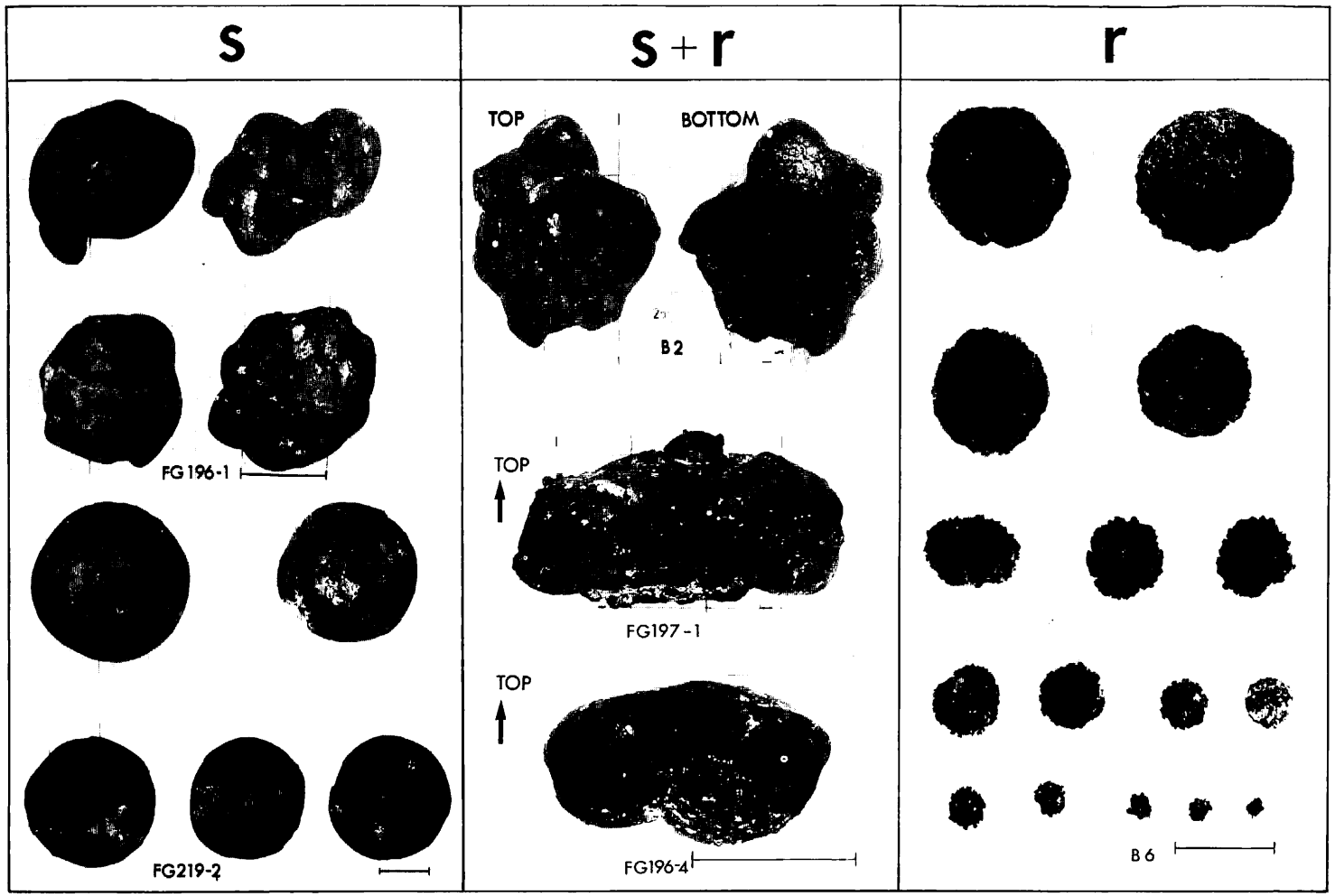

Fig. VII-4 Types of nodule surface texture. Type "s" in the figure includes smooth types from the northern Central Pacific Basin (FG196–1) and from the Penrhyn Basin (FG219–2). Type "s+r" is locally distributed in the northern Central Pacific Basin. Type "r" is dominant in the central to southern Central Pacific Basin. Scale bar: 25 mm.

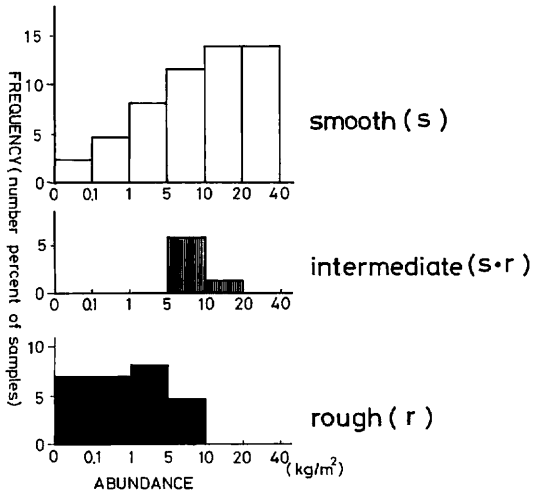

Fig. VII-5 Frequency distribution of abundance of each noodule type in terms of surface texture.

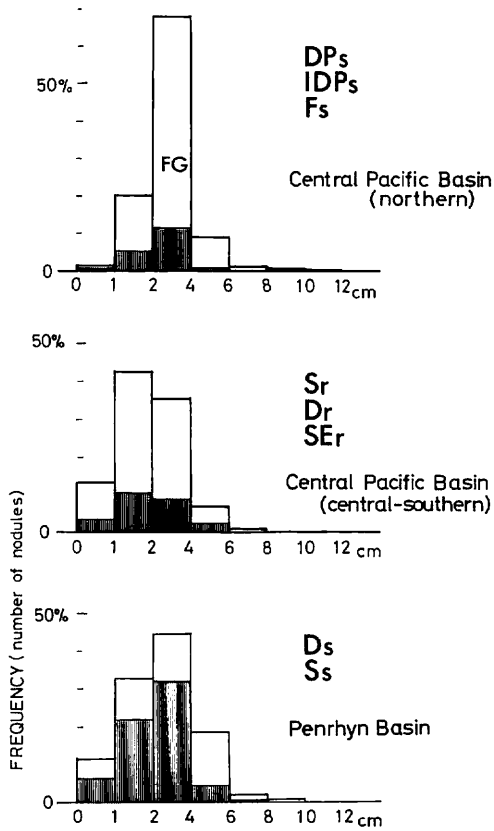

Fig. VII-7 Frequency distribution of nodule size, related to geological province and nodule morphology.

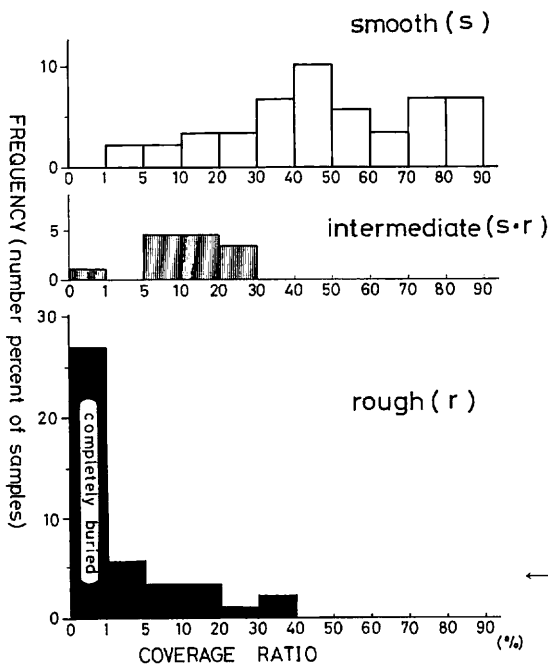

←—Fig. VII-6 Frequency distribution of nodule coverage of each nodule type in terms of surface texture. Coverage was visually determined on the bottom photographs.

Newly defined terms for nodule surface texture are "s·r" and "s+r". The former denotes the intermediate feature between typical "s" and "r". The feature is related to thin coating of 10 Å manganite cusps on smooth surfaces. Most of nodules with s·r surface feature are similar to that of typical "s" in internal characteristics except for surface feature. The "s+r" denotes the feature of nodules characterized by the typical smooth surface on top side and rough surface on bottom side (Fig. VII-4). Frequency

Table VII-1 Summary of occurrence and characteristics of manganese nodules.

Province	Mid-Pacific Mts.	Central Pacific Basin				Penrhyn Basin
surface feature	s	s	s+r	s·r	r	s
Occurrence on sediment surface	exposed	exposed	exposed or half buried	usually exposed with thin sediment blanket	buried	exposed
Mode of size fraction	2–4 cm	2–4 cm	4–6 cm	1–4 cm	1–2 cm	2–4 cm
Dominant shape	S	IS, ID	IDP, DP	IDP, DP, S	S, D	S, D, I
Internal structure	massive and compact, surrounding layer slightly laminated	massive and compact, surrounding layer slightly laminated	massive and compact, surrounding layer slightly laminated	massive or laminated	laminated concentric layers	massive and compact
Polynucleation	rare	common	common	rare	rare	rare
Internal cracks	dominant	dominant	dominant	occasionally	rare	common
Dominant surface sediment associated	zeolitic clay	zeolitic or pelagic clay	siliceous clay	siliceous or pelagic clay	siliceous ooze or clay	zeolitic clay or mud
Regional distribution	—	northern part of C.P.B.	northern part of C.P.B.	northern and central of C.P.B.	central and southern parts of C.P.B.	—
Mineral composition*	δ-MnO_2	δ-MnO_2	top and interior: δ-MnO_2, bottom: 10 Å manganite	10 Å manganite and δ-MnO_2	10 Å manganite	δ-MnO_2 and minor amount of 10 Å manganite
Chemical composition**						
(average) Mn/Fe	—	1.4***	1.7	2.4	4.1	1.3
Cu+Ni	—	0.8%***	1.1%	1.6%	2.4%	0.8%

*USUI (this cruise report).
**USUI and MOCHIZUKI (this cruise report).
***Including the nodule from the Mid-Pacific Mountains.

distributions of nodule abundance, coverage, and size are well correlated to the nodule surface features (Figs. VII-5, 6 and 7). Several characteristics of the nodule types are summarized in Table VII-1.

Mode of occurrence and distribution

Relationship to surface sediments

Manganese nodules of the ocean floors other than manganese crusts and micronodules are generally concentrated on unconsolidated sediment surface (CRONAN and TOOMS, 1967; PIPER and FOWLER, 1980), although they are occasionally found in the DSDP cores deeply buried in sediments (MENARD, 1976).

As for the top few meters of sediment column, manganese nodules from the Lines A and B occur within the top ten centimeters of the unconsolidated sediments, except for the nodules from B20(St. 1623) buried 15 cm deep within calcareous clay. Nodules deeply buried were also found in five piston cores.

It has been reported for the nodules recovered from the Hakurei-Maru cruise areas in the Central Pacific Basin that the rough type nodules are mostly or completely buried within surface sediments and the smooth type nodules are partly or completely exposed to sea water. The present results of box coring and bottom photographing revealed more details of the sea-bed occurrence of nodules.

Penetration depth of a trigger weight for camera release may indicate the consistency or water content of the sediments. The depth was visually determined on the photographs and was graded into H(hard), M(medium), and L(loose) (Appendix VII-1). The relationship between the penetration depth and nodule occurrence supports that the growth of rough surface (10 Å manganite) is optimal in the loose surface sediments but the smooth surface (δ-MnO_2) at the interface between solid objects and sea water (Table VII-2). Exceptional occurrences were, however, observed at a few stations. The rough type nodules are partly exposed to sea water and partly covered by thin sediment blanket at Sts. 1640 and 1641, where the nodule abundance is greater than 5 kg/m^2. Nodules of s·r type are commonly exposed to sea water, even if the abundance is less than 5 kg/m^2. The nodules with "s+r" surface feature, which contain an older nodule as nuclei, are half-exposed to sea water and half-buried within sediment surface. The occurrence suggests that the bottom rough surface is preferentially developed on the interface between sediment and older nodules.

The rough surface composed of 10 Å manganite cusps (USUI *et al.*, 1978) is commonly associated with the surface loose sediment as stated. These sediments are usually siliceous clay or ooze, suggesting the relationship between the accretion of the 10 Å manganite and the diagenesis of siliceous sediments.

Table VII-2 Relationship between nodule type and consistency of associated sediment.

Consistency of surface sediment	type of nodules (number of samples)		
	s	s·r and s+r	r
H	23	5	0
M	0	10	9
L	1	0	15

Local variation

The results of box coring and bottom photography have revealed a consistent regional variation of nodule deposits with geological provinces and a great local variation at a few stations. Local variations such as abrupt change in nodule abundance and morphology were encounted in the vicinity of the Magellan Trough and the Nova-Canton Trough during this cuise (Sts. 1606, 1635, 1640). For instance, at St. 1635 the nodule type varies from Sr to IDPs·r and Mn/Fe ratio from 5.4 to 1.3. This type of local variability is not probably exceptional case, but rather common in manganese provinces of the central to eastern Pacific as reported by CRAIG (1979), MIZUNO *et al.* (1980), and

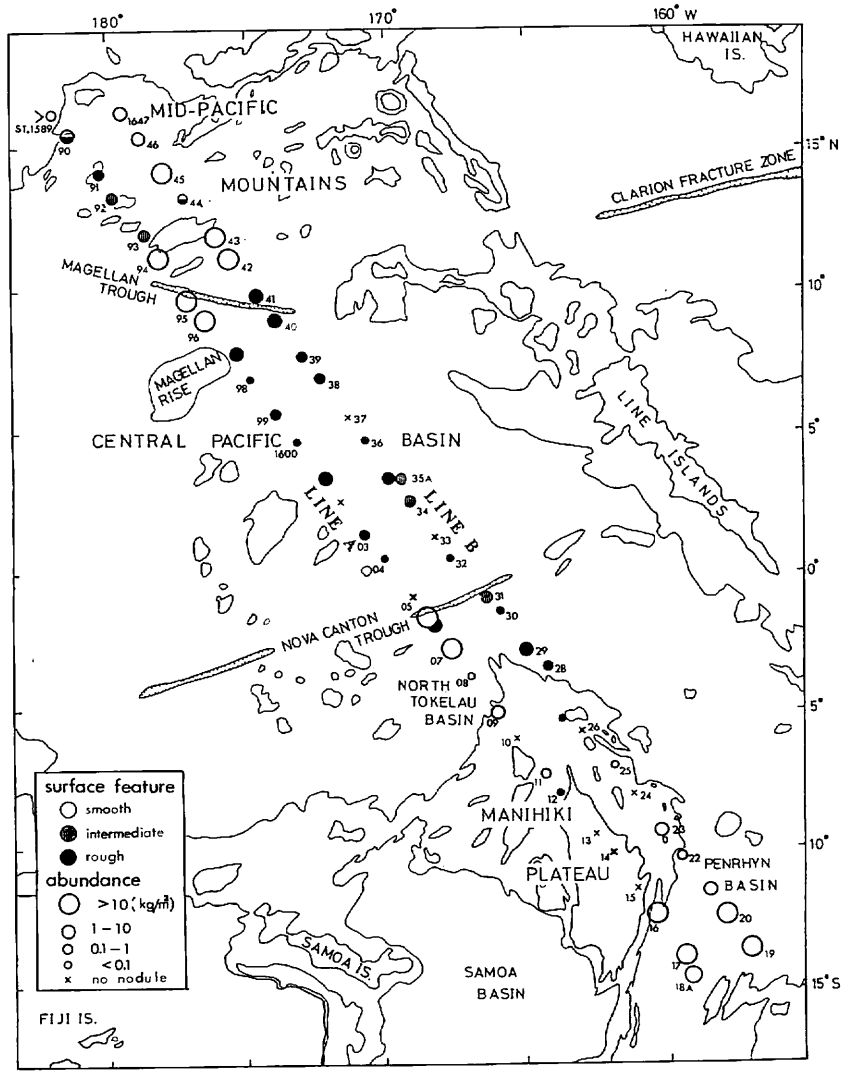

Fig. VII-8 Regional variability of nodule abundance and surface feature with geological provinces. Two contour lines denotes 2000 fathoms (ca. 3660 m) and 2600 fathoms (ca. 4750 m).

others.

Regional variation

It is of interest that the characteristics of nodule deposits consistently vary with the geological provinces despite the local variations. Figures VII-8 and VII-9 show the regional variability of nodule abundance and surface feature along the Lines A and B. The mode of variation is generally similar in the two traverses, though a slight difference is recognized in the vicinity of the Mid-Pacific Mountains and the Nova-Canton Trough Sts. 1592, 1593, 1606, and 1607).

Based on the mentioned criteria of morphological classification, nodules distributed along the traverses can be categorized into three dominant types. Two of them have been already described by MORITANI *et al.* (1977) and USUI (1979). Namely, 1) rough type: nearly spherical and discoidal nodules composed exclusively of concentric layers of 10 Å manganite cusps with entirely gritty texture, and small to medium in size (Appendix VII-2, Sts. 1601, 1635). They generally occur buried within surface loose sediments. 2) smooth type: irregular and discoidal nodules composed of internal older nodule fragments and surrounding layer of several millimeters thick. The size is generally large and they occur exposed to sea water (Appendix VII-2, Sts. 1594, 1645). The surface is generally smooth but occasionally rough on the bottom side.

The third is the s-type nodules from the Penrhyn Basin. The nodules are significantly different in color and internal structure from type s of the Central Pacific Basin. They are rather similar to older nodules inside type s of the Central Pacific Basin and the nodules from the Mid-Pacific Mountains in chemistry and mineralogy (USUI,

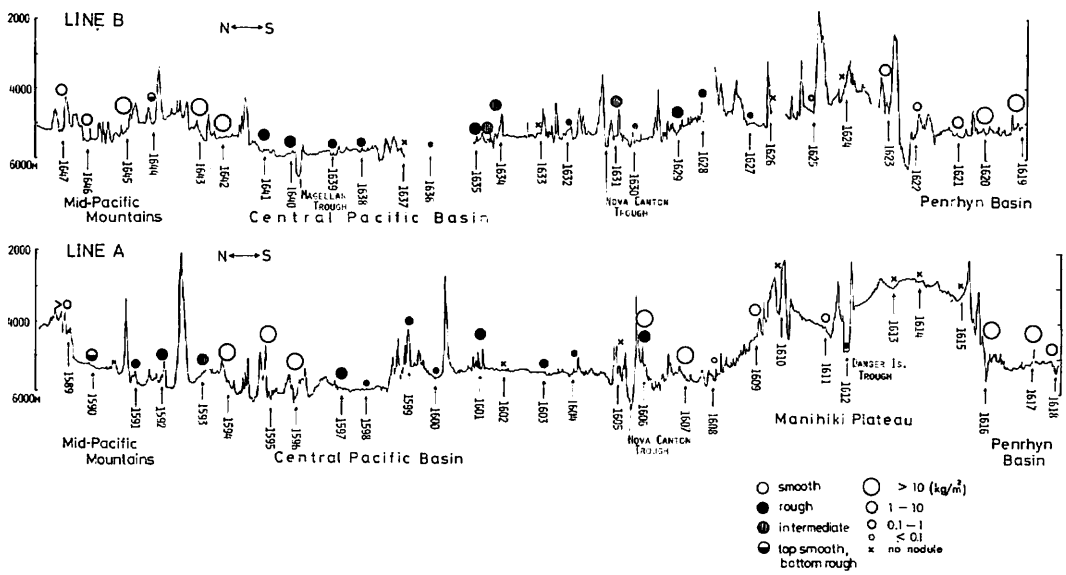

Fig. VII-9 Regional variability of nodule abundance and surface feature along the two traverses Lines A and B. The vertical exaggeration is approximately ×150. Nodule abundance of each station is represented by the maximum among some samplers of the station.

this cruise report).

Table VII-2 summarizes the regional variability of nodule characteristics from various geological provinces.

In the Mid-Pacific Mountains area smooth-surface and fairly large nodules (type s) are dominant. They cover the sea floor sporadically. Fragmentation along radial cracks of nearly spherical nodules are characteristic. Gritty surface of 10 Å manganite cusps rarely develops on the bottom surfaces.

In the northern part of the Central Pacific Basin, type s is extensively distributed. The shape is similar to that from the Mid-Pacific Mountains area, but internal cracks and fragmentation are more frequent. The abundance is large, ranging from 10 to 40 kg/m^2, and the nodules appear to cover continuously the sea floor as pavement. The internal double structure mentioned above is characteristic of this type. Mineralogically, internal fragmented older nodules always consist of the δ-MnO_2 phase while surrounding layers of the δ-MnO_2 and/or 10 Å manganite phases (USUI, this cruise report). It is interesting that the internal double structure is peculiar not only to these Central Pacific nodules but often found in nodules from the Northeastern Pacific (HEYE, 1975), suggesting a similarity in the growth history of nodules.

In the central to southern parts of the Central Pacific Basin, rough type nodules are preferentially distributed especially in the central part, and the abundance varies from trace to nearly 10 kg/m^2. The shape varies from spherical to irregular controlled by the shape of nuclei. This type of nodules always is associated with the surface loose sediments which generally cover the entire nodules except for the intermediate type(s·r) nodules. The greatest abundance of rough type is encountered at St. 1606 (8.3 kg/m^2) and the next at St. 1635 (5.0 kg/m^2). Noticeable is that these stations are located in the westward extention of so-called manganese belt between the Clarion and Clipperton fracture zones. The morphology, chemistry, and mineralogy (Chapters XVI and XVII, of this cruise report) of the nodules are very similar to those of the DOMES sites within the manganese belt (PIPER *et al.*, 1977). These results on the rough type nodules as well as on the smooth type nodules suggest a possibility that conditions and/or processes of nodules formation have been common between the Central Pacific Basin and the manganese belt in the Northeastern Pacific.

The Manihiki Plateau and adjacent basins are in general a barren zone. Surface sediments are characterized by calcareous clay or ooze (NAKAO and MIZUNO, this cruise report). Only at Sts. 1609 and 1611 in the flank of the plateau, smooth coatings of manganese oxide on zeolitic and/or clayey rock fragments were collected. Nodules from St. 1623 show abnormal occurrence. Nearly spherical to ellipsoidal nodules ranging from 1 to 4 cm in diameter are distributed between the sediment surface and the depth of 15 cm in calcareous sediments (B20), while accompanied freefall grabs collected no nodule.

It has been reported that considerably abundant manganese nodules are distributed in the South Pacific Basins (LANDMESSER *et al.*, 1976; and others). The nodules from the Penrhyn Basin are significantly different from the nodules mentioned above in occurrence, abundance, and physical and chemical characteristics. They are rather similar to the nodules from the Samoan Basin (MEYLAN *et al.*, 1978) and the southwestern region of the Cook Islands (BÄCKER *et al.*, 1976). The shape is spherical, discoidal, and very

irregular. The surface is soiled and brownish black, and appears smooth without typical gritty feature. Cross sections exhibit fairly compact structure lacking in distinct laminations. The nodule abundance is great and the monolayer of closely pakced nodules covers the sea bed.

Associated bottom materials are zeolitic clay and/or zeolitic rock fragments. The principal mineral constituent is 2 line form δ-MnO_2 according to the X-ray diffraction analysis, though a small amount of 10 Å manganite is sometimes detected (Usui, this cruise report). The differences of the Penrhyn nodules from the Central Pacific nodules in morphology, mineralogy, chemistry, abundance, and internal structure may be attributable to the different source of metals and mechanism of mineral deposition. It is of interest to study the origin of the Penrhyn basin nodules with reference to volcanic activity and sea floor weathering.

Buried nodules

The nodules buried deeply in sediment sequence were found at several levels of five piston cores, P161(St. 1607), P170(St. 1628), P173(St. 1634), P178(St. 1642), and P179 (St. 1644) out of 22 piston cores along Lines A and B (Appendix VII-3). Those nodules are mostly of smooth surface features. They are similar in type s in surface feature and shape, though we have no chemical data as yet. It seems that they occur at the upper horizons of pelagic clay than underlying zeolitic sediments. Future stratigraphic investigation of these cores may provide an important relationship of the sedimentary condition and nodule formation.

Problems on nodule origin

Marine manganese nodules are sedimentary rocks with very complex structure consisting of authigenic, terrigenous, volcanic, and biogenic materials, and their physical and chemical characteristics significantly vary with locality. The chemical characteristics and surface features are mainly controlled by the amount and mode of development of the major manganese minerals, the 10 Å manganite and δ-MnO_2 phases. It is my belief that the variability of nodule characteristics and distribution is closely related to the sedimentary and diagenetic processes of underlying sediments. Probable factors related to nodule growth are sedimentation rate, bottom current, benthic organic activity, volcanic and hydrothermal activity, and tectonic movement. However, only a few systematic studies have been carried out regarding these geological factors. I here mention some clues on nodule growth history encountered during this cruise and some problems to be studied.

The first problem is what are the factors controlling the regional variation of physical and chemical characteristics of nodules. The surface structure is the most important characteristics which may be correlated to the recent marine environments. One of the most interesting results is that the rough surface consisting of 10 Å manganite is usually associated with siliceous sediments in the Central Pacific Basin. Our investigation as regards stratigraphy and geochemistry of surface sediments and substrata would provide important suggestion.

The second is what geological events and environmental changes are correlated to the unconformity of the growth in the smooth type (type s) nodules from the northern part

of the Central Pacific Basin. The unconformity indicates the fragmentation of older nodules and followed deposition of surrounding layers in most of all the Central Pacific nodules. This unconformity has been discussed in relation to the sedimentary history of associated substrata (MIZUNO *et al.*, 1980). Comparative investigation is to be extended to the similar evidence observed in the Northeastern Pacific nodules.

The third is supply source and formation process of the nodules extensively distributed in the vicinity of the Mid-Pacific Mountains and the Penrhyn Basin. Dominant distribution of zeolite(phillipsite and clinoptilolite) and palagonitized volcanic glass in nodules and sediments suggest a possible relation of nodule formation to the Pre-Quaternary volcanism in these regions and weathering of basaltic materials. Deposition of manganese oxide minerals near the mid-ocean ridges (TOTH, 1980) and near the archipelagic aprons (FRANK *et al.*, 1976) could have influenced the vast expanse of the smooth type nodules of these regions. Although this is the possible mechanism, important is what mechanism is locally dominant.

Summary

The regional variation of manganese deposits from the Mid-Pacific Mountains area to the Penrhyn basin was outlined during the GH80–1 cruise. A corresponding variation of nodule characteristics with geological provinces was evidenced along the two traverses, although great local variations were encountered with the diversed topography near the troughs.

Previously defined two nodule types "s" and "r" are almost exclusively distributed in the Central Pacific Basin. Type "s" is dominant in the Mid-Pacific Mountains area and the northern Central Pacific Basin. The expanse of type "r" distribution was found in the central to southern Central Pacific Basin which is located in the westward extention of the manganese belt between the Clarion-Clipperton Fracture Zones. The present results of bottom sampling and sea-sed observation reconfirmed the characteristic occurrence of the two types on the sediment surface. The nodules from the Penrhyn Basin are of smooth surface and very similar in chemical composition to type s from the Central Pacific Basin, though their shape and color are significantly different.

The difference of the three types in morphology, chemistry, mineralogy, occurrence, and internal structure may be correlated to the present and/or past geological conditions. Most likely geological processes are diagenesis of siliceous sediment for the rough type nodules and volcanic activity or submarine weathering of basaltic rocks for the Penrhyn nodules. However, further detailed investigations are needed before we attain the conclusive discussion of the growth mechanism of manganese nodules.

References

BÄCKER, H., GLASBY, G. P., and MEYLAN, M. A. (1976) Manganese nodules from the Southwestern Pacific Basin. *N. Z. O. I. Oceanogr. Field Rept.*, no. 6, 88p.

CRAIG, J. D. (1979) The relationship between bathymetry and ferromanganese deposits in the Northern Pacific. *Mar. Geol.*, vol. 29, p. 165–185.

CRONAN, D. S. and TOOMS, J. S. (1967) Sub-surface concentrations of manganese nodules in Pacific sediments. *Deep-Sea Res.*, vol. 14, p. 117–119.

FRANK, D. J., MEYLAN, M. A., CRAIG, J. D., and GLASBY, G. P. (1976) Ferromanganese

deposits of the Hawaiian Archipelago. *HIG Rept.*, HIG-76-14, 71p.

HALBACH, P., ÖZKARA, M., and HENCE, J. (1975) The influence of metal content on the physical and mineralogical properties of pelagic manganese nodules. *Mineral. Deposita,* vol. 10, p. 397–411.

HEYE, D. (1975) Wachstumsverhältnisse von Manganknollen. *Geol. Jb.,* Ser. E, no. 5, p. 3–122.

LANDMESSER, C. W., KROENKE, L. K., GLASBY, G. P., SAWTELL, G. H., KINGAN, S., UTANGA, E., UTANGA, A., and COWAN, G. (1976) Manganese nodules from the South Penrhyn Basin, Southwest Pacific. *South Pacific Marine Geological Notes,* vol. 1, no. 3, p. 17–40.

MENARD, H. W. (1976) Time, chance, and origin of manganese nodules. *Amer. Sci.,* vol. 64, p. 519–529.

MEYER, K. (1973) Surface sediment and manganese nodule facies, encountered on R. V. Valdivia cruises 1971/1973. *In* MORGENSTEIN, M. (*ed.*), *The Origin and Distribution of Manganese Nodules in the Pacific and Prospects for Exploration,* HIG. Honolulu, p. 125–130.

MEYLAN, M. A. (1974) Field description and classification of manganese nodules. *In Ferromanganese Deposits of the Ocean Floor, HIG Rept.*, HIG-74-9, p. 158–168.

————, GLASBY, G. P., MCDOUGALL, J. C., and SINGLETON, R. J. (1978) Manganese. nodules and associated sediments from the Samoan Basin and Passage. *N. Z. O. I. Oceanogr. Field Rept.*, no. 11, 61p.

MIZUNO, A., MIYAZAKI, T., NISHIMURA, A., TAMAKI, K., and TANAHASHI, M. (1980) Central Pacific manganese nodules, and their relation to sedimentary history. *Proc. 12th Ann. Offshore Tech. Conf., Houston,* vol. 3, p. 331–340.

MORITANI, T., MARUYAMA, S., MATSUMOTO, K., OGITSU, T., and MORIWAKI, H. (1977) Description, classification, and distribution of manganese nodules. *In* MIZUNO, A. and MORITANI, T. (*eds.*), *Geol. Surv. Japan Cruise Rept.,* no. 8, p. 136–158.

PIPER, D. Z., CANNON, W., and LEONG, K. (1977) Composition and abundance of ferromanganese nodules at DOMES sites A, B and C: relationship with bathymetry and stratigraphy. *In* PIPER, D. Z. (*ed.*), Deep Ocean Environmental Study: Geology and Geochemistry of DOMES Sites A, B, and C, Equatorial North Pacific. *U. S. Geol. Surv. Open File Rept.* 77–778, p. 217–266.

———— and FOWLER, B. (1980) New constraint on the maintenance of Mn nodules on the sediment surface. *Nature,* vol. 286, p. 880–883.

TOTH, J. R. (1980) Deposition of submarine crusts rich in manganese and iron. *Geol. Surv. Am. Bull.*, part 1, vol. 91, p. 44–54.

USUI, A. (1979) Minerals, metal contents, and mechanism of formation of manganese nodules from the Central Pacific Basin (GH76–1 and GH77–1 areas). *In* BISCHOFF, J. L. and PIPER, D. Z. (*eds.*), *Marine Geology and Oceanography of the Pacific Manganese Nodule Provinces.* Plenum Publ. Co., p. 651–679.

————, TAKENOUCHI, S., and SHOJI, T. (1978) Mineralogy of deep sea manganese nodules, synthesis of manganese oxides: implications to genesis and geochemistry. *Mining Geol.,* vol. 28, p. 405–420.

Appendix VII-1 Sample list and results of on-site

Station/sample no.		Seabed Photography		Sediment type	Manganese nodules							
		nodule coverage	sediment consistency		Morphological type	Abundance	Size fraction (nos.)					
		%				(kg/m²)	>10	10–8	8–6	6–4	4–2	2–1	<1(cm)
1589	BI	60			(DPs)						2		
	FG191 -1					0							
	-2	30	H′			0							
1590	B2			zrC	DPs+r, IDPs+r	6.2			1	8	168	108	6
	FG192 -1	40	H′	zM	Ds, IDPs	5.5		1	2	0	8	25	8
	-2	25		zM	Ds, Ss	1.1				2	4	6	3
1591	P158			zC		0							
	FG193 -1	1		zrC	Sr	0.1					1	4	
	-2	2		zrC	Sr, SEr	0.1					2	1	
1592	B3			pC		0							
	FG194 -1	5	M	pC	DPs·r, IDs·r	1.5				2	13	4	
	-2	8		pC	DPs·r, Ss·r	0.9					9	15	1
1593	FG195 -1			pC	Ds·r, Ss·r	1.3				2	5	9	2
	-2	10	L	pC	IDPs+r, Ss·r	0.9					8	12	2
1594	FG196 -1	80		pC	IDPs, DPs	16.1				18	109	17	
	-2			pC	IDPs, DPs	6.4				6	45	2	
	-3	30		pC	D*	12.1			5	17	23	2	
	-4	50	H′	sfrC	IDs+r, DPs+r	27.6			1	21	106	3	
	-5	70	H′	pC	DPs	20.1			1	9	92	11	
1595	FG197 -1	40	H′	sfrC	IDPs+r, DPs+r	31.7	4	3	7	12	26	1	
	-2	50	H′	pC	IDPs, DPs	22.4			3	25	33		
	-3			pC	IDPs	11.9				8	117	23	
	-4	(40)			IDPr	(0.5)				1			
1596	FG198 -1	(10)		sfrC	IDPs	(1.9)		1		3			
	-2	30	H′	sfrC	IDPs+r	4.8			1	7	23	1	
	-3	40	H′	sfrC	IDPs	21.0			3	26	115	35	
	-4	40		sfrC	IDPs	19.6		2	1	22	126	22	
1597	FG199 -1	10	M	sfrC	SPr, Sr	0.7					7		
	-2			sfrC	SPr, Sr	5.0			1	0	33	54	6
1598	B4			sfrC	Sr	tr.							2
	FG200 -1	0	L	sfrC	Sr	0.1					1		
	-2	0		sfrC	Sr	tr.					1	0	2

observation of manganese nodules and associated data.

Total weight	Position on/in sediment	Internal structure	Nucleus	Polynucleation	Associated material
(g)				(no. %)	
13				0	chert? basaltic rock fragment (Mn oxide coated)
1534	half buried	surrounding layer (1 mm) internal cracks	fragmented older nodules	20	zeolite?
634		thick compact layer around nuclei	zeolite aggregate	0	do
122		thin layer surrounding nuclei	do.	0	chert
12				0	shark's teeth
11				0	chert?
178		distinct concentric band	fragmented older nodules	10	shark's teeth
107		do.	do.	0	do.
150		do.	do.	0	do.
106		do.	do.	0	chert, shark's teeth
1866		surronding layer (1 mm), internal cracks	fragmented older nodules	20	
742		do.	do.	40	
1400		internal cracks	do.	0	*completely coated by clay
3187		surrounding layer (0.5 mm), internal cracks	do.	10	chert
2321				20	
3668		compact surrounding layer, internal cracks	fragmented nodules, zeolite	10	zeolite?
2595		do.		10	do.
1373				50	altered volcanic rocks
55				0	
225		compact outer layer, similar to manganese crusts	clay aggregate	0	altered volcanic rocks
557		do.	do.	50	
2423			do.	70	
2269			do.	60	
78		distinct concentric band	zeolite aggregate	70	
576		do.	do.	50	
1	buried			0	pumice
9		concentric band	zeolite aggregate?	0	do.
4		do.	do.	0	do.

Appendix VII–1 (Continued)

Station/sample no.		Seabed Photography		Sediment type	Manganese nodules								
		nodule coverage	sediment consistency		Morphological type	Abundance	Size fraction (nos.)						
		%				(kg/m²)	>10	10–8	8–6	6–4	4–2	2–1	<1(cm)
1599	FG201 –1	(5)				0							
	–2	0	M	cmO	Sr	1.0					14	23	11
	–3			cmO	Sr	0.2					4	7	13
	–4			cO	Sr, SPr	tr.						6	1
	–5	0	M	scO	Sr	tr.							8
1600	B5			sM		0							
	FG202 –1	0	L	sM		0							
	–2	0	L	sM	Sr	tr.						1	
1601	B6			sM	Sr	1.2				1	7	23	9
	FG203 –1	1		sM	Sr	2.6				1	12	17	
	–2	1	L	sM	Sr	8.3				5	36	34	8
1602	B7			sM		0							
	FG204 –1	0	L	sM		0							
	–2	0		sM		0							
1603	P159			sM		0							
	FG205 –1	0	L	sM	Sr	tr.					1	1	1
	–2	0	L	sM	Sr, SPr	0.3				1	1	1	1
1604	B8			sM		0							
	FG206 –1	0		sM		0							
	–2	0	L	sM	Sr	0.1					1	1	
1605	P160			crsM		0							
	FG207 –1	0	M	crsM		0							
	–2	0	L	crsM		0							
1606	B9	0	M	sM	DPs	(57)	1	0	1				
	FG208 –1	5		scO		0							
	–2	0	M	scO	Sr, SEr	2.7			2	0	1	0	3
1607	P161			sM	DPs, SPs	(7)					4		
	FG209 –1	10		sM	IDPs	12.0				9	115	3	
	–2	30	H	sM	IDPs	11.6			1	14	107	2	
1608	B10			nfO	(DPs)	tr.							
	FG210 –1	(10)	M	sM	(DPs)	tr.							
	–2	(10)		nfO	(DPs)	tr.							
1609	P162			nO	(DPs)	tr.							
	FG211 –1	2		nfO	DPs	tr.					1		
	–2				DPs, IDPs	1.2			1	0	4	2	

Total weight	Position on/in sediment	Internal structure	Nucleus	Polynucleation	Associated material
(g)				(no. %)	
121				0	zeolite aggregate
26				0	do.
5				0	
2				0	
2				0	
188	buried	distinct concentric band	none or very small	0	benthic foram.
305		do.	do.	0	shark's teeth
959		do.	shark teeth	0	do.
3				0	
31				(50)	
11				0	
8639	half buried	laminated surrounding layer	zeolite aggregate?	0	
			do.	0	
317		[Inner] compact [Outer] concentric band	do.	0	
33	9 buried noduls from 8 horizons	banded but not distinct		50	
1391		surrounding layer (2 mm) internal cracks	zeolite aggregate	70	
1343		compact and massive	do.	50	
—			unknown brown rock	0	(coating on rocks)
—			do.	0	do.
—			do.	0	do.
—			fossil?	0	do.
5				0	do.
135		compact surrounding layer radial cracks	phosphorite?	70	

Appendix VII-1 (Continued)

Station/sample no.		Seabed Photography		Sediment type	Manganese nodules							
		nodule coverage	sediment consistency		Morphological type	Abundance	Size fraction (nos.)					
		%				(kg/m²)	>10	10–8	8–6	6–4	4–2	2–1	<1(cm)
1610	FG212 -1	0	H			0							
	-2	0	H			0							
	-3	0	H			0							
	-4	0	H			0							
1611	B11			nO	Vs	0.8		1	1	1	14	11	
	FG213 -1	5	H	frnO	Vs	0.1					4	1	
	-2	2	H	frnO		0							
1612	P163			cM		0							
	FG214 -1	0		nM		0							
	-2	0		nM	(Sr)	tr.							1
1613	B12	0	H			0							
	FG215 -1					0							
	-2	0	H			0							
1614	B13	0		nfO		0							
	FG216 -1	0	H			0							
	-2	0	H			0							
1615	P164			nfO		0							
	FG217 -1	0				0							
	-2	0		nfO		0							
1616	B14	70	H'	pC	Ss, Ts, SPs	18.3				17	124	102	64
	FG218 -1	60	H'			0							
	-2	50		pC	Ss, DPs, Fs	8.6				5	84	230	320
1617	B15	60	H'	pC	Ss	31.0			1	32	99	23	1
	FG219 -1	40	H'	pC	Ss, DPs, IDPs	3.2				2	21	2	14
	-2	50	H'	pC	Ss	18.8		1	6	3	10	3	
1618	B16	2	H	pC	Ss, SPs, Is	1.0					9	82	72
	FG220 -1	5		pC	DPs, Is	tr.							2
	-2	2	M	pC	Ss, Is	0.5					7	18	11
1618A	P165			pC		0							
	FG221 -1	8		pC	Is, DPs, Ss	3.9					35	240	66
	-2	10		pC	Is, DPs	2.8				2	19	6	4
1619	P166				DPs, IDPs	(15)					2		
	B17	20		zM	DPs, IDPs	6.1					63	195	41
	FG222 -1	15		zM	DPs, Ts+r	12.8		1	6	9	77	64	6
	-2	20	L	zM	DPs, SPs, ISPs	9.4				11	78	80	17

Total weight	Position on/in sediment	Internal structure	Nucleus	Polynucleation	Associated material
(g)				(no. %)	
117	half buried	compact, lamination indistinct	zeolite aggregate (fossil?)	0	shark's teeth
15		do.	do.	0	zeolite aggregate
1				0	
2777	exposed	radial and concentric cracks	zeolite aggregate?	5	shark's teeth
993		fragmented, compact		0	zeolite aggregate
4728	exposed	compact, lamination indistinct	shark tooth	10	
365		do.	do.	10	
2170		do.	do.	0	
149	buried, partly exposed	clastic structure, lamination indistinct	zeolite?	50	shark's teeth, zeolite
2				(100)	
58		compact, lamination indistinct	unknown brown rock	60	
448		clastic structure	shark tooth, zeolite?	70	shark's teeth, zeolite
322		compact surrounding layer around irregular nuclei	zeolite?	40	zeolite
12	half buried			(0)	
931				40	shark's teeth, zeolite
1484		clastic structure	zeolite aggregate	50	shark's teeth, zeolite
1089		very thin coating on chert fragments	zeolite aggregate	50	shark's teeth

Appendix VII–1 (Continued)

Station/sample no.		Seabed Photography		Sediment type	Manganese nodules							
		nodule coverage	sediment consistency		Morphological type	Abundance	Size fraction (nos.)					
		%				(kg/m²)	>10	10–8	8–6	6–4	4–2	2–1	<1(cm)
1620	B18	(30)		zM	Ds	0.1					3	1	
	FG223 –1	40	H′	zM	Ss, SEs	23.9		1	3	16	56	74	27
	–2	40	H′	zM	Ss, SEs	26.1		2	7	10	36	17	1
1621	B19	40	H′	zrM	Ds, Ss	6.7		1	3	4	27	20	4
	FG224 –1	30			Ss, Ds	3.8				3	16	5	1
	–2			zrM	DPs, Ts	10.5	1			1	20	17	11
1622	P167			zrM		0							
	FG225 –1	1		zrM	Ss, Ds	0.2						8	3
	–2	1	H′	zrM	Ss, SPs, Ds	0.2						13	8
1623	B20	60	H′	cmO	Ss, SPs	16.0				11	108	98	2
	B20X				Ss, SPs	(20)				18	117	100	2
	FG226 –1					0							
	–2					0							
1624	P168			nfO		0							
	FG227 –1	0		fnO		0							
	–2	0	H	fnO		0							
1625	B21	0		nO	DPs, Ds	0.1					2	7	9
	FG228 –1	0	M	nO	Ss, Is	0.1					1	3	9
	–2	0		nO	Ds, Is	tr.						1	2
1626	P169			nO		0							
	FG229 –1	0		nO		0							
	–2	0	M			0							
1627	B22	0		scfr	Sr	tr.							1
	FG230 –1	0		scfrM		0							
	–2	0		scfrM		0							
1628	P170			sfrnO		0							
	FG231 –1	0		sfrnO		0							
	–2	0			Ir	0.2					4		
1629	B23	0		sM	Ir, IDPr, Sr, Ts+r	6.1	1	1	2	1	31	55	30
	FG232 –1	0	L	cfrsM	Sr, Ds·r, Ts+r	7.0		4	0	1	3	6	3
	–2	0	L	cfrsM	Sr, SEr	0.4					1	2	5

Total weight	Position on/in sediment	Internal structure	Nucleus	Polynucleation	Associated material
(g)				(no. %)	
14				(0)	chert
2760		surrounding layer (1 mm), internal cracks		10	
3012		do.		10	
1022	half buried	radial and concentric cracks		20	shark's teeth
434		compact, lamination indistinct	shark tooth	20	
1212				10	shark's teeth
21				(10)	shark's teeth, pumice
25				10	shark's teeth
	half buried	lamination present but indistinct, surrounding layer (1 mm)	zeolite aggregate	20	
3134	buried in 0–15 cm depth				
	buried	thin coating	zeolite?	0	shark's teeth, zeolite
		clastic structure	do.	0	zeolite
				0	zeolite
1	completely buried			(0)	
	1 nodule buried in 7 m depth				
6				0	
930	half or completely buried	relatively compact	zeolitic rocks	10	zeolite
814		interal radial and concentric cracks	zeolitic rocks	0	zeolite
43				0	pumice

Appendix VII–1 (Continued)

Station/sample no.		Seabed Photography		Sediment type	Manganese nodules								
		nodule coverage	sediment consistency		Morphological type	Abundance	Size fraction (nos.)						
		%				(kg/m^2)	>10	10–8	8–6	6–4	4–2	2–1	<1(cm)
1630	P171			sM		0							
	FG233 –1	0		sM	Sr	tr.							1
	–2	0	(M)	sM	Sr	tr.							1
1631	B24	0	M	csO	Sr	2.5					18	33	8
	FG234 –1	0	M	csO	SPs·r, Ss·r	9.0					96	38	
	–2	5	M	csO	SPs·r, Ss·r	10.4				7	79	17	
1632	P172			snM		0							
	FG235 –1			csM		0							
	–2	1		csM	Sr	tr.						1	1
1633	B25	0		sO		0							
	FG236 –1	0	L	csO		0							
	–2	0		csO		0							
1634	P173			scmO	Dr	(6)				1			
	FG237 –1	5	M	sO	IDPs·r, DPs·r	6.8				5	61		
	–2	10	M	sO	IDPs·r, DPs·r	7.7				10	48	1	
1635	B26	0		sO	Sr, Dr	2.6				4	5	13	8
	FG238 –1	5	L	sO	Sr, Dr	5.0			1	5	10	6	1
	–2	0		sO	Sr, Dr	2.0				1	10	14	
1635A	P174			sO									
	D377				Ir, Vr, Sr		1	0	4	6	7	1	
	FG239 –1	15	M	sO	IDPs·r, DPs·r, Ts·r	5.9	1	0	2	2	18	8	
	–2	0	M	cfrsO	IDPr, Dr	1.2			1	0	2		
1636	P175			sM		0							
	FG240 –1	2	L	sM	Vr	tr.						1	
	–2	0		sM		0							
1637	B27	0	M	sM		0							
	FG241 –1	0	L	sM		0							
	–2	0		sM		0							
1638	P176			sM		0							
	FG242 –1	0	L	sM	Sr, Dr	0.4			1	1	1	1	1
	–2	0	L	sM	Ir, Vr, SPr	0.1					1	1	1
1639	B28			sM	Vr, Sr	0.1				1	1	2	1
	FG243 –1	0	L	sfrC	Dr, Sr	0.2					2	8	1
	–2	0		sfrC	Sr, Vr	0.6				1	1	7	4

Total weight	Position on/in sediment	Internal structure	Nucleus	Polynucleation	Associated material
(g)				(no. %)	
1				(0)	
1				(0)	
284	completely buried			10	
1035		concentric but indistinct	zeolite?	60	
1205		do.	do.	50	
2				(0)	shark's teeth
27	11 buried nodules from 7 horizons			(0)	
789		surrounding layer (2 mm), internal cracks	fragmented older nodules	60	
894				70	
393	completely buried			0	
575		distinct concentric band	small particle less than 1 mm	0	
232		do.	do.	0	
481				0	
686				20	
133				0	unknown rocks
1				0	
44				0	
6				0	shark's teeth
19	completely buried			0	pumice
28				0	
65				0	pumice, whale ear bone?

Appendix VII-1 (Continued)

Station/sample no.		Seabed Photography		Sediment type	Manganese nodules							
		nodule coverage	sediment consistency		Morphological type	Abundance	Size fraction (nos.)					
		%				(kg/m^2)	>10	10–8	8–6	6–4	4–2	2–1	<1(cm)
1640	P177			sM	Dr	(2)					1		
	FG244 -1	5	L	sM	Sr, Ts+r	3.7		2	0	4	13	16	
	-2	15		sM	Sr, SEr, SPr	10.0			1	7	32	27	1
1641	B29	30	M	sfrC	Sr, SPr, Dr	7.8				14	37	9	
	FG245 -1	30	M		Sr, SEr	1.8				3	3	3	
	-2	20	L	pC	Sr, SEr	9.4			2	6	35	21	1
1642	P178			sfrC	Ds	(1)					1		
	FG246 -1	80		sfrC	DPs, IDPs	27.2			2	30	88	6	
	-2	70	H′	sfrC	DPs, IDPs	22.4			1	24	56	9	
1643	D378				DPs, IDPs								
	FG247 -1	70	(H′)	zrC	DPs, IDPs	9.8				5	32	3	
	-2	70	H′	zrC	DPs, IDPs	21.8			2	29	77	3	
1644	P179			zM		0							
	FG248 -1	10		zM		0							
	-2	8	H		SPs+r	0.2					2		
1645	B30	80	H′	zrC	Ds, DPs	20.2				23	259	61	
	FG249 -1	80	H′	zrC	DPs, IDPs, Ts	23.4				25	172	26	
	-2	80	H′	zrC	DPs, IDPs	21.8				10	199	47	
1646	B31	30	M	zrC	Ds, DPs, Ts	2.1				3	32	43	6
	G250 -1	40	M	zM	Ts, Ds	7.2				6	121	217	23
	-2	30		zM	DPs, Ts	5.5				3	86	43	
1647	B32	80	H′	zM	Ds	15.4				10	245	65	
	FG251 -1	50	H′	zM	Fs	6.2					19	526	~200
	-2	70		zM	Ds, Ss	13.5				5	127	33	

Table note

1. Data in parentheses or with "?" are uncertain.
2. Total weights in the table represent the values for surface nodules.
3. Sediment consistency; L: loose, M: medium, H: hard, H′: hit nodules.

Total weight	Position on/in sediment	Internal structure	Nucleus	Polynucleation	Associated material
(g)				(no. %)	
11	completely buried			0	
433		distinct concentric band	zeolite aggregate	5	
1158		do.	do.	20	
1185		do.	zeolite?	20	
213		do.		40	pumice
1091		do.		20	
4	4 buried nodules from 2 horizons			(0)	
3147		surrounding layer, internal cracks	fragmented older nodules	20	shark's teeth
2591			zeolite?	20	
~40 kg					
1134				50	
2515			fragmented older nodules	30	
	3 buried nodules from 2 horizons				
21				(100)	unknown rocks
3080	completely exposed	surrounding layer (1 mm), internal cracks	fragmented older nodules	10	
2703		do.	do.	10	
2520				30	
239	exposed	surrounding layer (1 mm), internal cracks	fragmented older nodules	0	chert
828				5	
635		surrounding layer (1 mm), internal cracks	fragmented older nodules	10 10	
2340	exposed			10	
720		surrounding layer (1 mm), internal cracks	fragmented older nodules	0	
1564				5	

4. Sediment type; s: siliceous, c: calcareous, m: marly, n: nanno, f: foram, p: pelagic, z: zeolitic, fr: fossils rich, zr: zeolite rich, C: clay, M: mud, O: ooze.
5. "tr." denotes that nodule abundance is less than 0.05 kg/m^2.

1589	B1	-		60%	(DPs)	-
	FG191-1	0	kg/m^2	-	-	-
	FG191-2	0		30	-	-

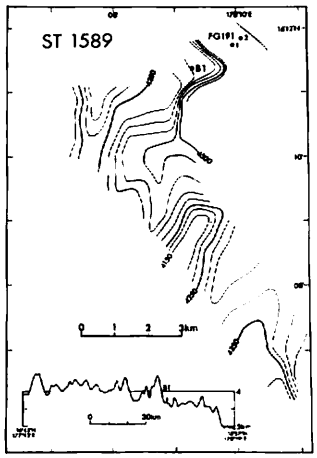

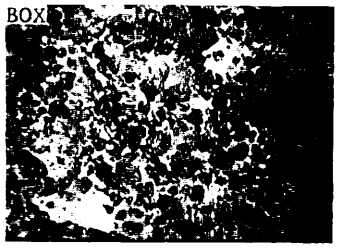

1590	B2	6.2kg/m^2		-	DPs+r, IDPs+r	Z rich clay
	FG192-1	5.5		40%	Ds, IDPs	Z mud
	FG192-2	1.1		25	Ds, Ss	Z mud

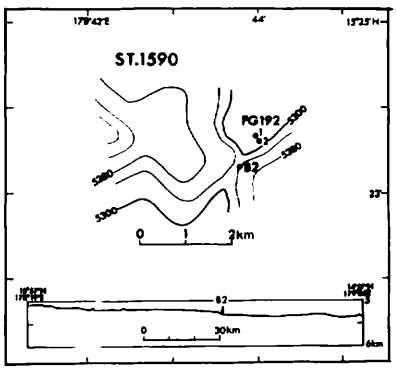

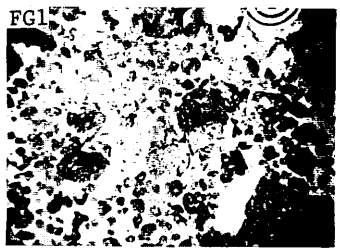

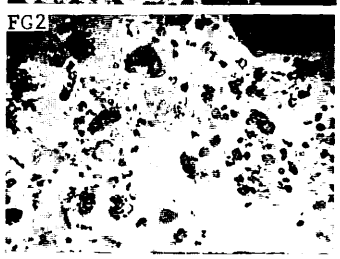

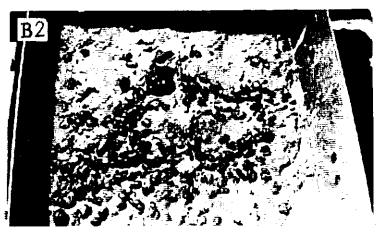

(1)

Appendix VII-2 Sampling sites, sea-bottom photographs, top surface of box cores, and external and internal morphology of selected nodules (1-57).

1) Related data in the upper column: Station no., Sample no., Nodule abundance, Visual nodule coverage ratio, Nodule type, and Type of surface sediment.

2) ( ): uncertain data, —: no available data P: pelagic, C: calcareous, S: siliceous, M: marly, Z: zeolitic, N: nannos, F: forams, f: fossils.

3) The trigger weight on the sea-bed photographs is 10 cm in diameter.

4) The width of the photographs of retrieved box corers (with the core number) is 40 cm.

5) The scale mesh under the photographs of whole nodules is 25 mm, and the scale bar with the nodule cross sections is 1 cm.

Local bathymetric map and/or profile were prepared by K. ONODERA.

BOX

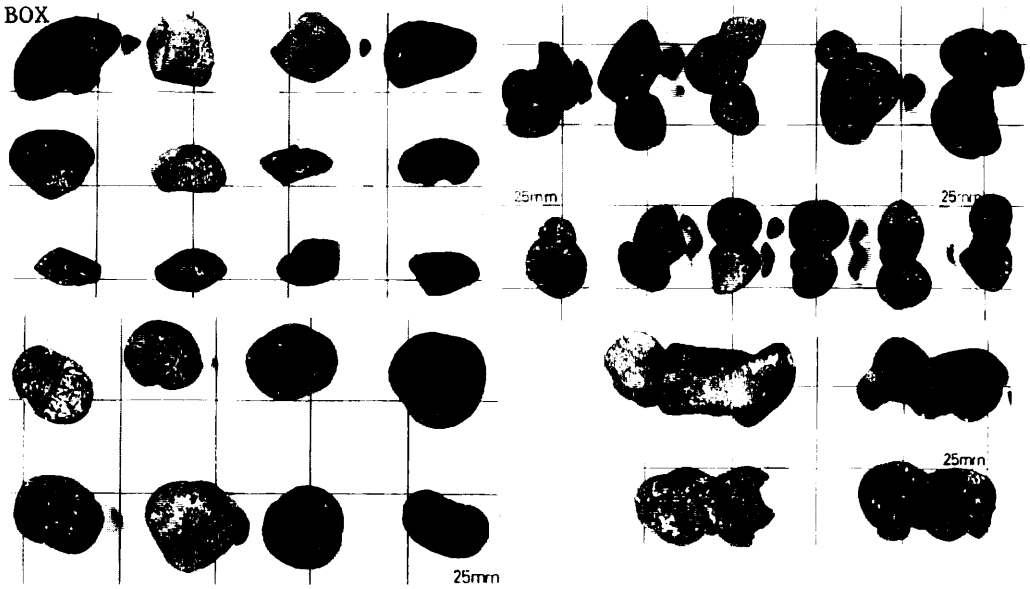

FG1

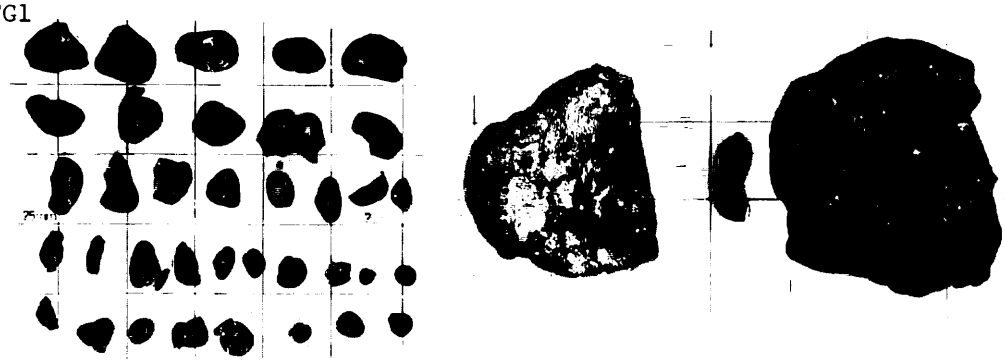

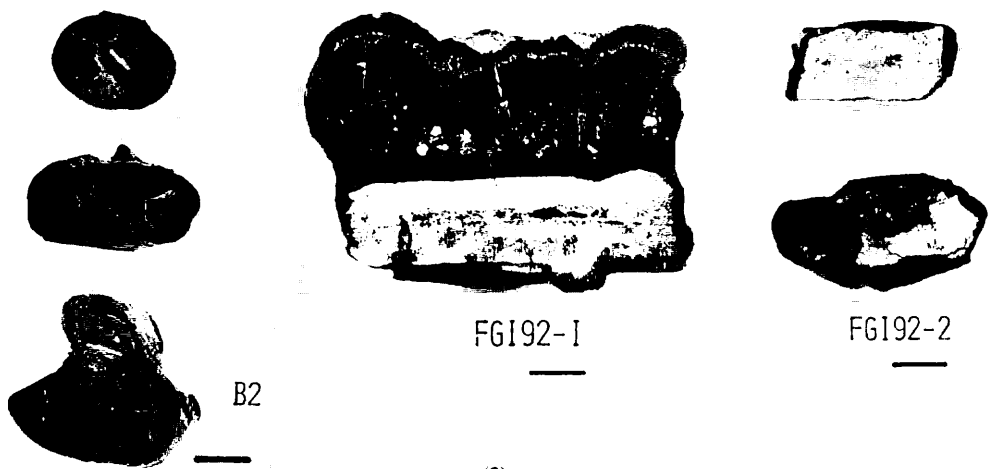

B2

FG192-I

FG192-2

(2)

1591	P158	0 kg/m^2	-	-	Z clay
	FG193-1	0.1	1%	Sr	Z rich clay
	FG193-2	0.1	2	Sr, SEr	Z rich clay

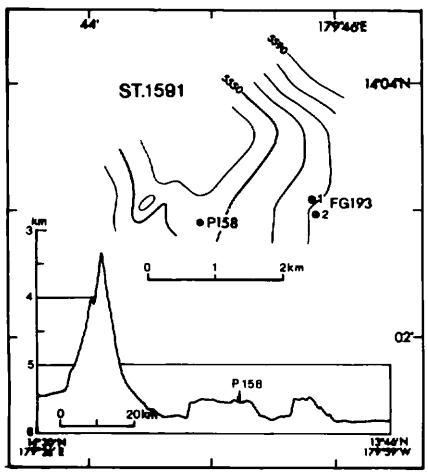

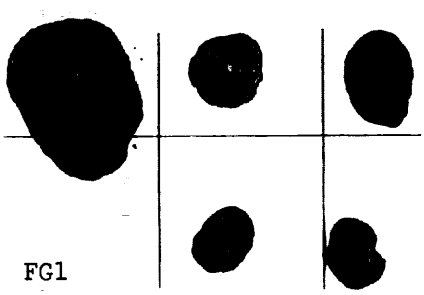

(3)

1592	B3	-	-	-	- (unsuccessful)
	FG194-1	1.5kg/m^2	5%	DPs·r, IDs·r	P clay
	FG194-2	0.9	8	DPs·r, Ss·r	P clay

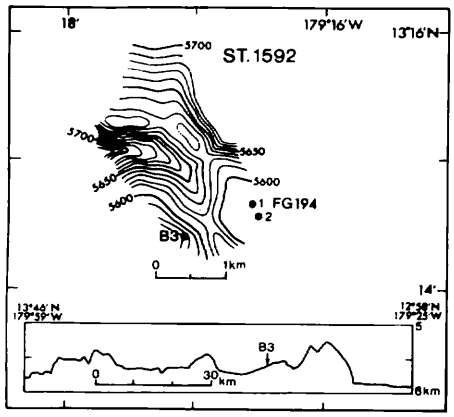

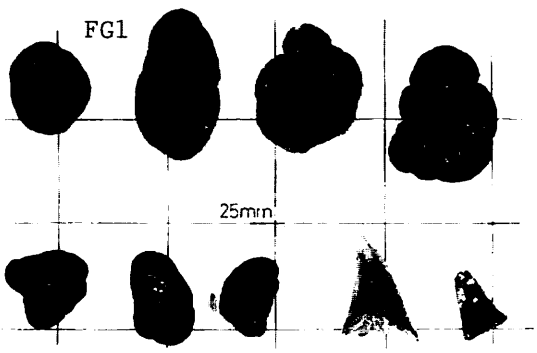

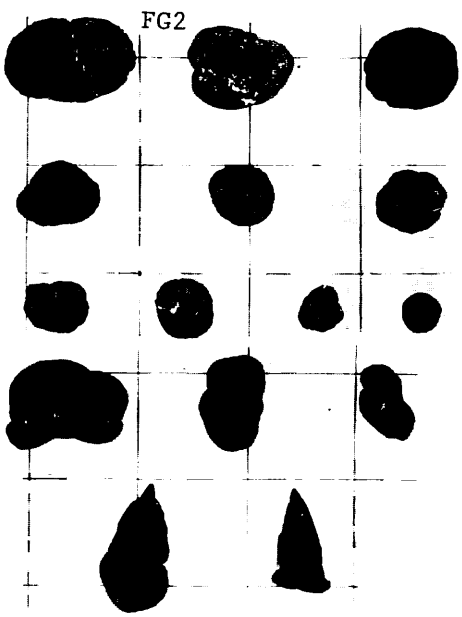

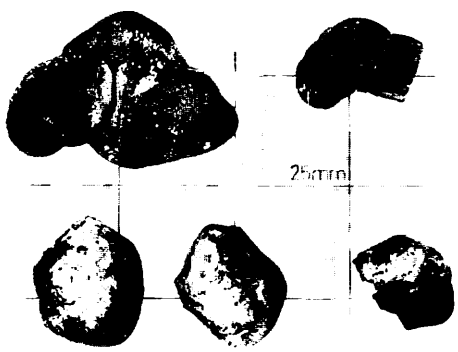

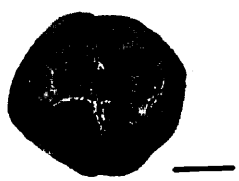

FG194-1 FG194-2

(4)

1593	FG195-1	1.3kg/m^2	-	Ds·r, Ss·r	P clay
	FG195-2	0.9	10%	IDPs+r, Ss·r	P clay

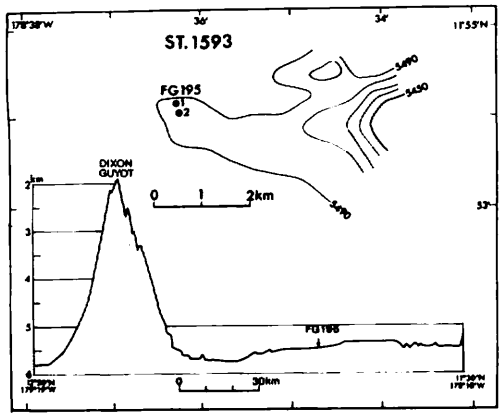

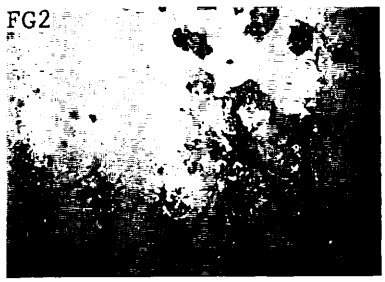

FG1

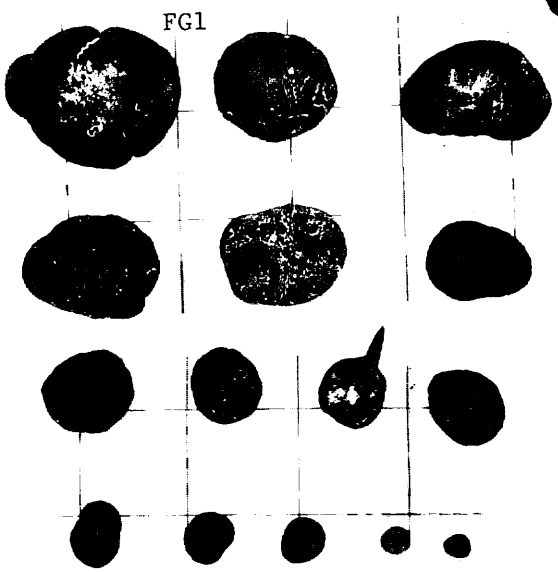

FG2

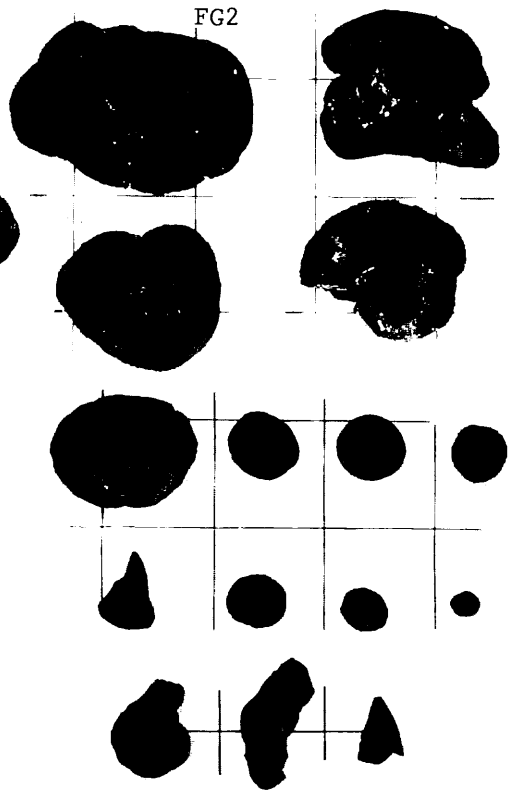

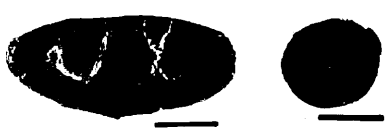

FGI95-1

FGI95-2

(5)

1594	FG196-1	16.1kg/m^2	80%	IDPs, DPs	P clay
	FG196-2	6.4	-	IDPs, DPs	P clay
	FG196-3	12.1	30	Ds	P clay
	FG196-4	27.6	50	IDPs+r, DPs+r	Sf rich clay
	FG196-5	20.1	70	DPs	P clay

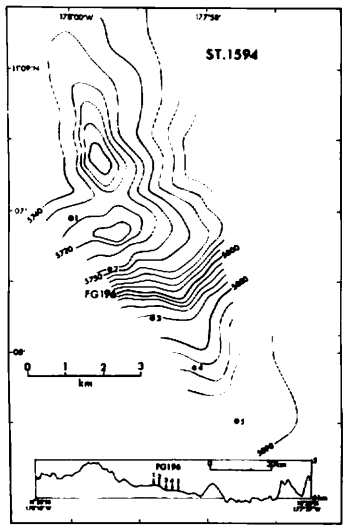

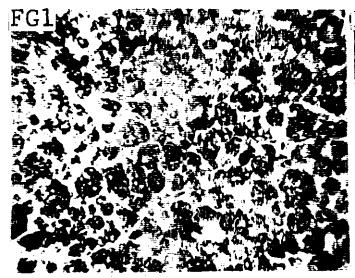

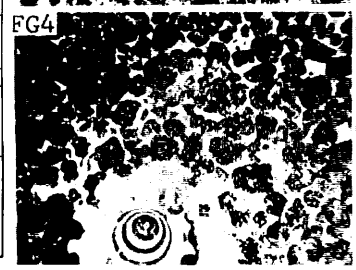

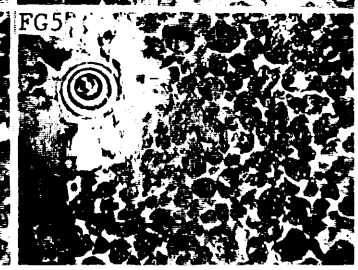

FG1

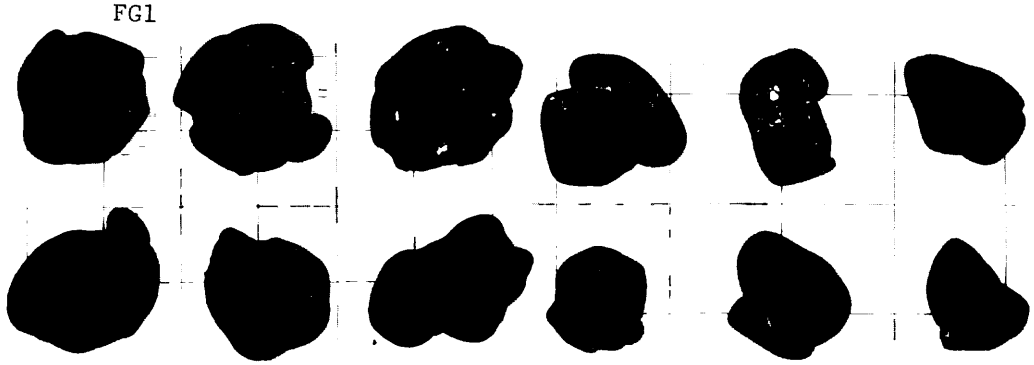

FG2

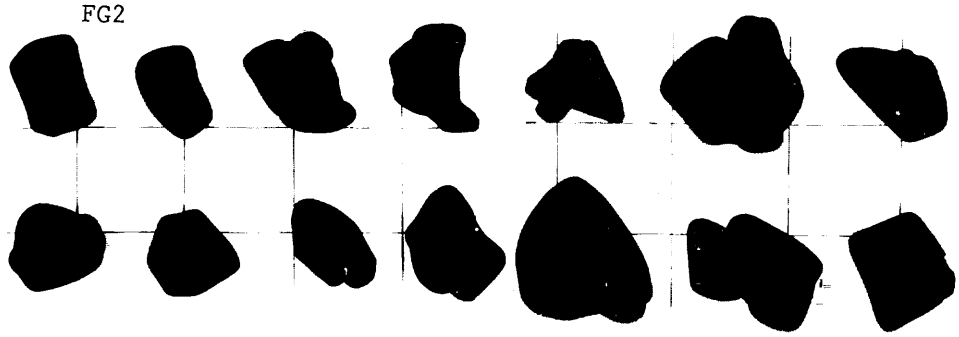

(6)

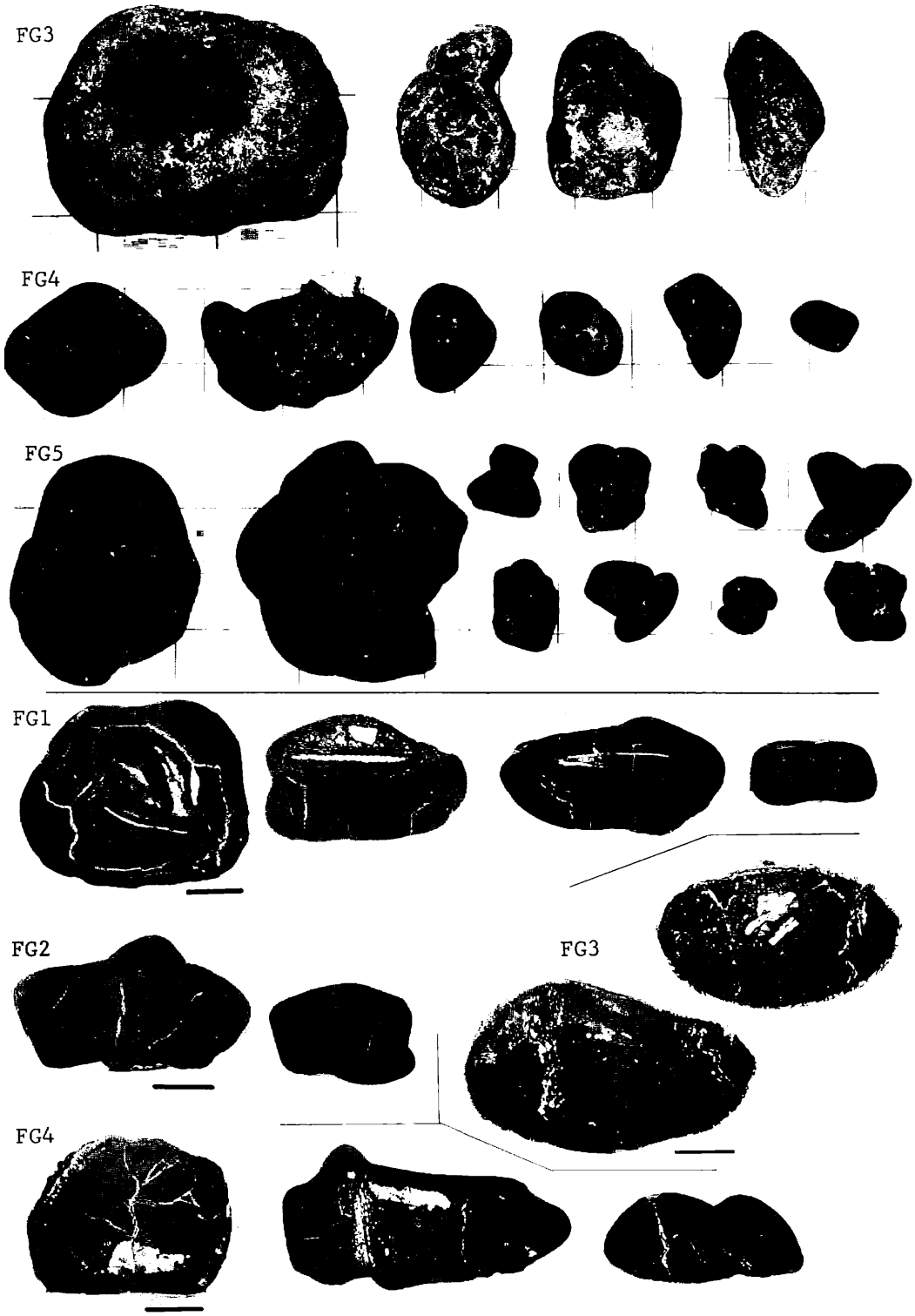

(7)

1595	FG197-1	31.7kg/m^2	40%	IDPs+r, DPs+r	Sf rich clay
	FG197-2	22.4	50	IPDs, DPs	P clay
	FG197-3	11.9	-	IDPs	P clay
	FG197-4	(0.5)	(40)	IDPr	-

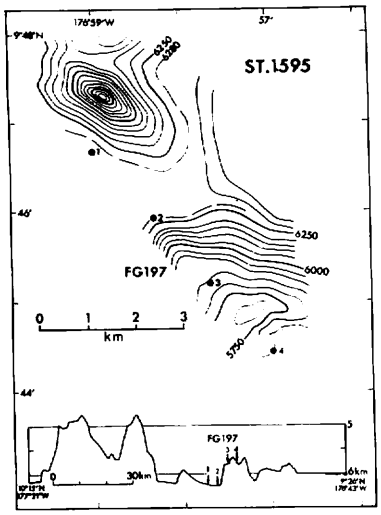

FG1

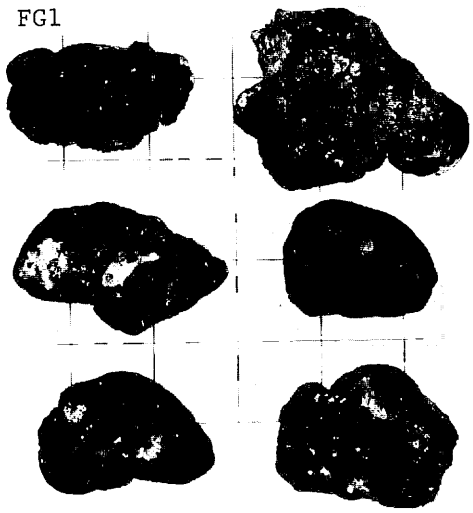

FG2

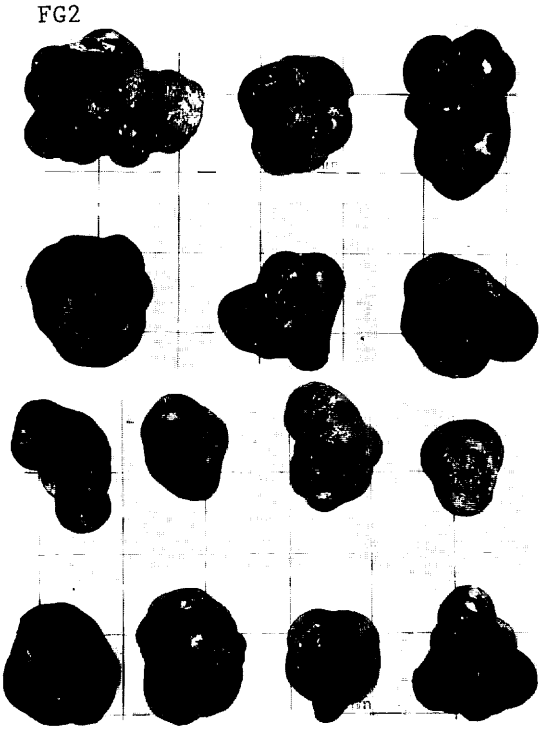

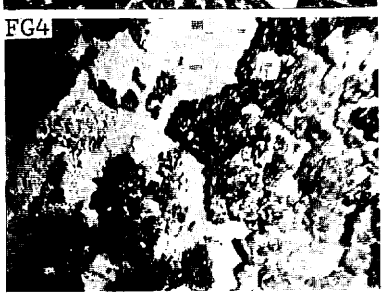

(8)

FG3

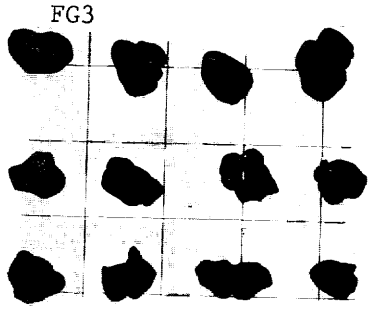

FG4

FG1

FG2

FG3

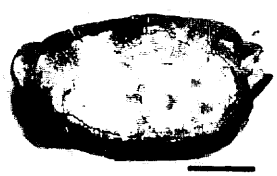

(9)

1596	FG198-1	(1.9)kg/m^2	(10)%	IDPs	Sf rich clay
	FG198-2	4.8	30	IDPs+r	Sf rich clay
	FG198-3	21.0	40	IDPs	Sf rich clay
	FG198-4	19.6	40	IDPs	Sf rich clay

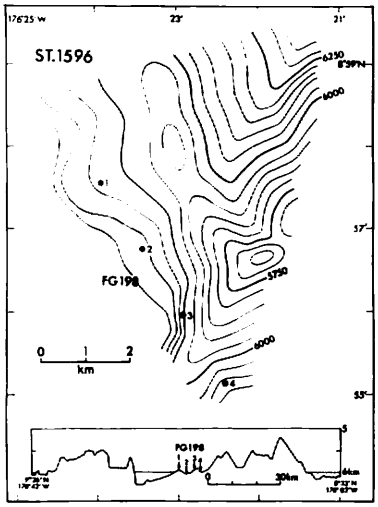

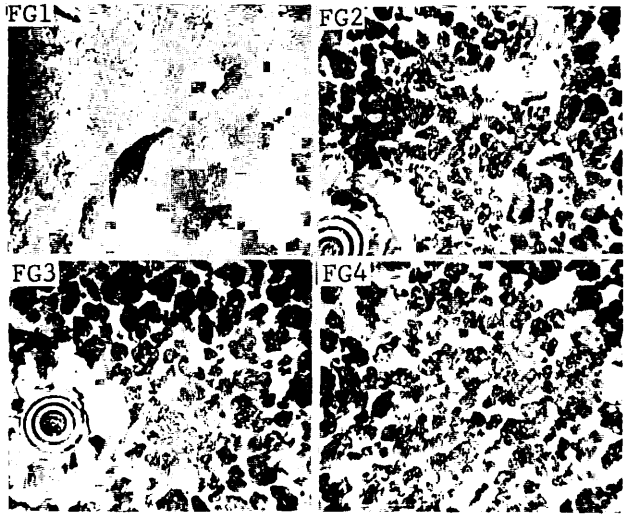

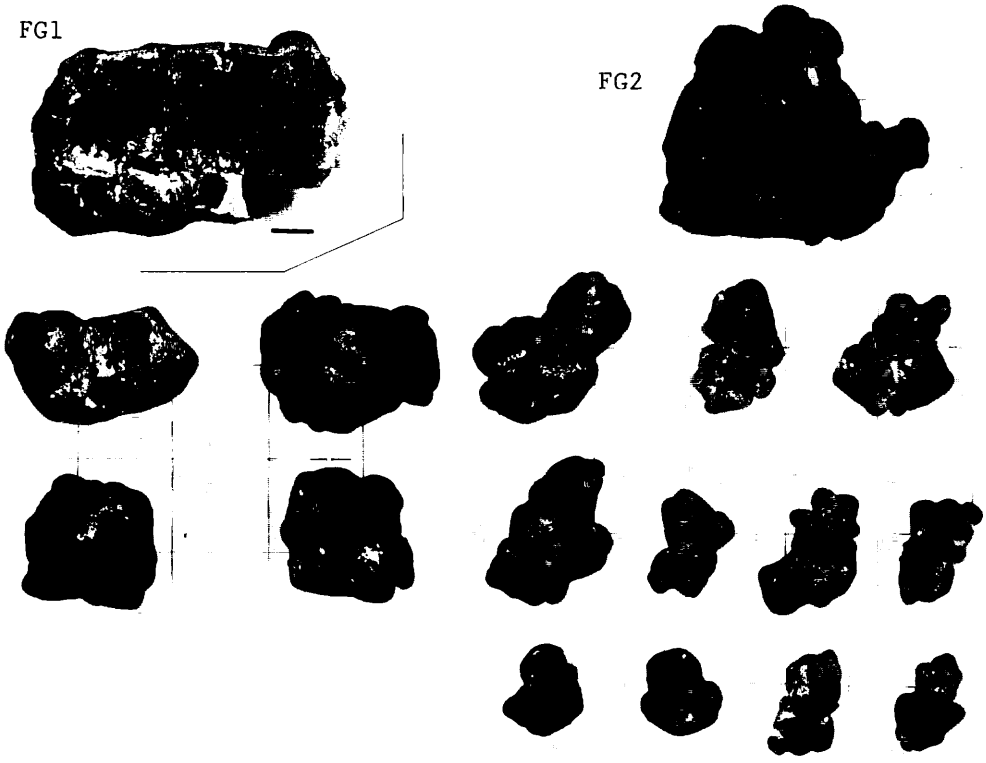

(10)

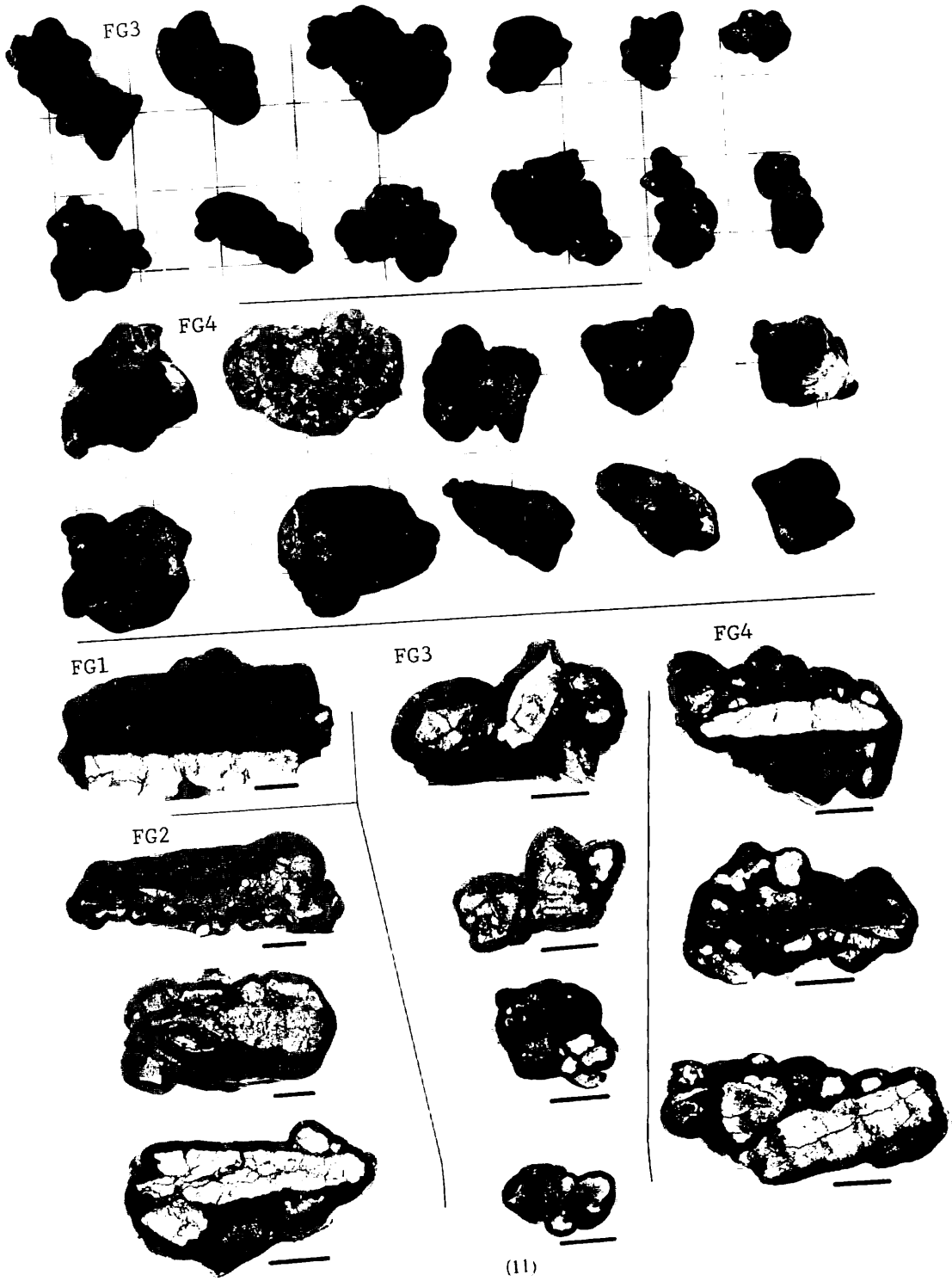

(11)

1597	FG199-1	0.7kg/m^2	10%	SPr, Sr	Sf rich clay
	FG199-2	5.0	-	SPr, Sr	Sf rich clay

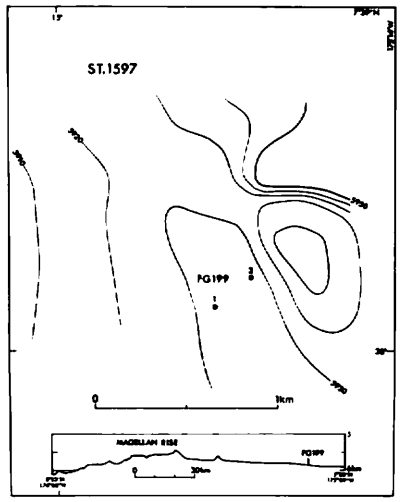

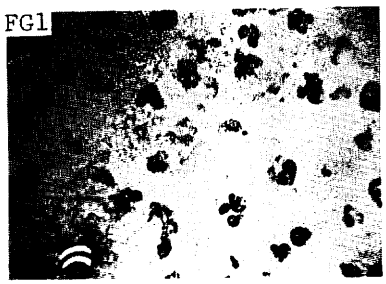

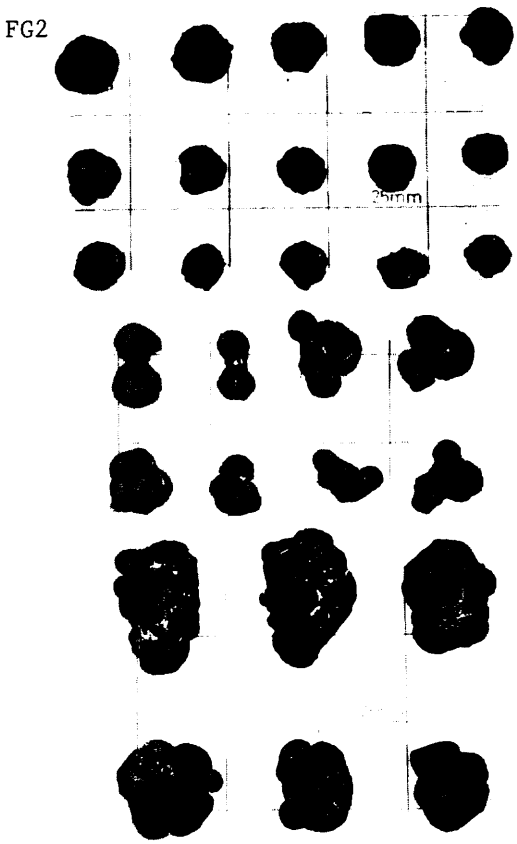

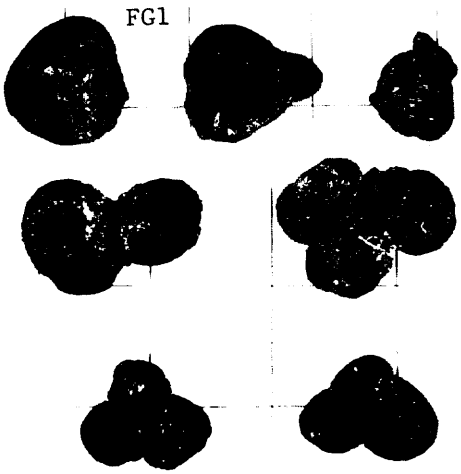

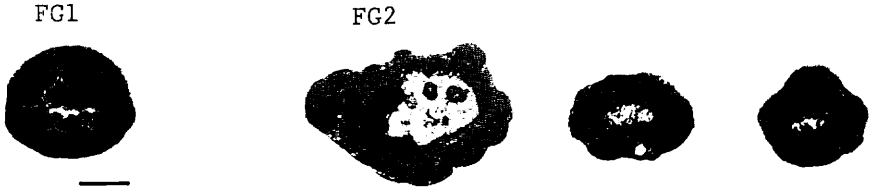

(12)

1598	B4	tr	-	Sr	Sf rich clay
	FG200-1	0.1kg/m^2	0%	Sr	Sf rich clay
	FG200-2	tr	0	Sr	Sf rich clay

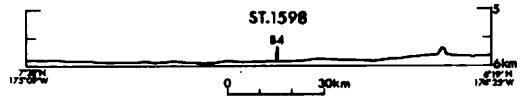

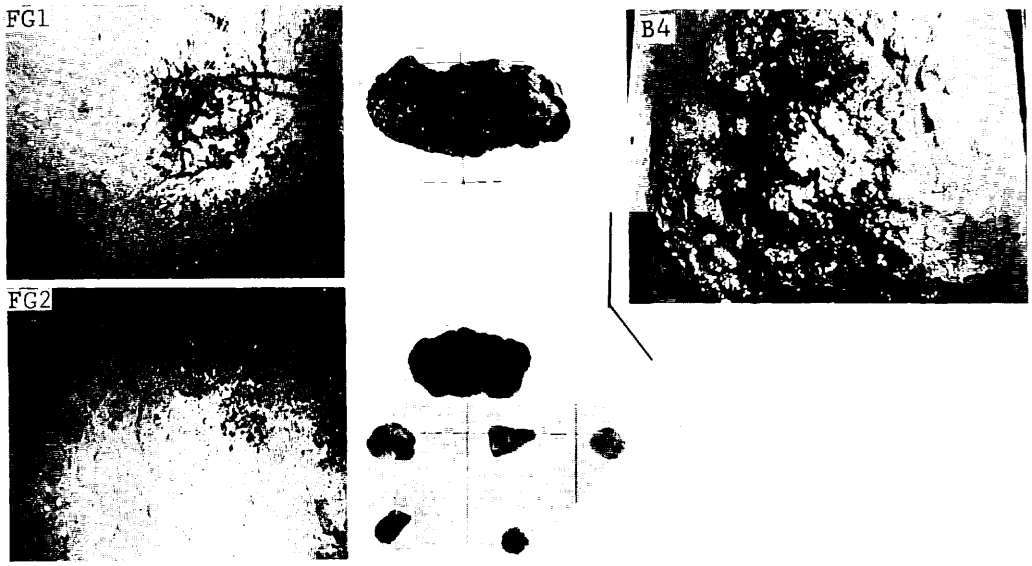

1599	FG201-1	0 kg/m^2	(5)%	-	-
	FG201-2	1.0	0	Sr	CM ooze
	FG201-3	0.2	-	Sr	CM ooze
	FG201-4	tr	-	Sr, SPr	C mud
	FG201-5	tr	0	Sr	SC mud

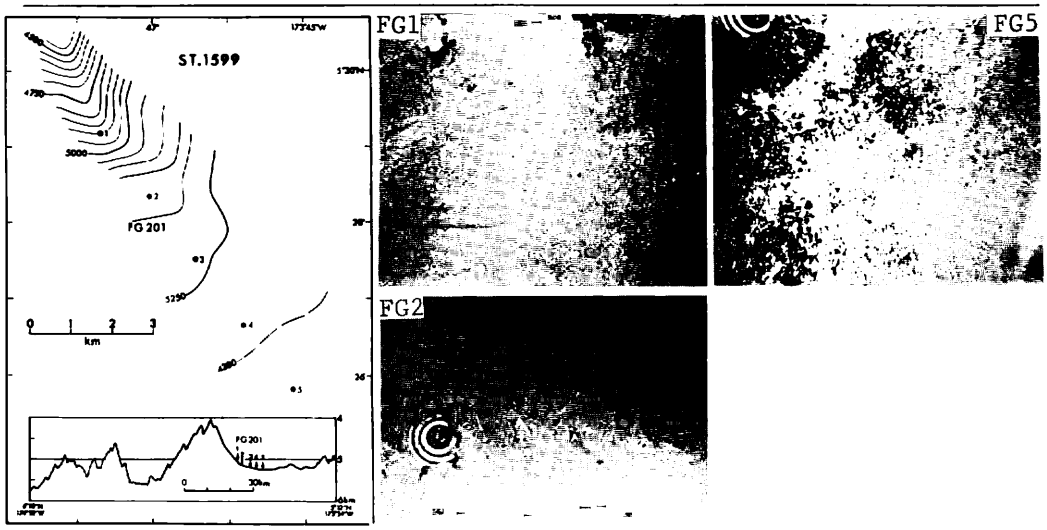

(13)

FG2

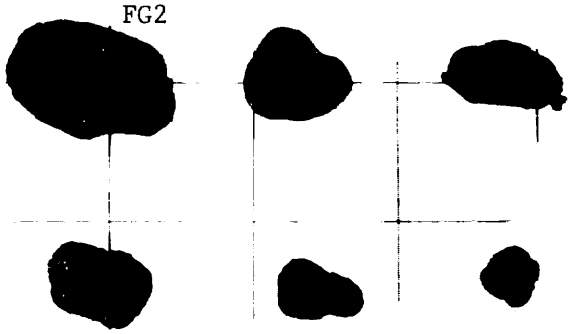

FG4

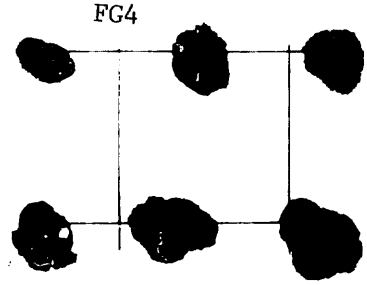

FG3

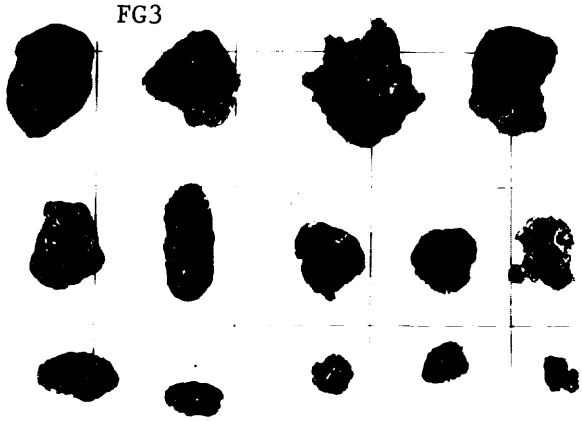

FG5

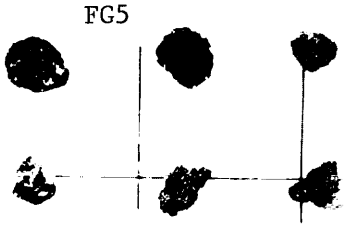

FG2

FG3

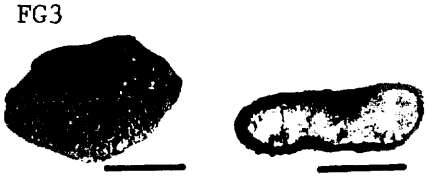

(14)

1600	B5	0	kg/m^2	-	-	S mud
	FG202-1	0		0%	-	S mud
	FG202-2	tr		0	Sr	S mud

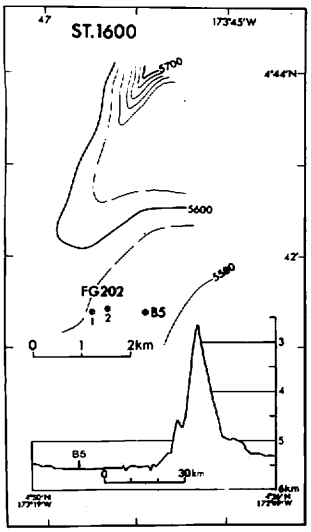

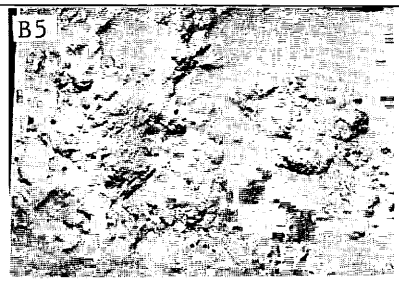

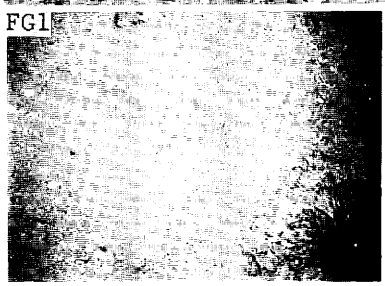

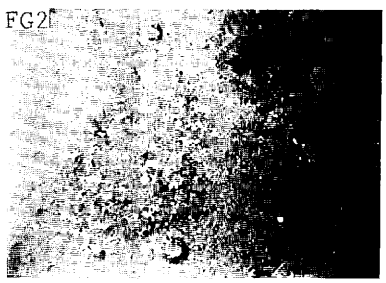

1601	B6	1.2kg/m^2		-	Sr	S mud
	FG203-1	2.6		1%	Sr	S mud
	FG203-2	8.3		1	Sr	S mud

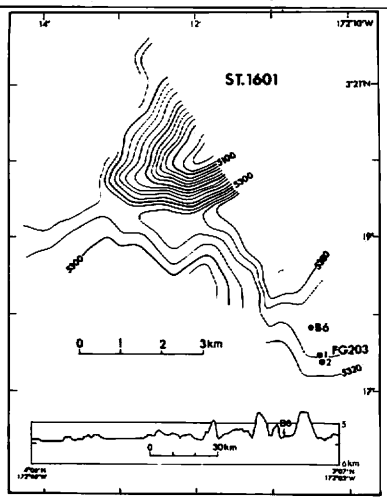

(15)

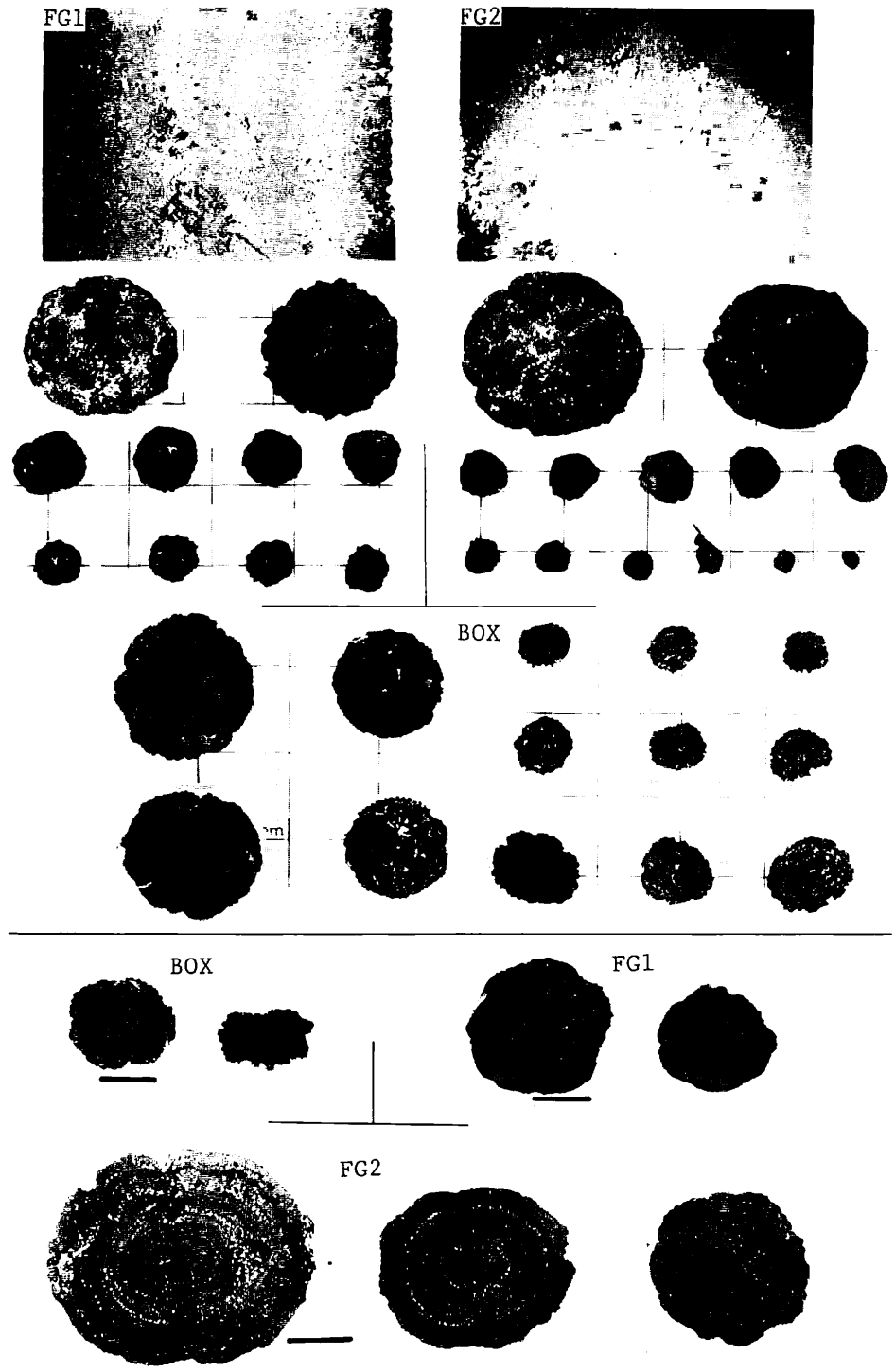

(16)

1602	B7	0	kg/m^2	-	-	S mud
	FG204-1	0		0%	-	S mud
	FG204-2	0		0	-	S mud

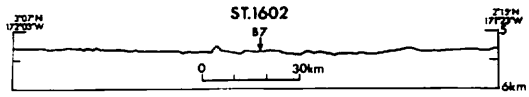

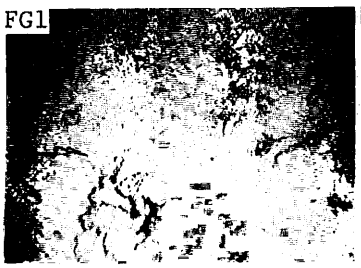

1603	P159	0	kg/m^2	-	-	S mud
	FG205-1	tr		0%	Sr	S mud
	FG205-2	0.3		0	Sr	S mud

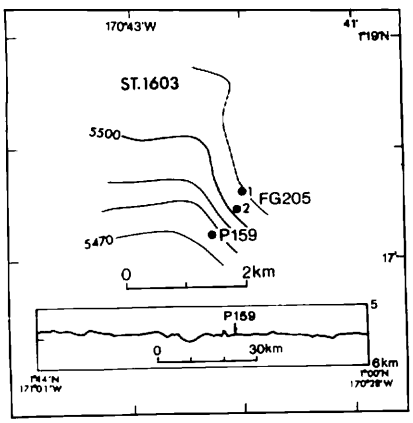

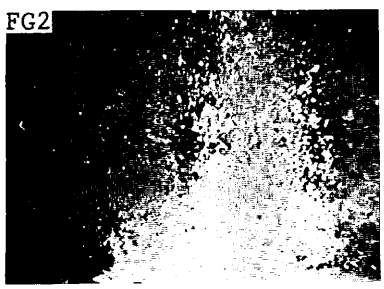

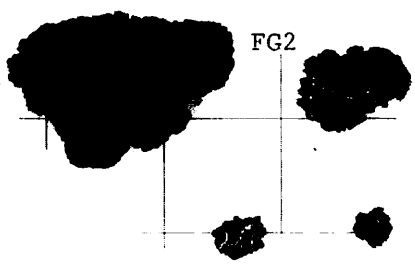

(17)

1604	B8	0	kg/m^2	-	-	S mud
	FG206-1	0		0%	-	S mud
	FG206-2	0.1		0	Sr	S mud

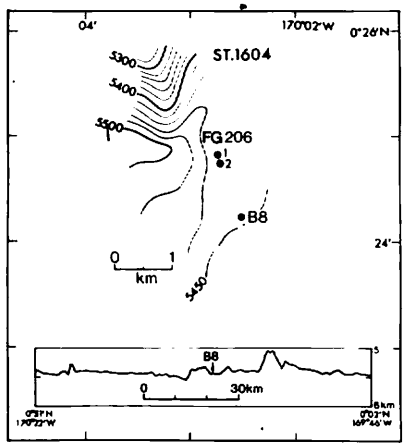

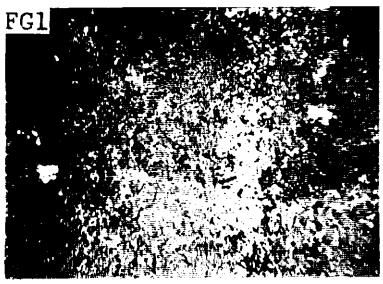

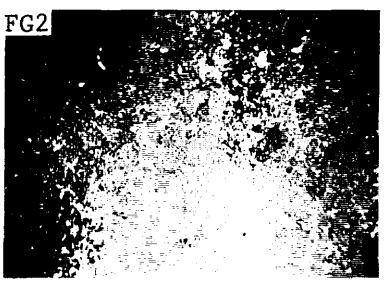

1605	P160	0	kg/m^2	-	-	Cb rich S mud
	FG207-1	0		0%	-	Cb rich S mud
	FG207-2	0		0	-	Cb rich S mud

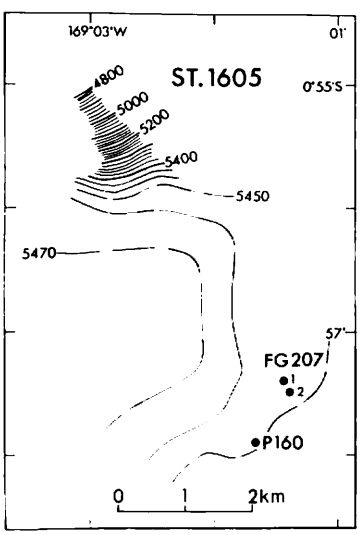

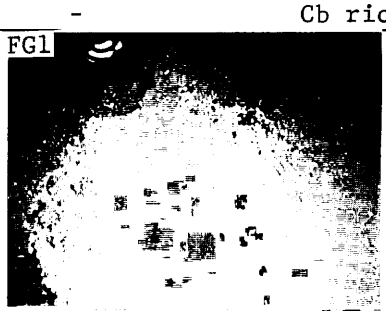

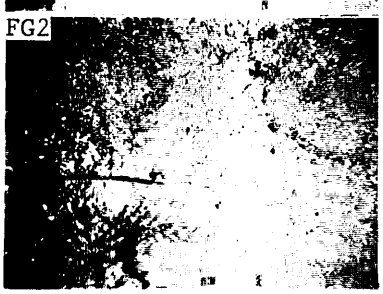

(18)

1606	B9	(56.8)kg/m^2	0%	DPs	S mud
	FG208-1	0	5	-	SC ooze
	FG208-2	2.7	0	Sr, SEr	SC ooze

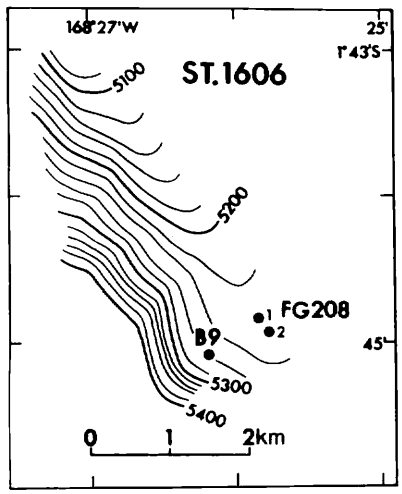

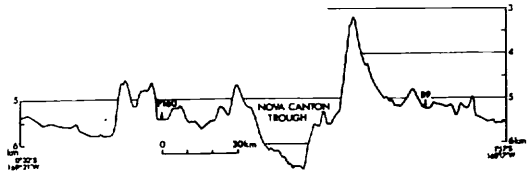

BOX

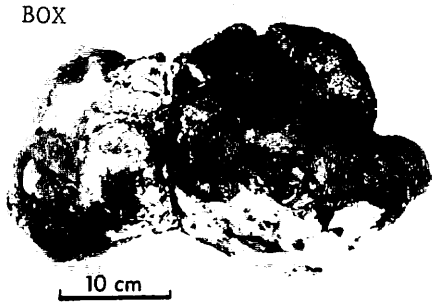

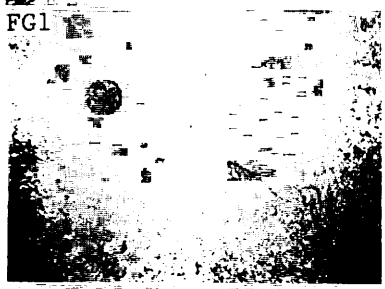

FG2

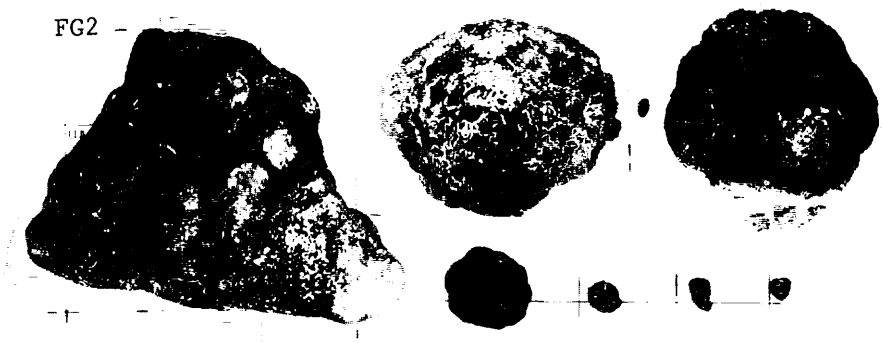

(19)

1607	P161	(7.3)kg/m^2	-	DPs, SPs	S mud
	FG209-1	12.0	10%	IDPs	S mud
	FG209-2	11.6	30	IDPs	S mud

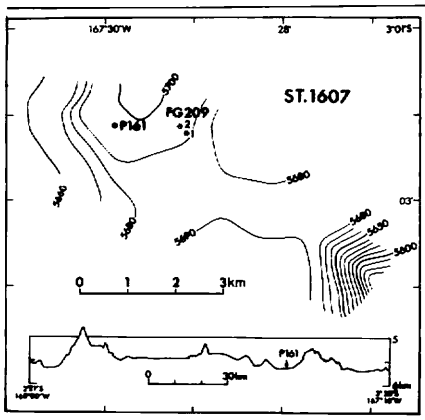

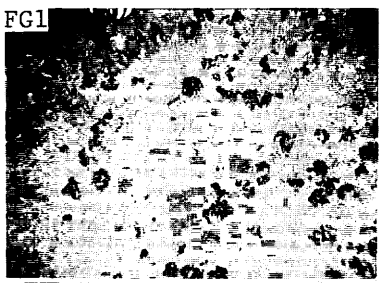

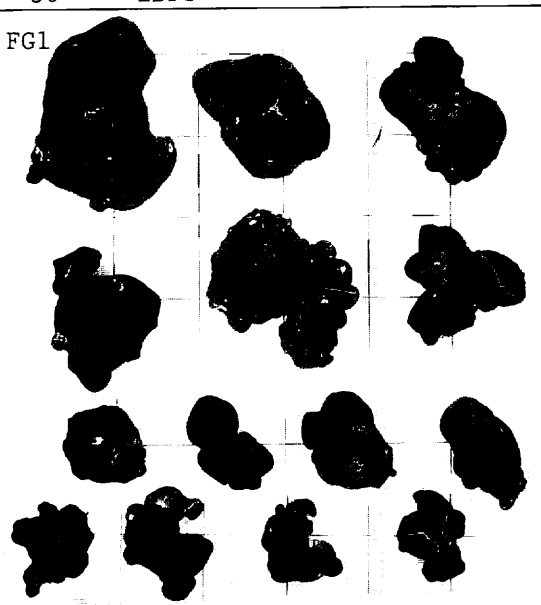

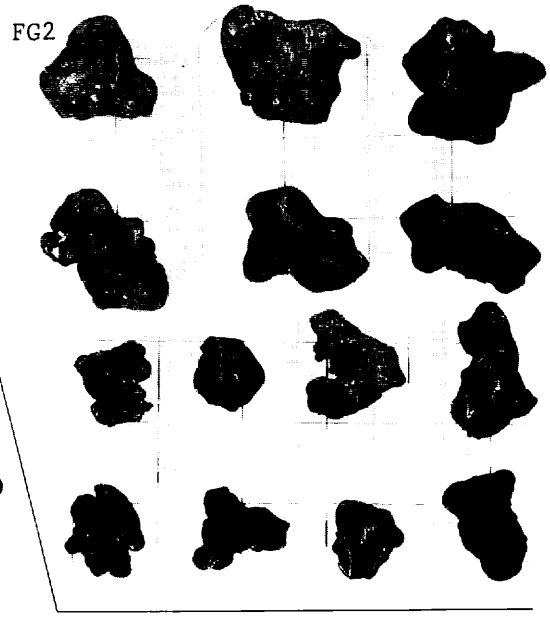

1608	B10	tr	-	(DPs)	NF ooze
	FG210-1	tr	(10)%	(DPs)	S mud
	FG210-2	tr	(10)	(DPs)	NF ooze

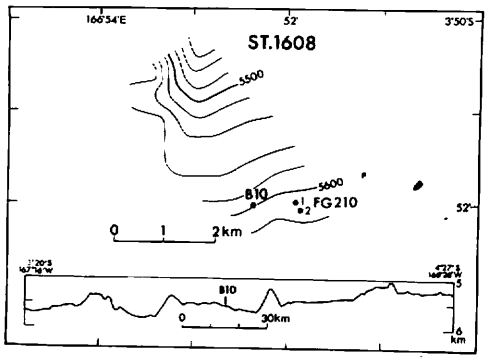

FG1

FG1

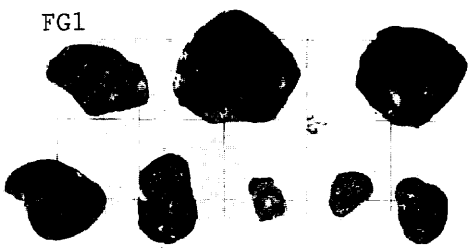

FG2

FG2

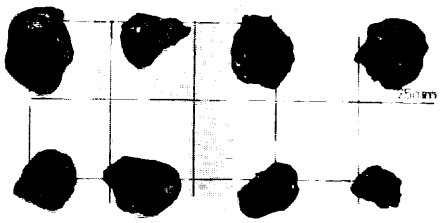

FG2

1609	P162	tr	-	(DPs)	N ooze
	FG211-1	tr	2%	DPs	NF ooze
	FG211-2	1.2kg/m^2	-	DPs, IDPs	-

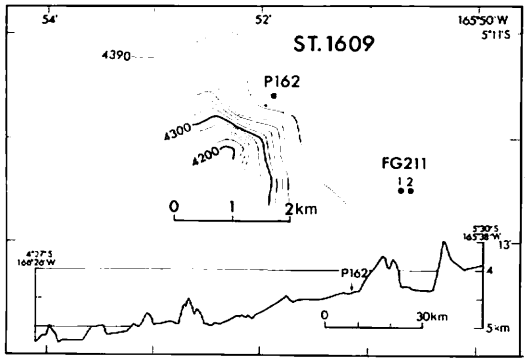

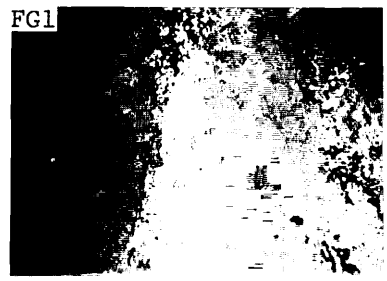

1610	FG212-1	0	kg/m^2	0%	-	-
	FG212-2	0		0	-	-
	FG212-3	0		0	-	-
	FG212-4	0		0	-	-

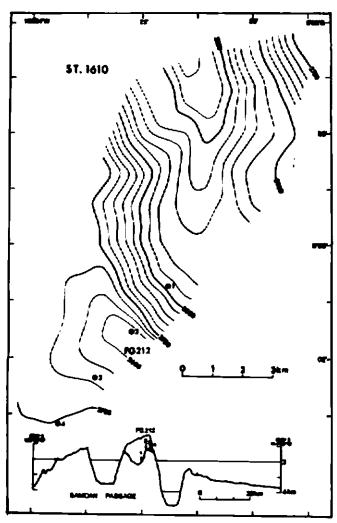

1611	B11	0.8kg/m^2	-	Vs	N ooze
	FG213-1	0.1	5%	Vs	F rich N ooze
	FG213-2	0	2	-	F rich N ooze

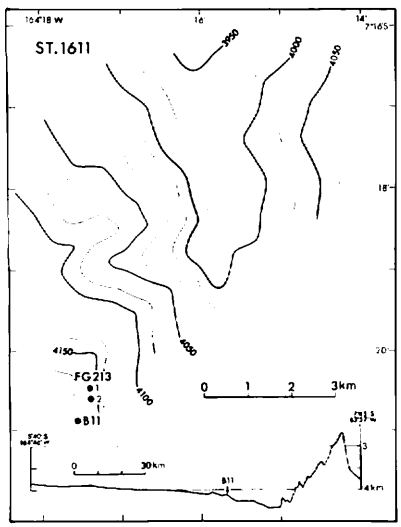

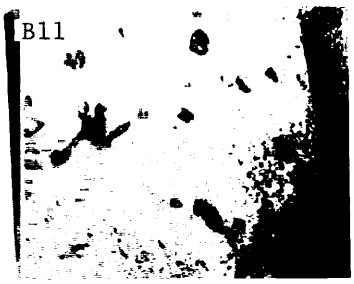

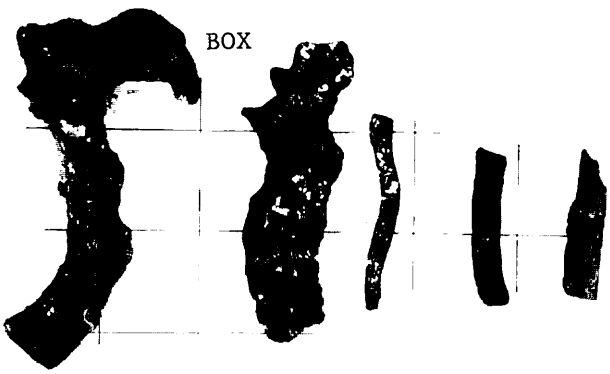

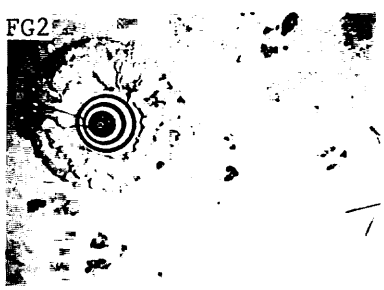

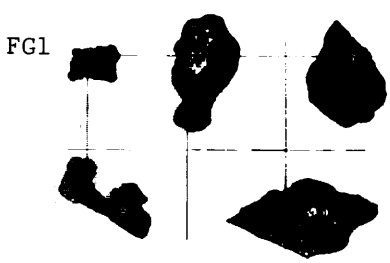

BOX

(23)

1612	P163	0	kg/m^2	-	-	C mud
	FG214-1	0		0%	-	N mud
	FG214-2	tr		0	(Sr)	N mud

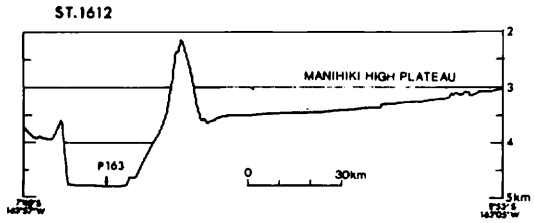

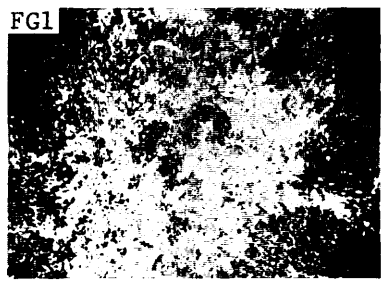

FG2

1613	B12	0	kg/m^2	0%	-	-
	FG215-1	0		-	-	-
	FG215-2	0		0	-	-

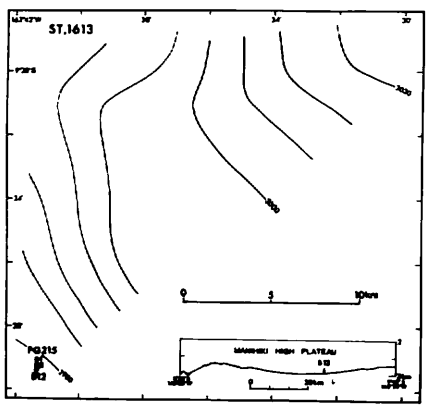

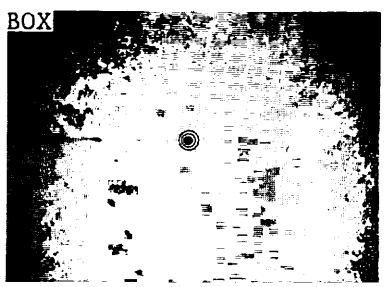

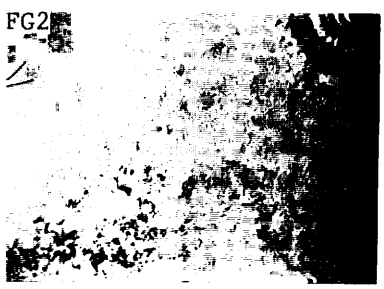

(24)

1614	B13	0	kg/m^2	0%	-	NF ooze
	FG216-1	0		0	-	-
	FG216-2	0		0	-	-

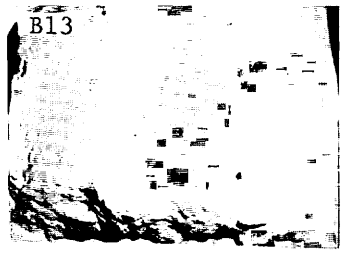

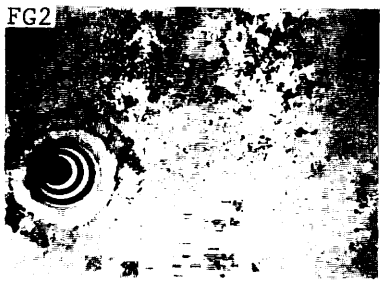

1615	P164	0	kg/m^2	-	-	NF ooze
	FG217-1	0		0%	-	-
	FG217-2	0		0	-	NF ooze

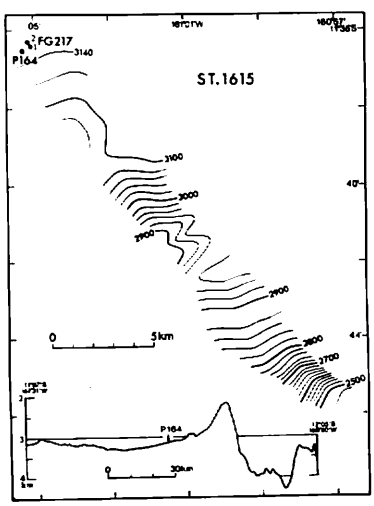

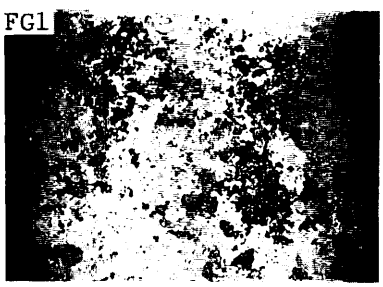

(25)

1616	B14	18.3kg/m^2	70%	Ss, Ts, SPs	P clay
	FG218-1	0	60	-	-
	FG218-2	8.6	50	Ss, DPs, Fs	P clay

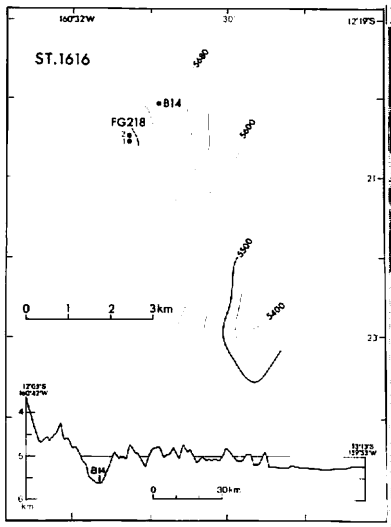

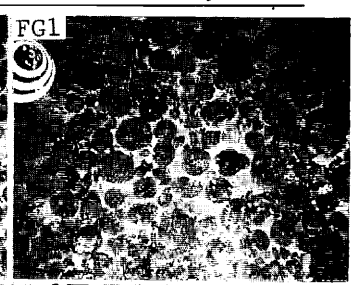

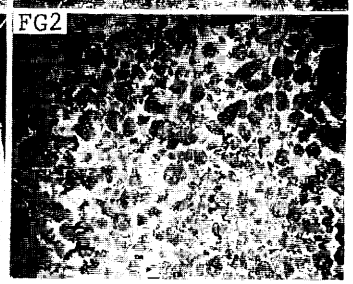

BOX

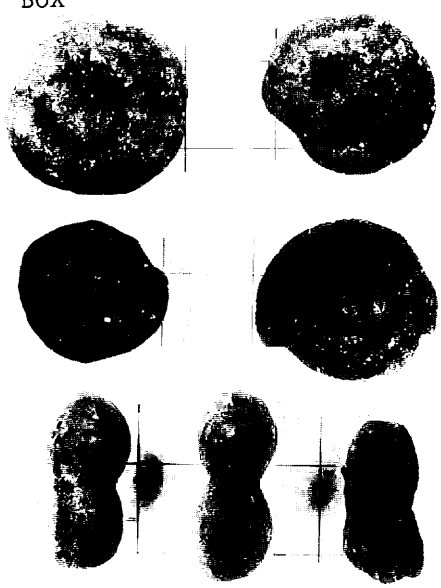

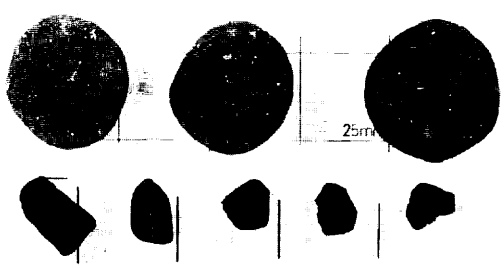

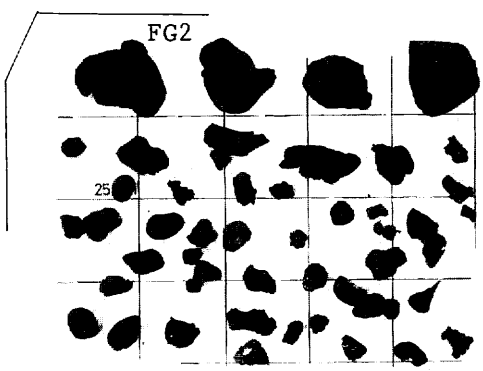

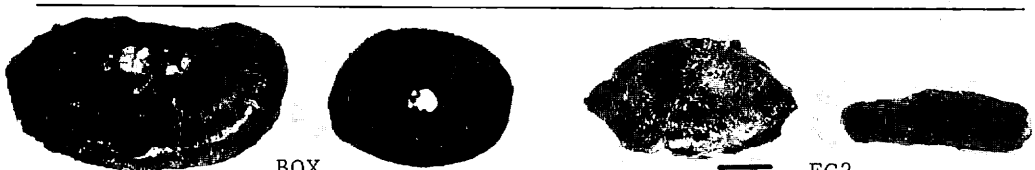

(26)

1617	B15	31.0kg/m^2	60%	Ss	P clay
	FG219-1	3.2	40	Ss, DPs, IDPs	P clay
	FG219-2	18.8	50	Ss	P clay

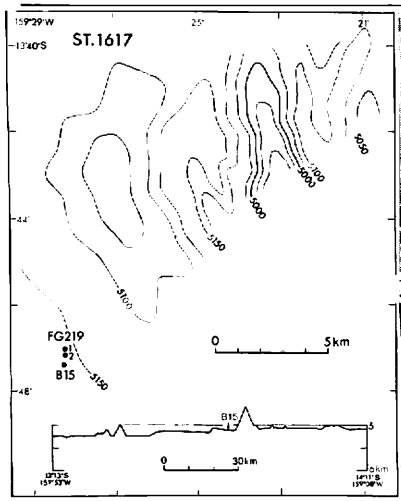

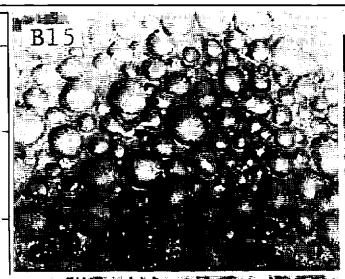

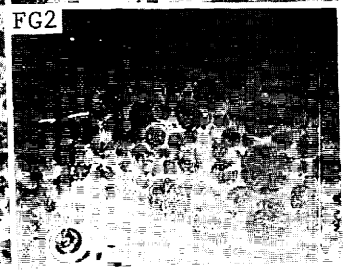

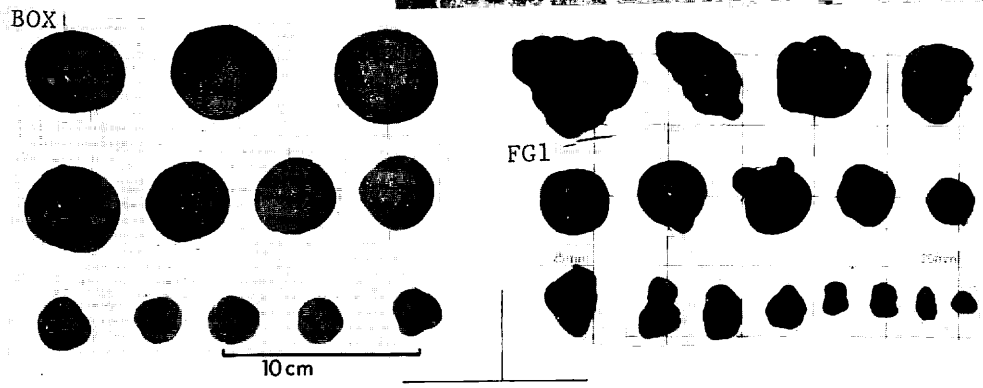

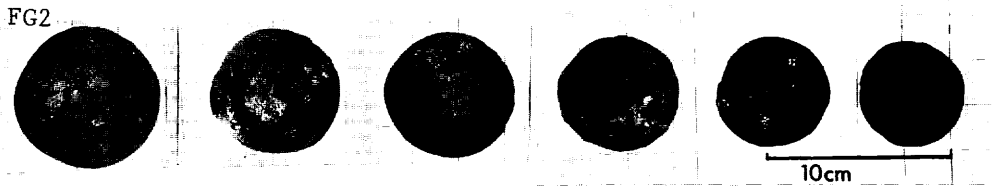

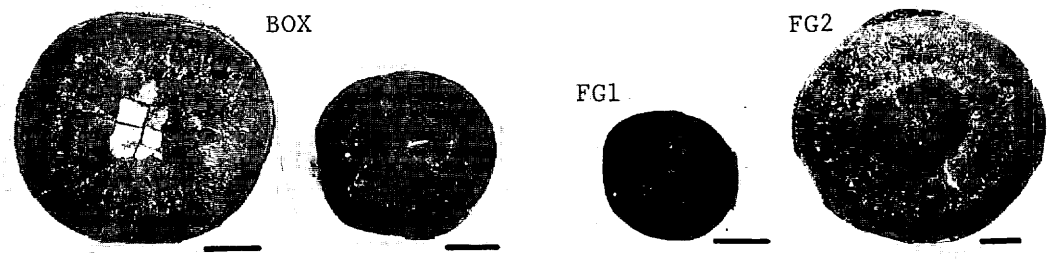

(27)

1618	B16	1.0kg/m^2	2%	Ss, SPs, Is	P clay
	FG220-1	tr	5	DPs, Is	P clay
	FG220-2	0.5	2	Ss, Is	P clay
A	P165	0	-	-	P clay
	FG221-1	3.9	8	Is, DPs, Ss	P clay
	FG221-2	2.8	10	Is, DPs	P clay

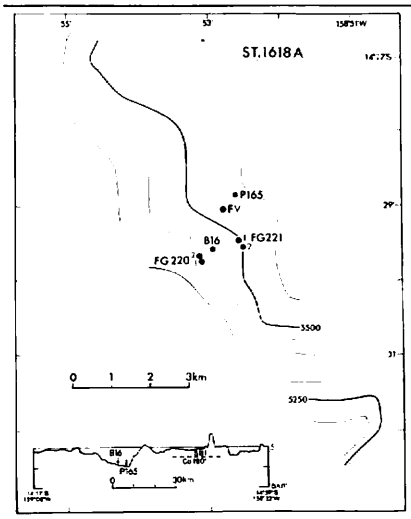

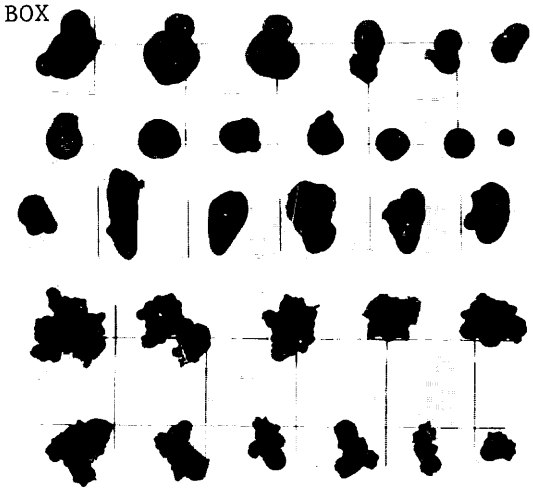

(28)

FG1

FG2

FG1A

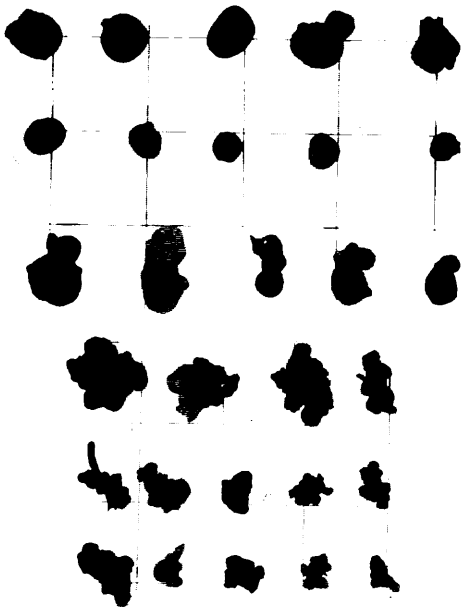

FG2A

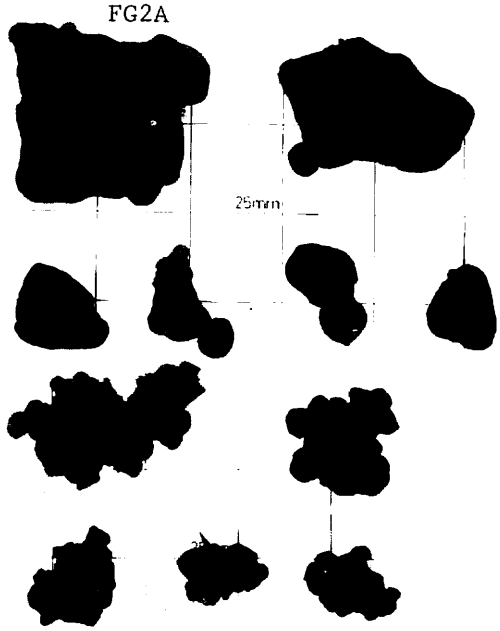

BOX

FG1A

FG2A

1619	P166	(15) kg/m^2	-	DPs, IDPs	Z mud
	B17	6.1	20%	DPs, IDPs	Z mud
	FG222-1	12.8	15	DPs, Ts+r	Z mud
	FG222-2	9.4	20	DPs, SPs, ISPs	Z mud

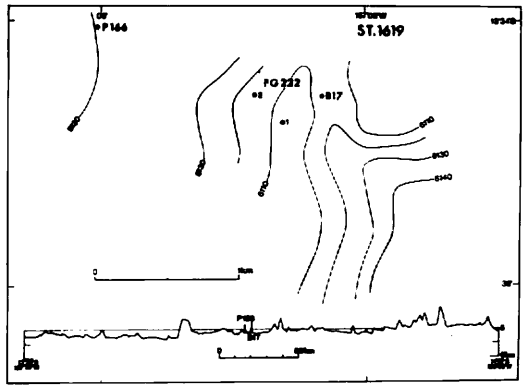

BOX

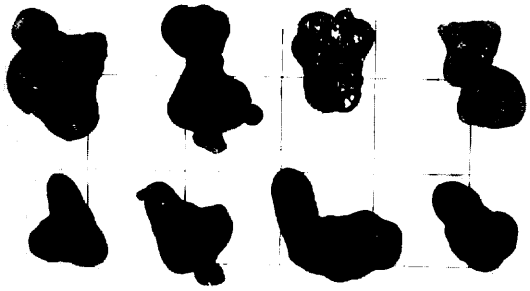

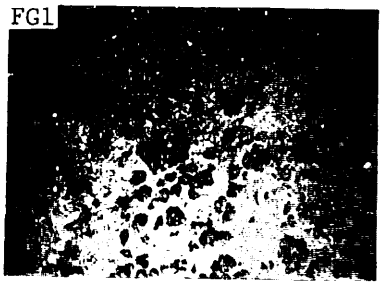

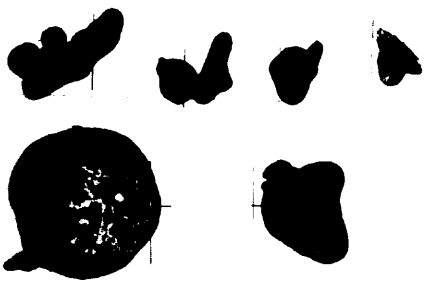

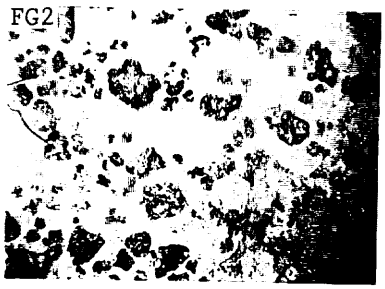

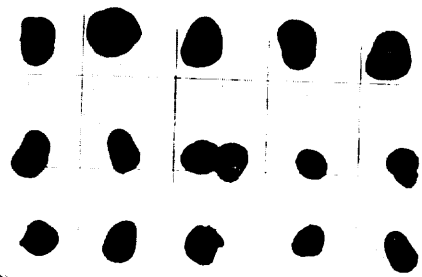

(30)

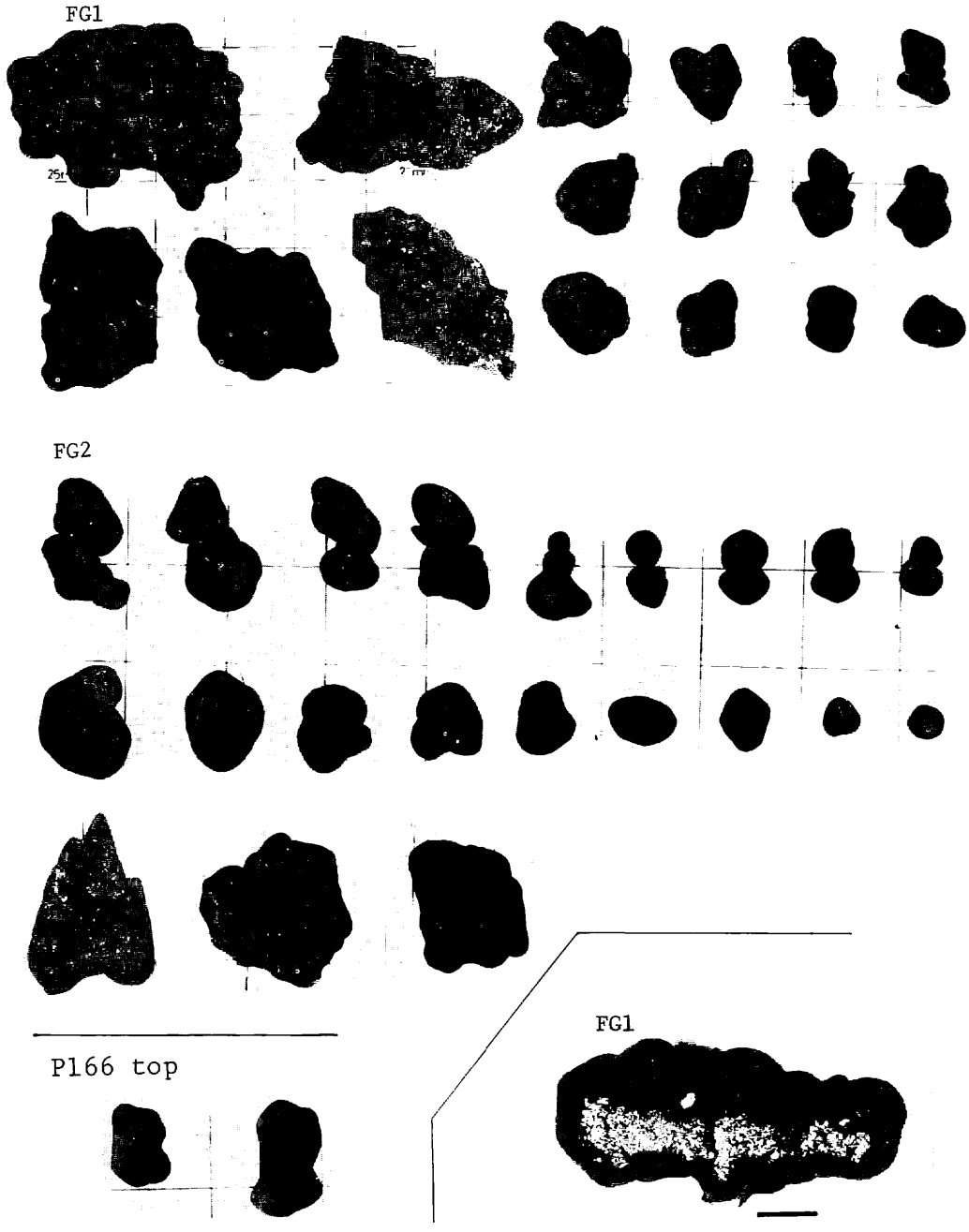

(31)

1620	B18	0.1kg/m^2	(30)%	Ds	Z mud
	FG223-1	23.9	40	Ss, SEs	Z mud
	FG223-2	26.1	40	Ss, SEs	Z mud

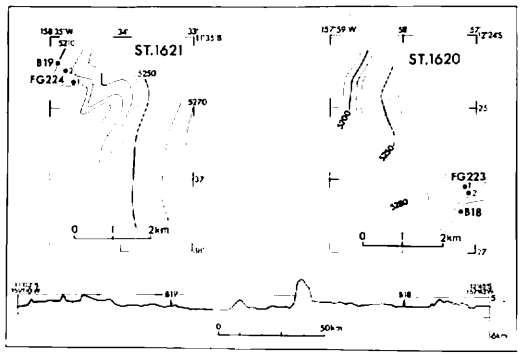

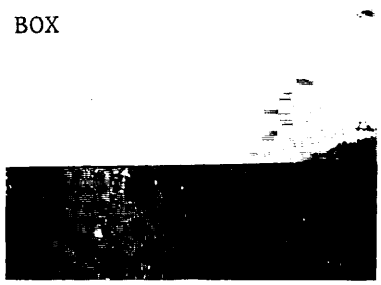

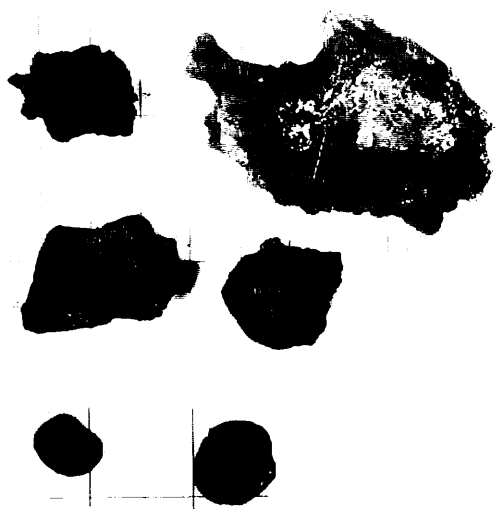

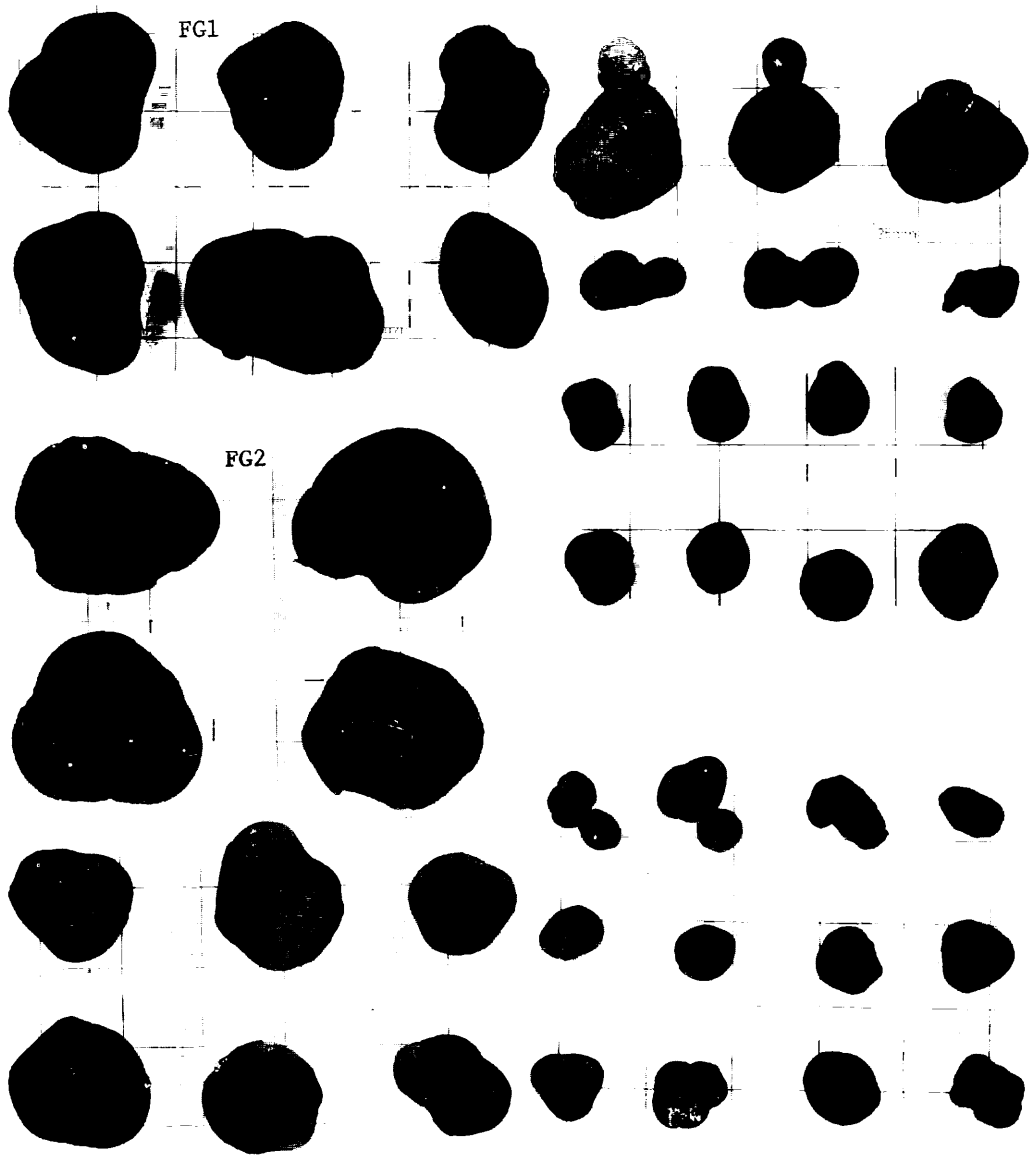

(33)

1621	B19	6.7kg/m^2	40%	Ds, Ss	Z rich mud
	FG224-1	3.8	30	Ss, Ds	-
	FG224-2	10.5	-	DPs, Ts	Z rich mud

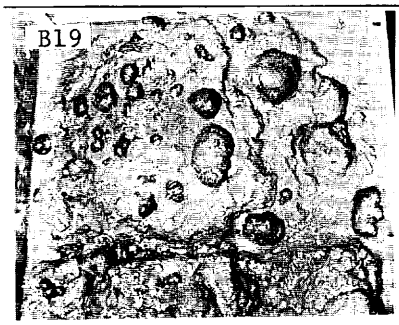

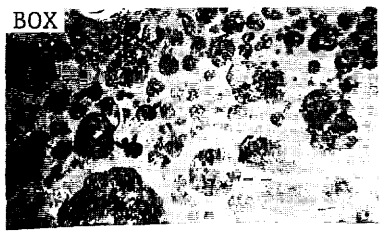

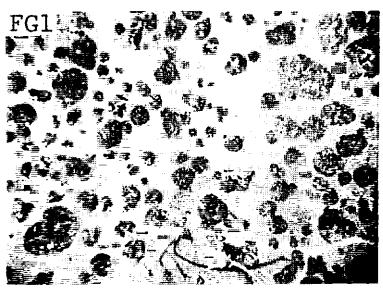

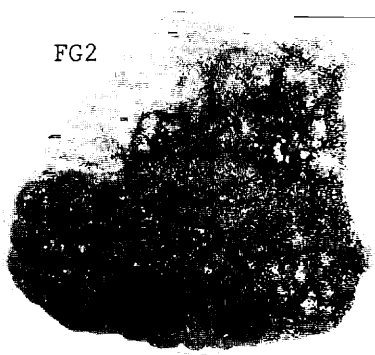

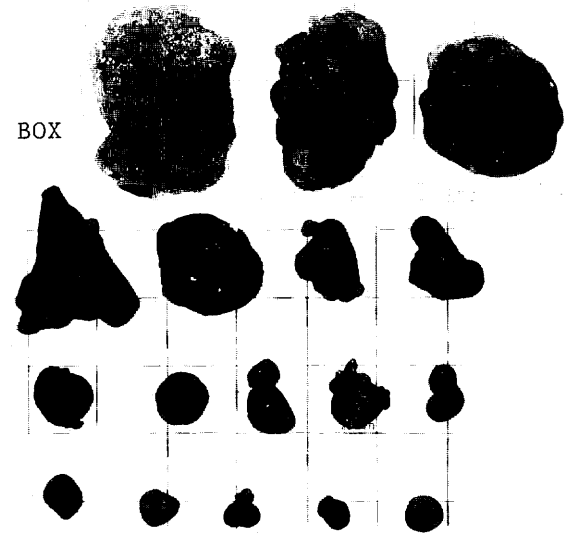

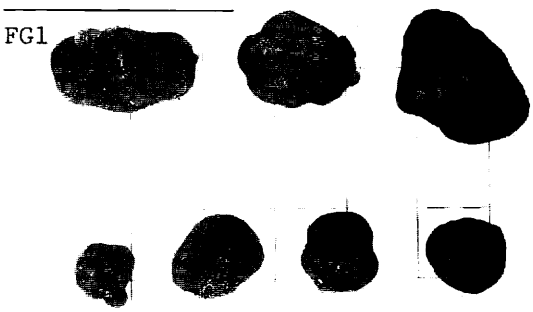

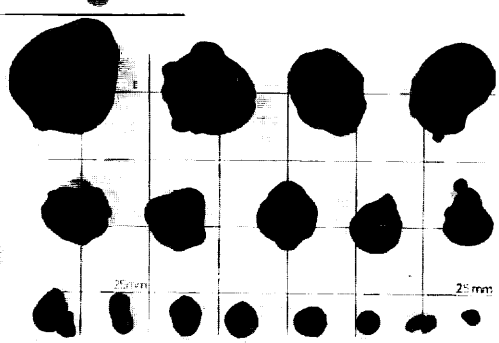

(34)

1622	P167	0 kg/m^2	-	-	Z rich mud
	FG225-1	0.2	1%	Ss, Ds	Z rich mud
	FG225-2	0.2	1	Ss, SPs, Ds	Z rich mud

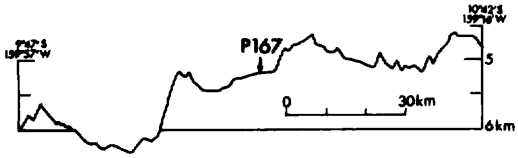

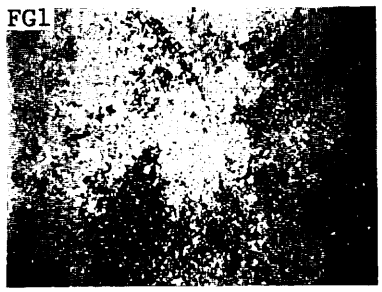

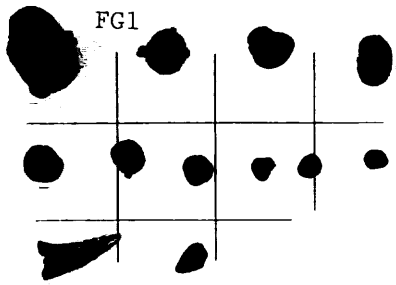

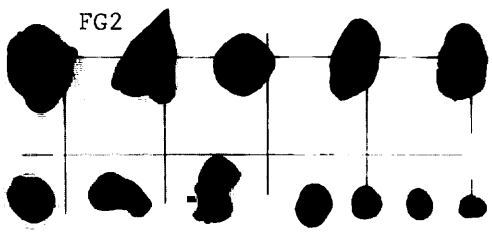

1623	B20	16.0kg/m^2	60%	Ss, SPs	CM ooze
	FG226-1	0	(0)	-	-
	FG226-2	0	(0)	-	-

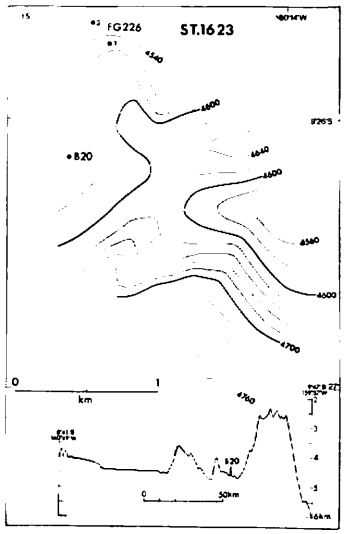

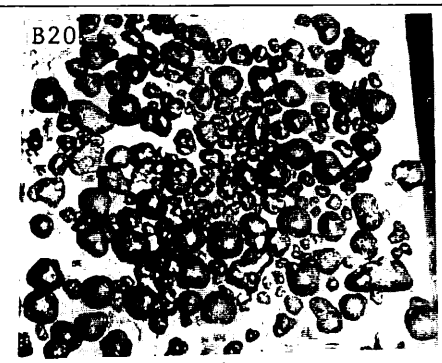

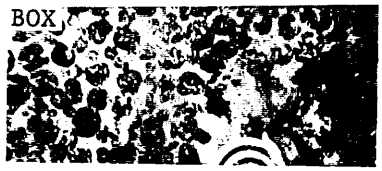

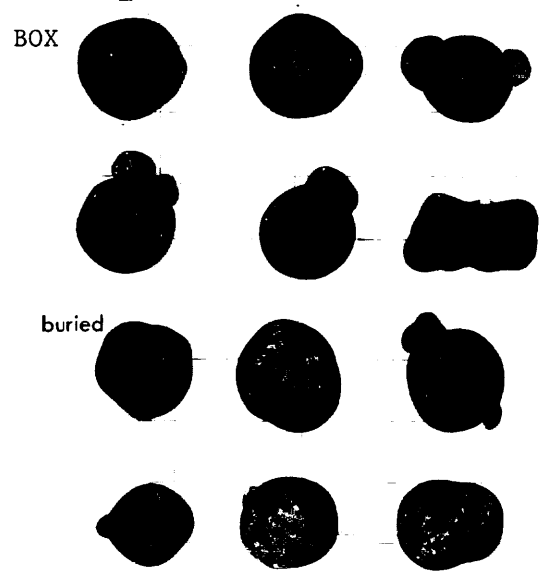

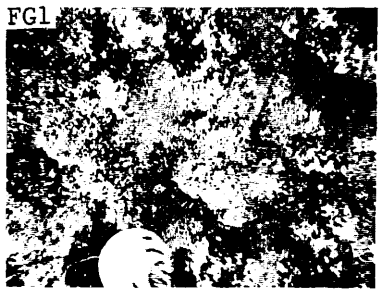

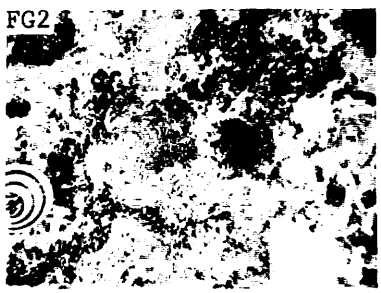

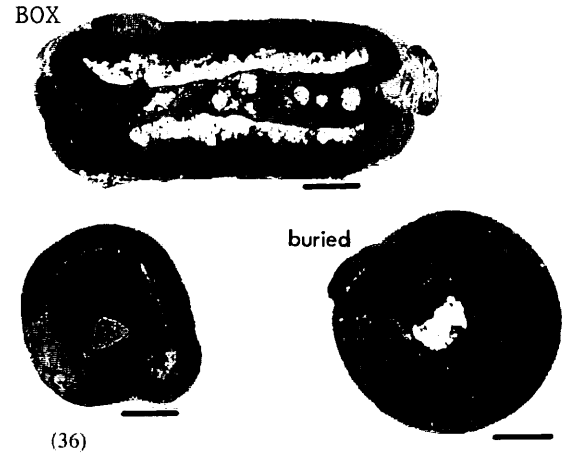

(36)

1624	P168	0	kg/m^2	-	-	NF ooze
	FG227-1	0		0%	-	FN ooze
	FG227-2	0		0	-	FN ooze

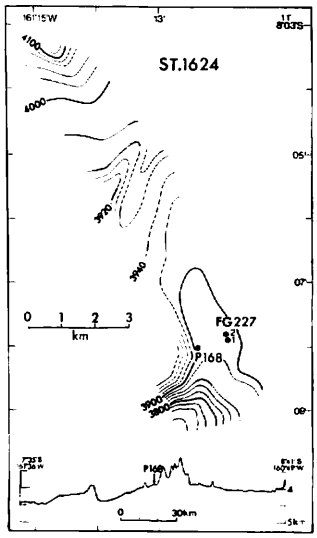

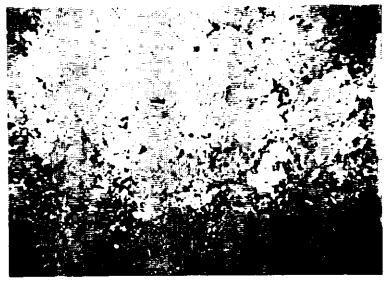

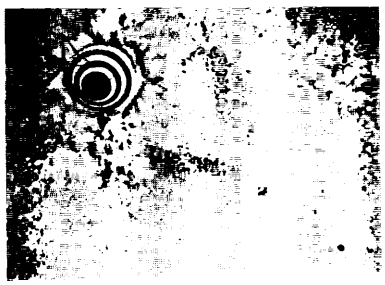

1625	B21	0.1kg/m^2		0%	(DPs, Ds)	N ooze
	FG228-1	0.1		0	Ss, Is	N ooze
	FG228-2	tr		0	Ds, Is	N ooze

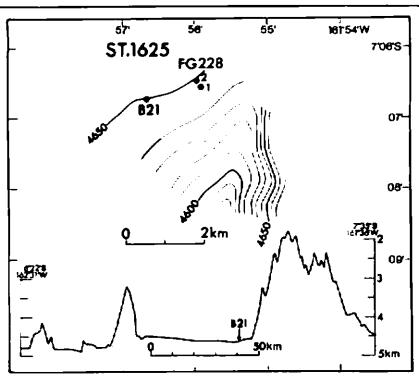

(37)

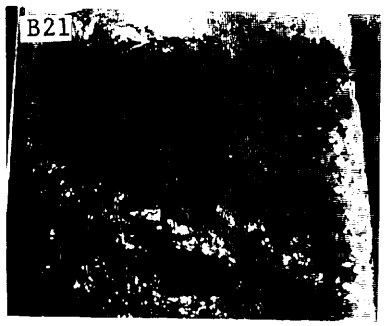

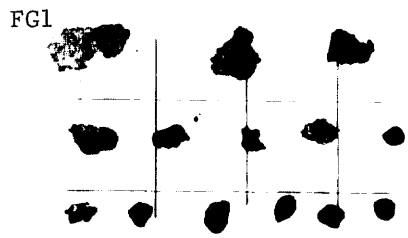

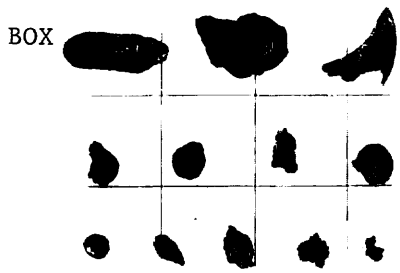

1626	P169	0	kg/m^2	-	-	N ooze
	FG229-1	0		0%	-	N ooze
	FG229-2	0		0	-	N ooze

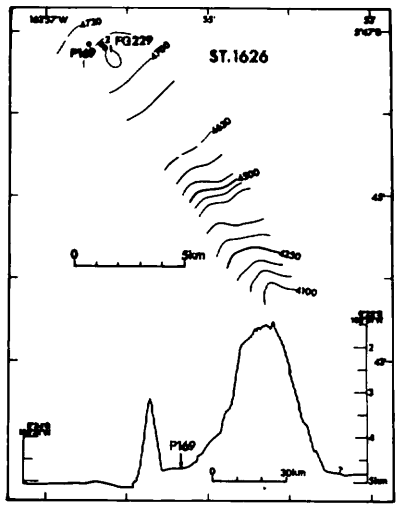

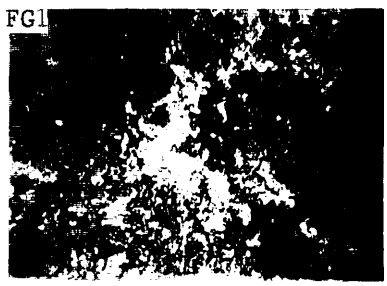

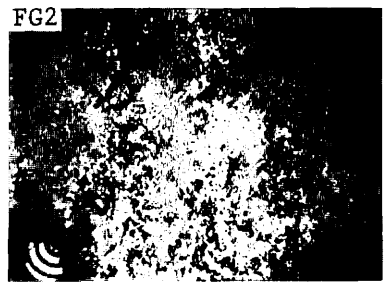

1627	B22	tr	0%	Sr	SCf rich mud
	FG230-1	0 kg/m^2	0	-	SCf rich mud
	FG230-2	0	0	-	SCf rich mud

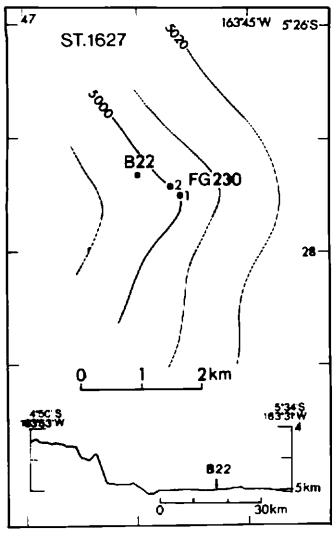

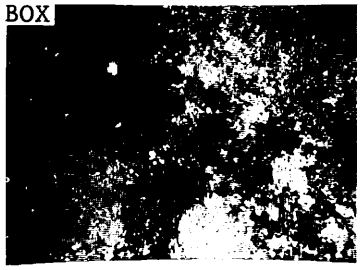

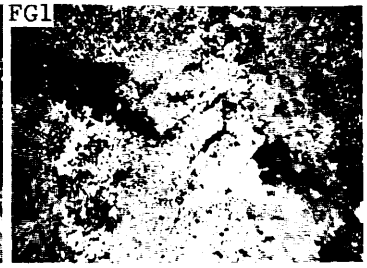

1628	P170	0 kg/m^2	-	-	Sf rich N ooze
	FG231-1	0	0%	-	Sf rich N ooze
	FG231-2	0.2	0	Ir	-

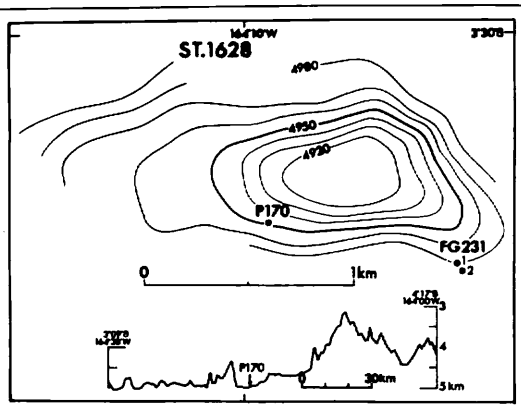

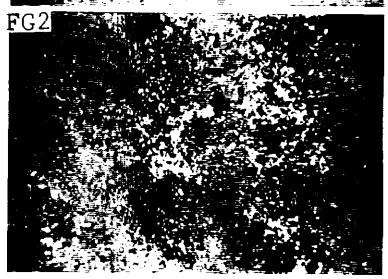

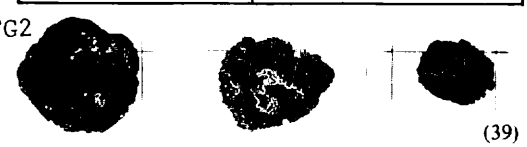

(39)

1629	B23	6.1kg/m^2	0%	Ir, IDPr, Sr, Ts+r	S mud
	FG232-1	7.0	0	Sr, Dr, Ts+r	Cf rich S mud
	FG232-2	0.4	0	Sr, SEr	Cf rich S mud

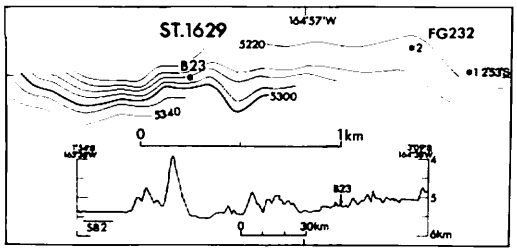

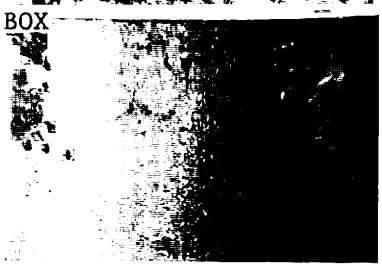

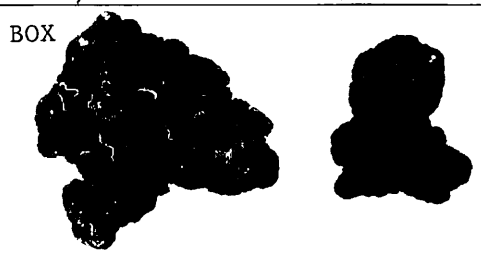

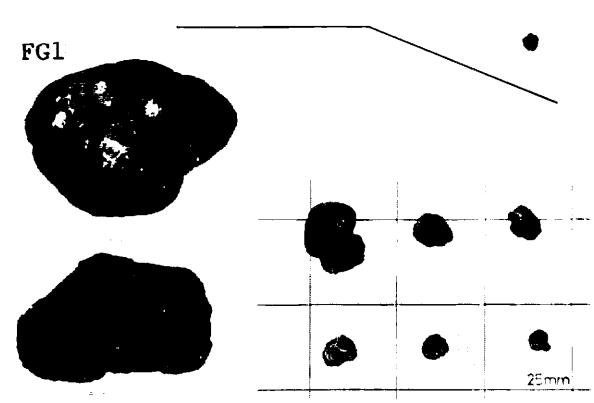

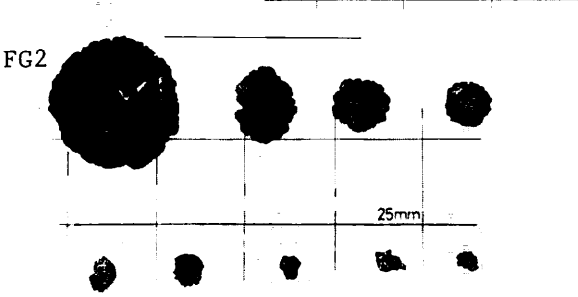

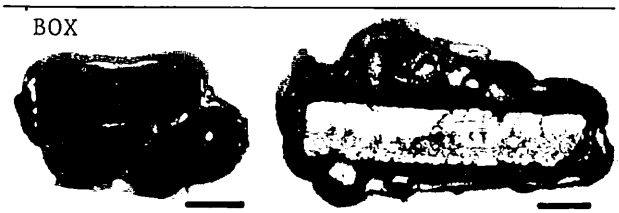

(40)

1630	P171	0 kg/m^2	-	-	S mud
	FG233-1	tr	0%	Sr	S mud
	FG233-2	tr	0	Sr	S mud

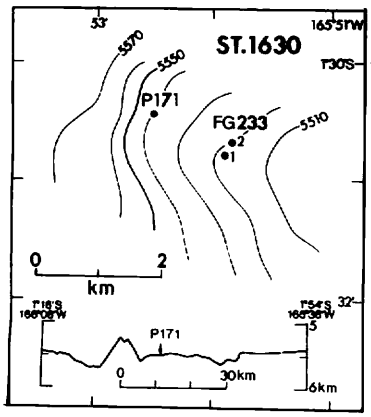

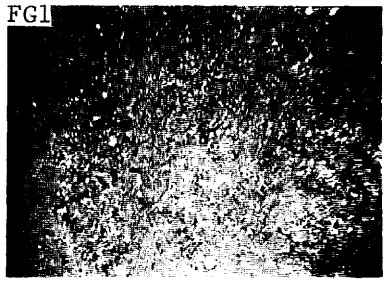

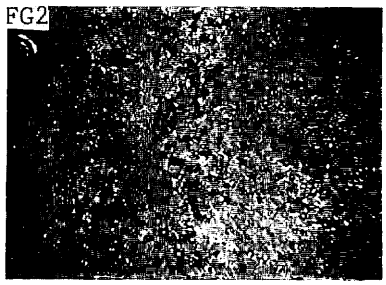

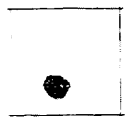

1631	B24	2.5kg/m^2	0%	Sr	CS ooze
	FG234-1	9.0	0	SPs·r, Ss·r	CS ooze
	FG234-2	10.4	5	SPs·r, Ss·r	CS ooze

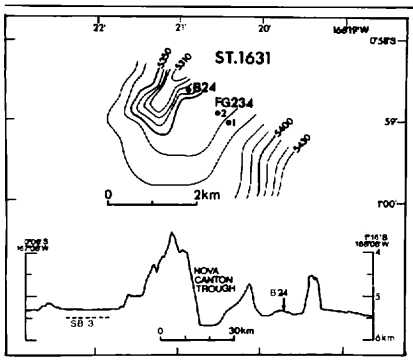

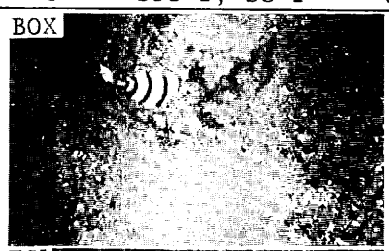

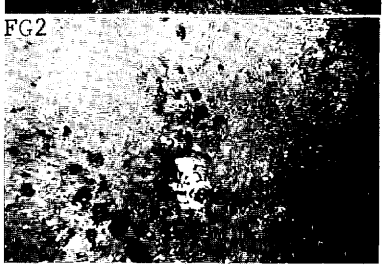

(41)

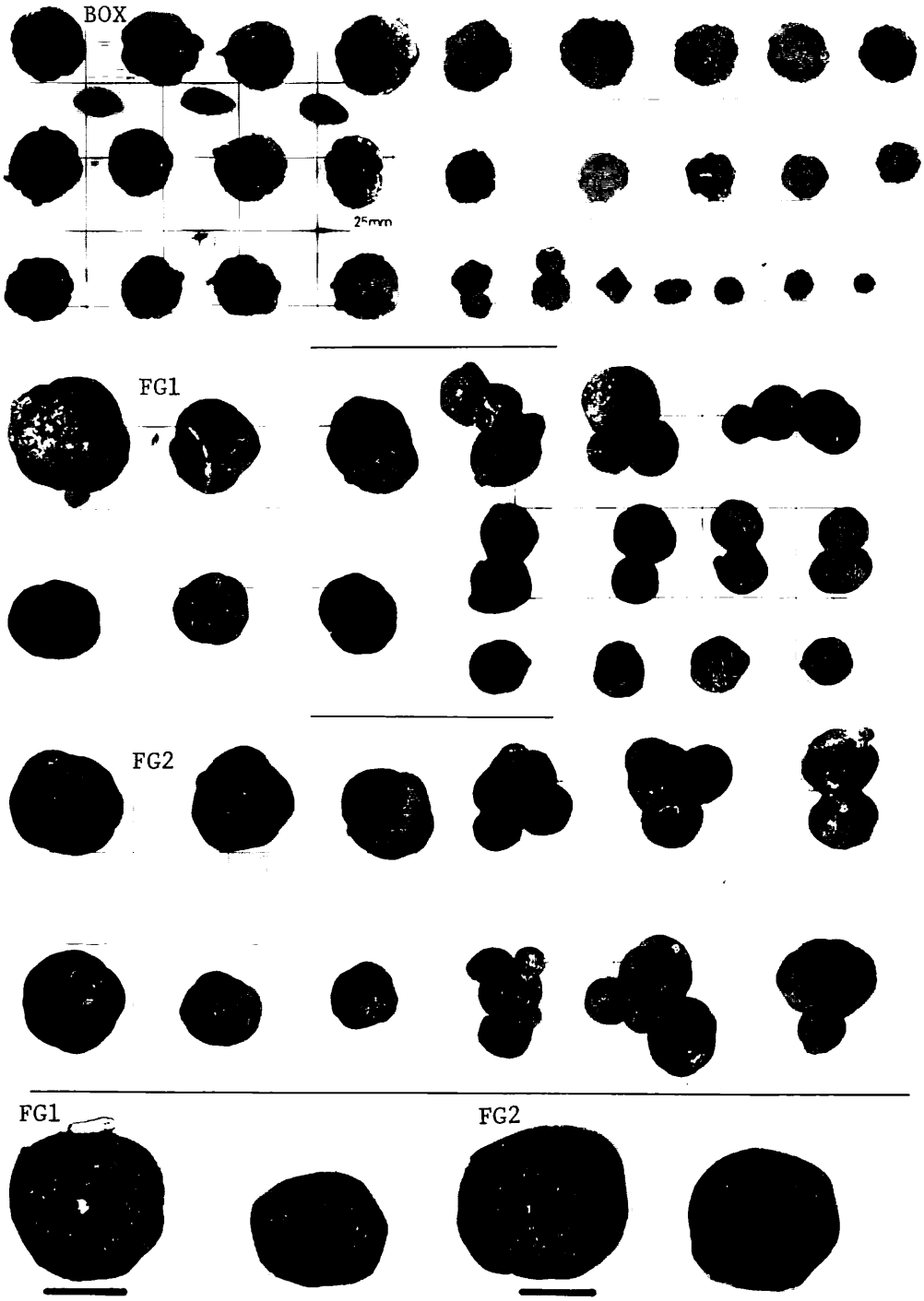

(42)

1632	P172	0	kg/m^2	-	-	SN mud
	FG235-1	0		-	-	CS mud
	FG235-2	tr		1%	Sr	CS mud

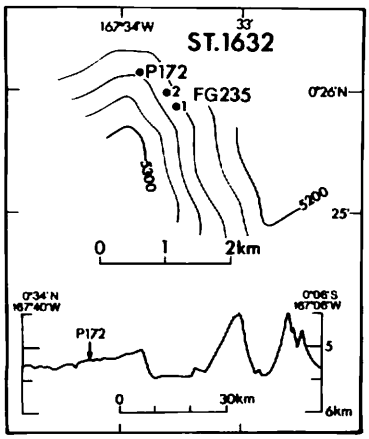

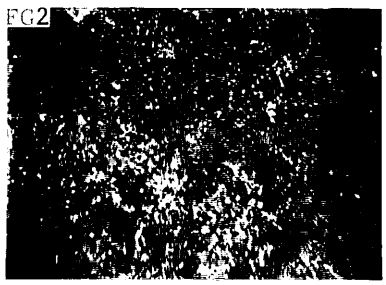

FG2

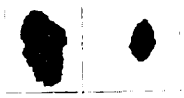

1633	B25	0	kg/m^2	0%	-	S ooze
	FG236-1	0		0	-	CS ooze
	FG236-2	0		0	-	CS ooze

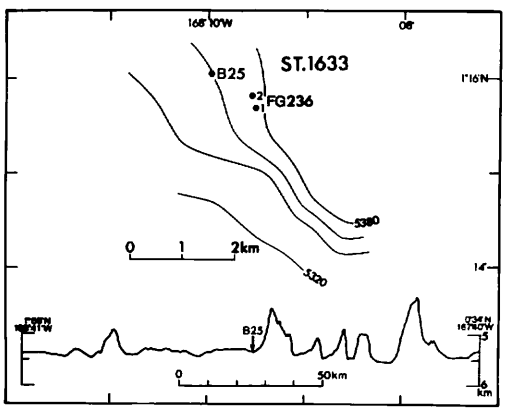

BOX

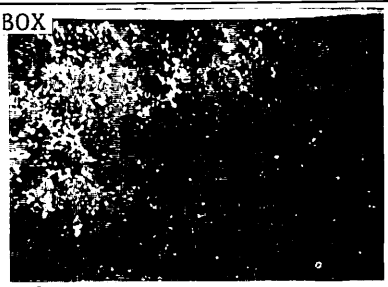

FG1

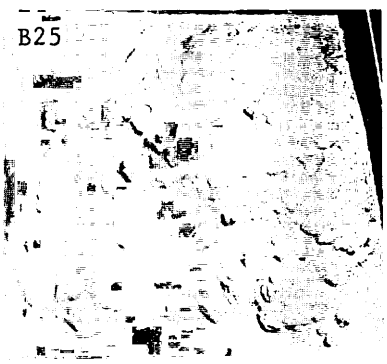

FG2

(43)

1634					
P173	(6.0)kg/m^2	-	Dr		SCM ooze
FG237-1	6.8	5%	IDPs·r,	DPs·r	S ooze
FG237-2	7.7	10	IDPs·r,	DPs·r	S ooze

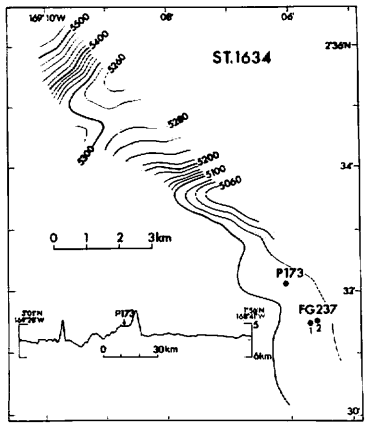

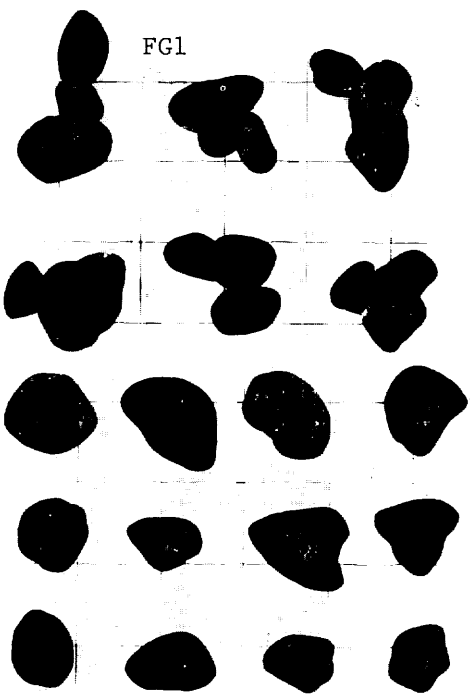

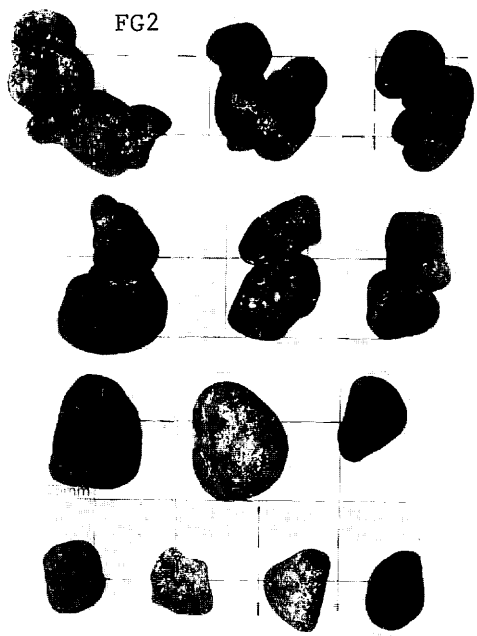

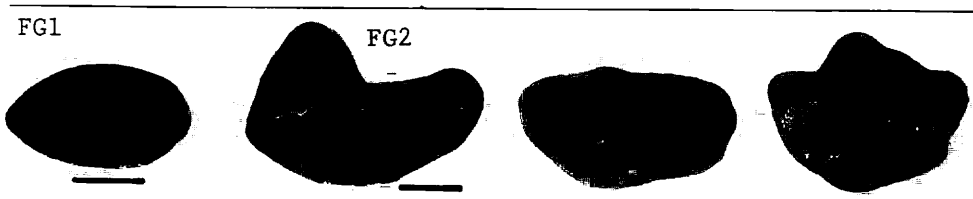

(44)

1635 A	B26	2.6kg/m^2	0%	Sr, Dr	S ooze
	FG238-1	5.0	5	Sr, Dr	S ooze
	FG238-2	2.0	0	Sr, Dr	S ooze
	D377	-	-	Ir, Vr, Sr	-
	P197	0	-	-	S ooze
	FG239-1	5.9	15	IDPs·r, DPs·r, Tr	S ooze
	FG239-2	1.2	0	IDPr, Dr	Cf rich S ooze

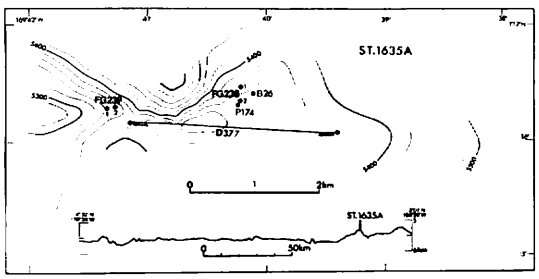

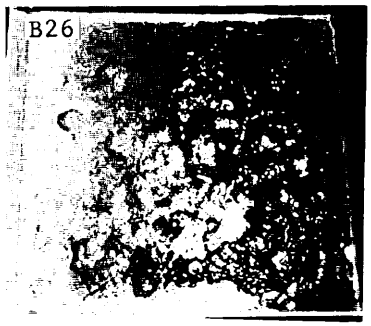

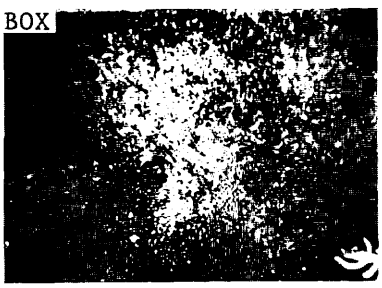

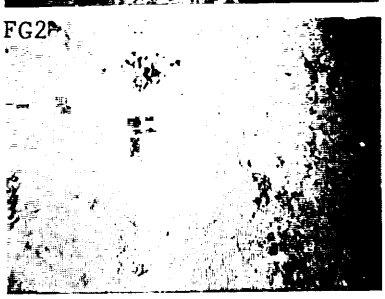

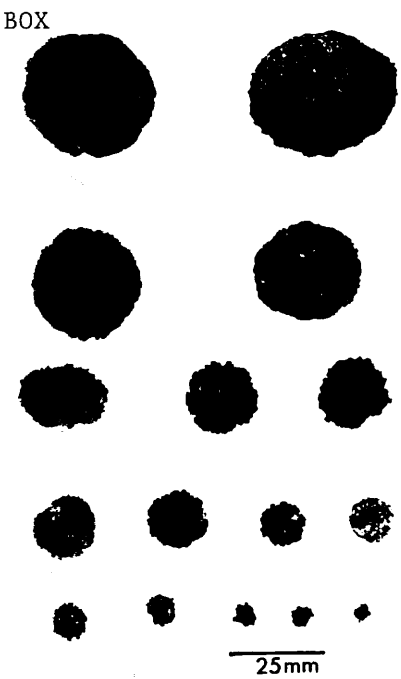

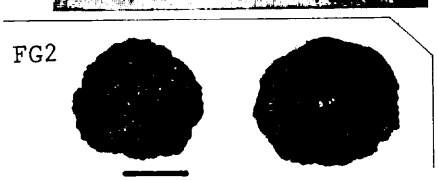

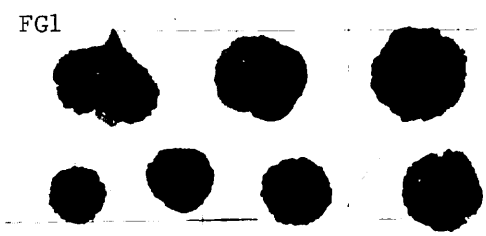

(45)

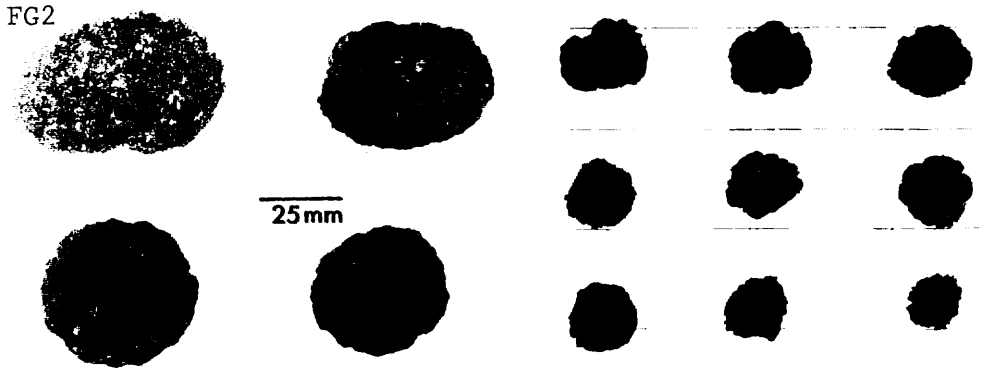
FG2
25mm

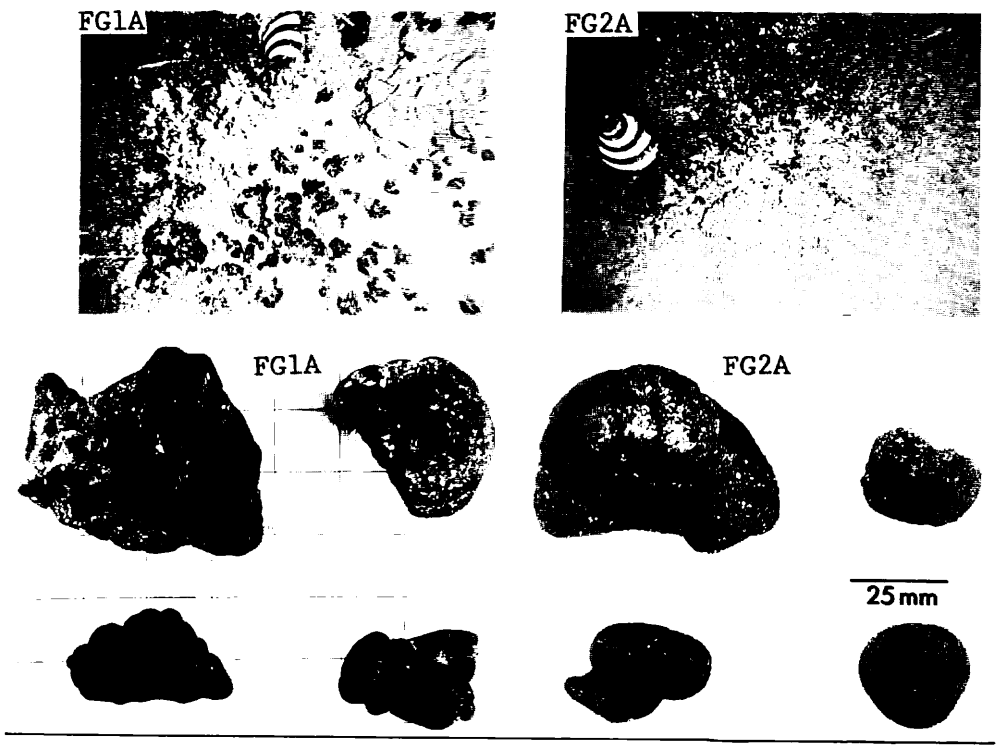
FG1A
FG2A
FG1A
FG2A
25mm

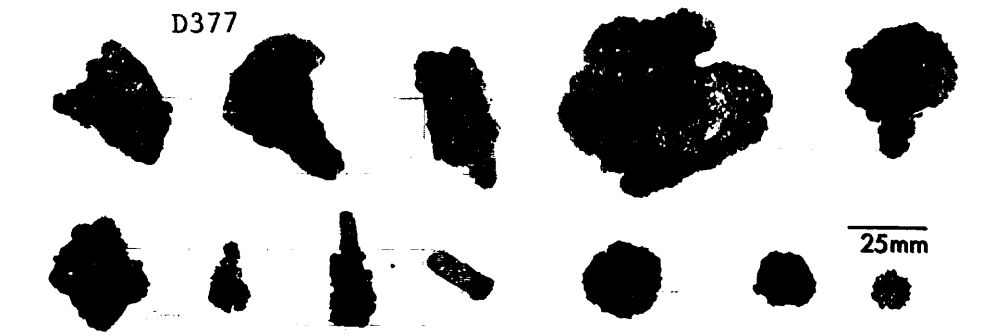
D377
25mm

1636	P175	0	kg/m^2	-	-	S mud
	FG240-1	tr		2%	Vr	S mud
	FG240-2	0		0	-	S mud

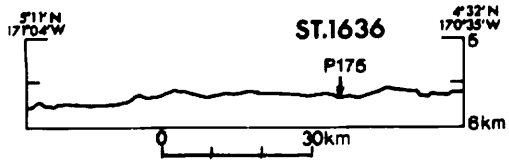

FG1

FG2

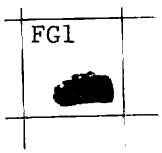

1637	B27	0	kg/m^2	0%	-	S mud
	FG241-1	0		0	-	S mud
	FG241-2	0		0	-	S mud

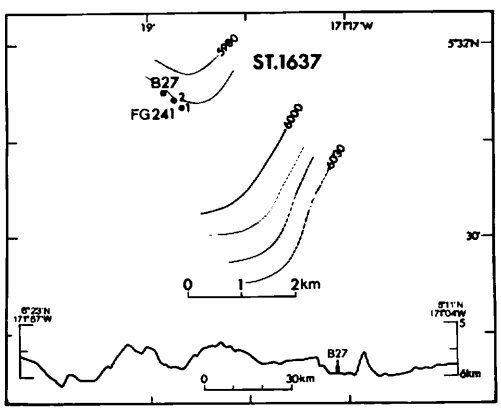

FG1

BOX

(47)

1638	P176	0 kg/m^2	-	-	S mud
	FG242-1	0.4	0%	Sr, Dr	S mud
	FG242-2	0.1	0	Ir, Vr, SPr	S mud

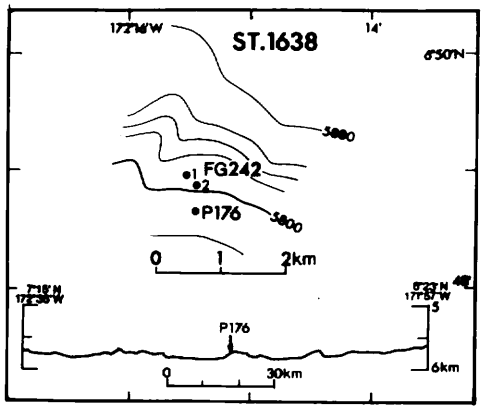

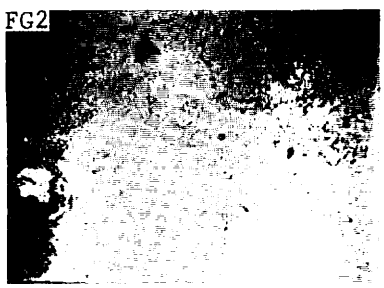

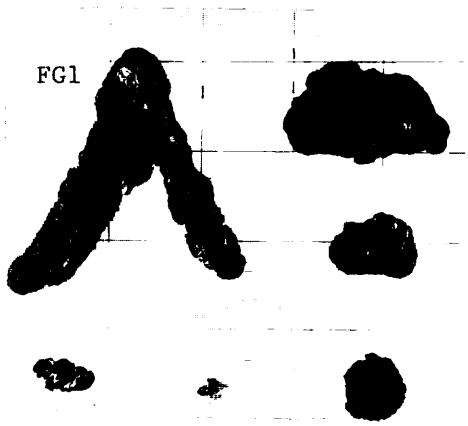

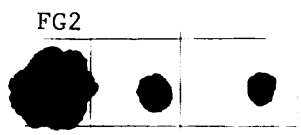

1639	B28	0.1kg/m^2	-	Vr, Sr	S mud
	FG243-1	0.2	0%	Dr, Sr	Sf rich clay
	FG243-2	0.6	0	Sr, Vr	Sf rich clay

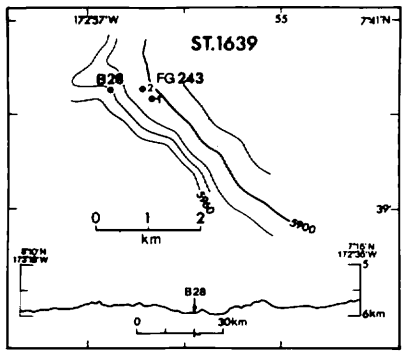

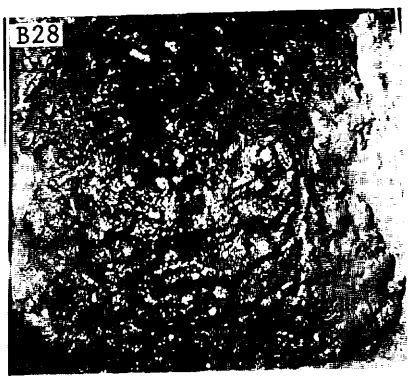

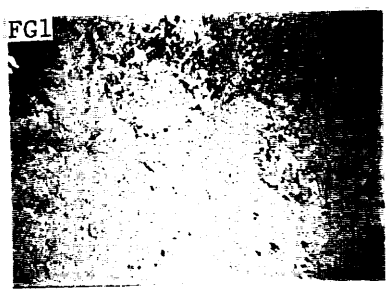

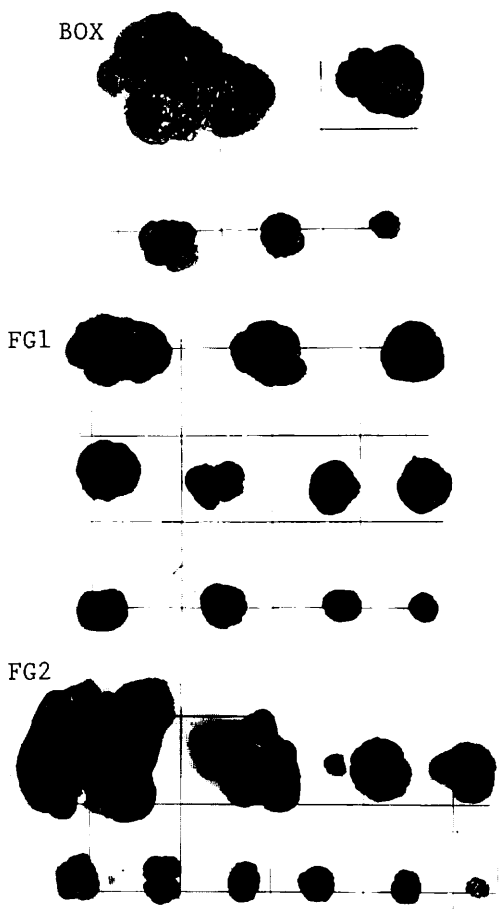

(49)

1640	P177	(2.4)kg/m^2	-	Dr	S mud
	FG244-1	3.7	5%	Sr, Ts+r	S mud
	FG244-2	10.0	15	Sr, SEr, SPr	S mud

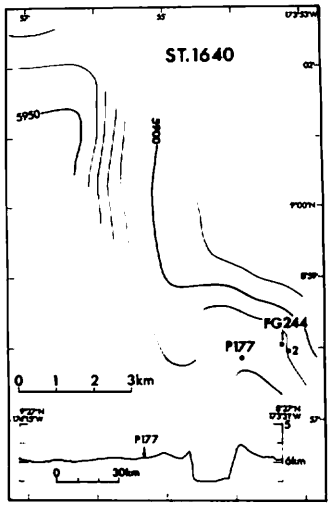

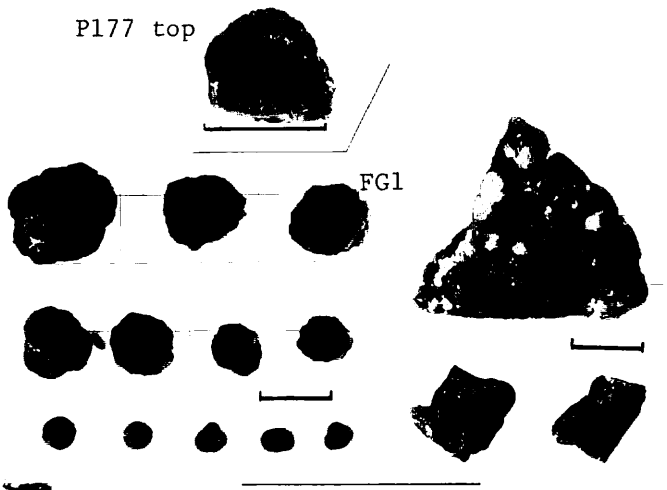

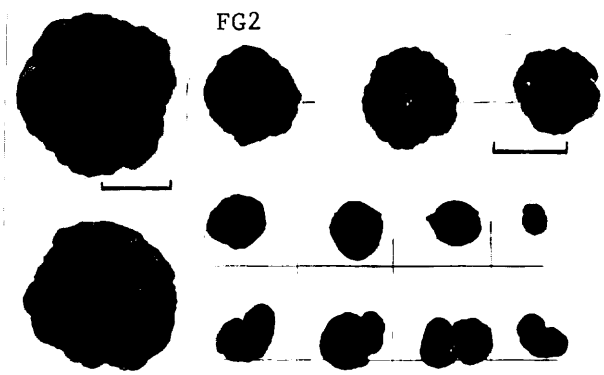

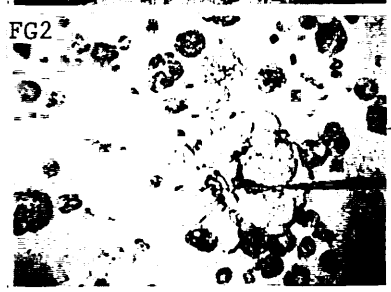

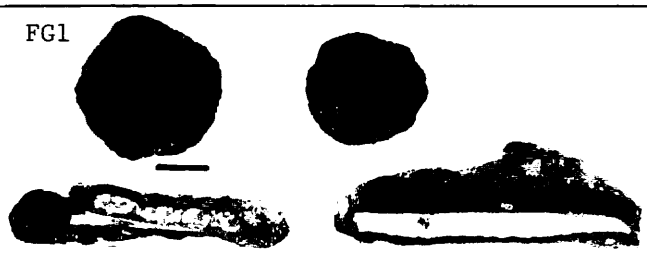

(50)

1641	B29	7.8kg/m^2	30%	Sr, SPr, Dr	Sf rich clay
	FG245-1	1.8	30	Sr, SEr	-
	FG245-2	9.4	20	Sr, SEr	P clay

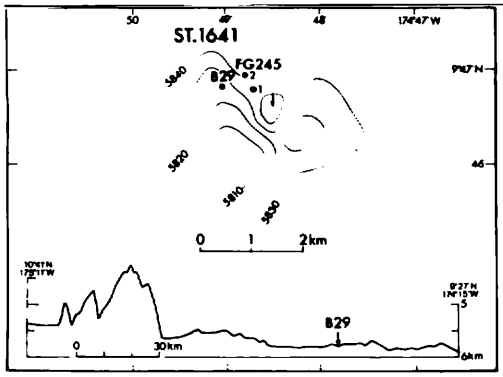

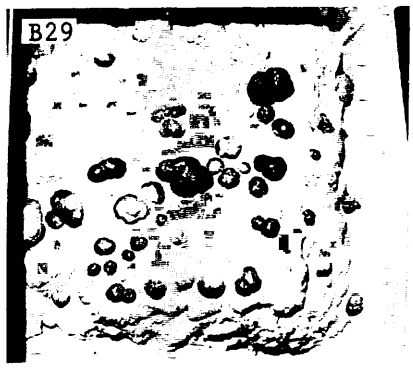

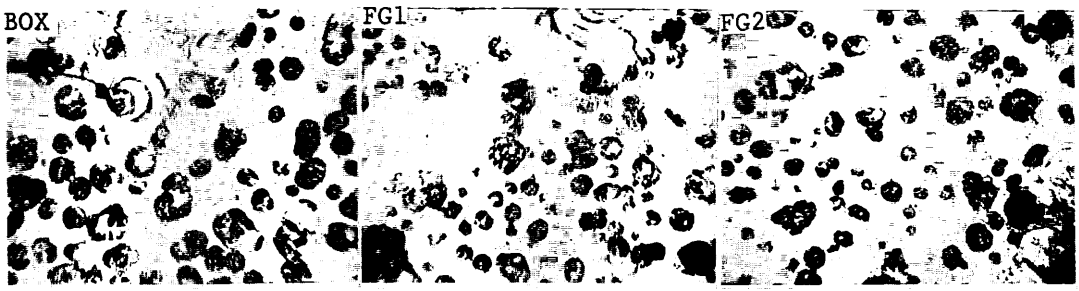

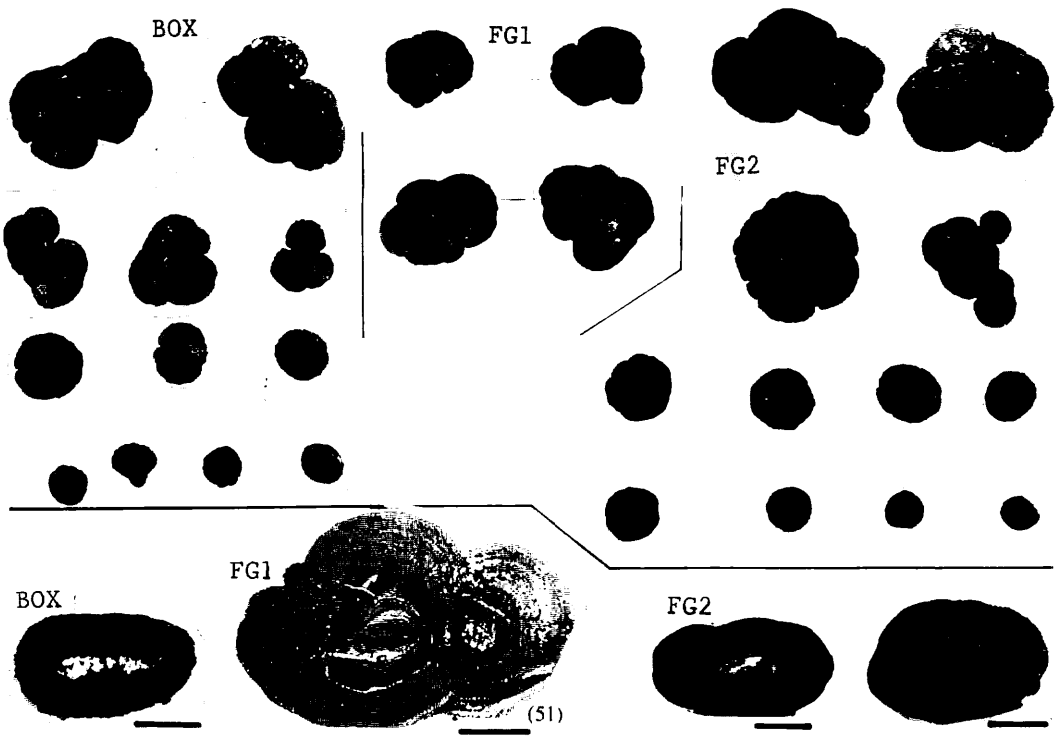

1642	P178	(1) kg/m^2	-	Ds	Sf rich clay
	FG246-1	27.2	80%	DPs, IDPs	Sf rich clay
	FG246-2	22.4	70	DPs, IDPs	Sf rich clay

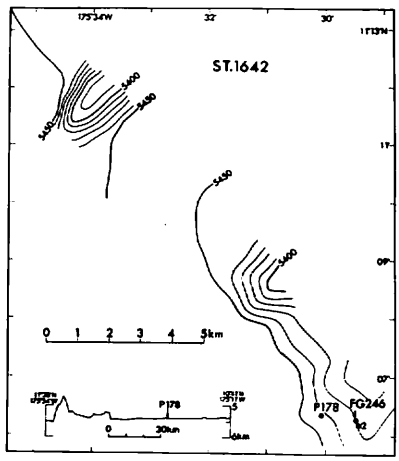

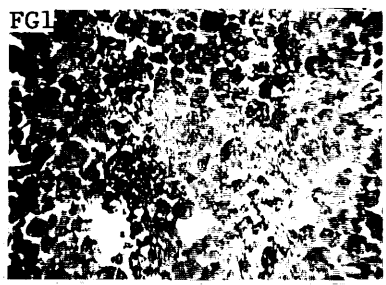

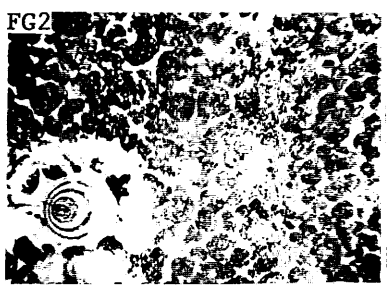

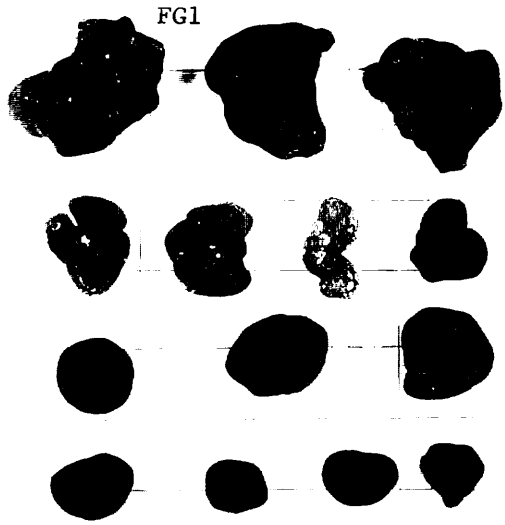

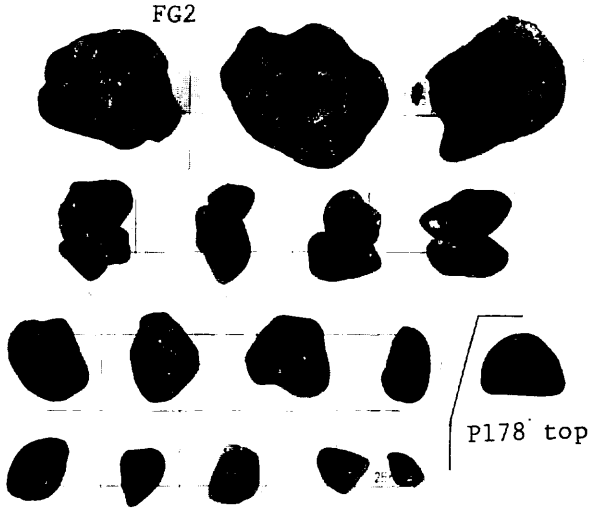

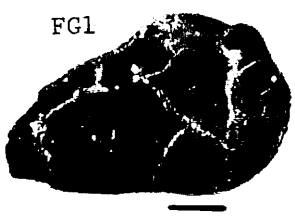

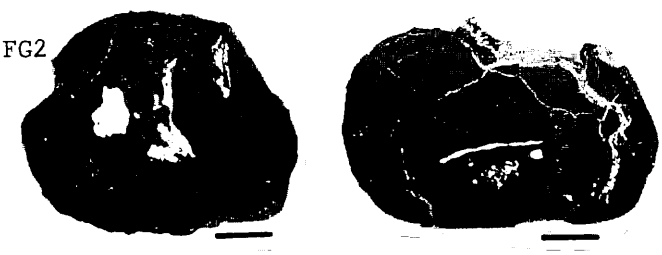

(52)

1643	D378	-	-	DPs, IDPs	-
	FG247-1	9.8kg/m^2	70%	DPs, IDPs	Z rich clay
	FG247-2	21.8	70	DPs, IDPs	Z rich clay

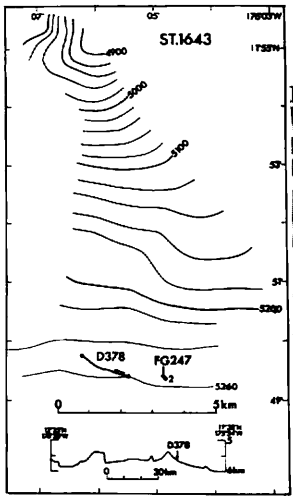

FG1

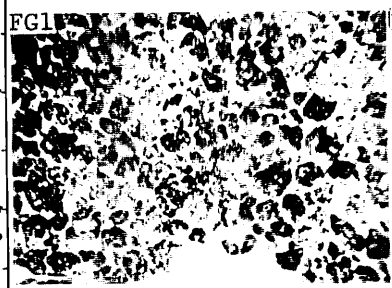

FG2

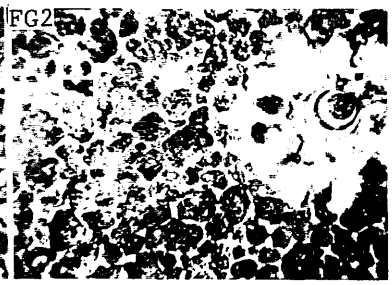

FG2

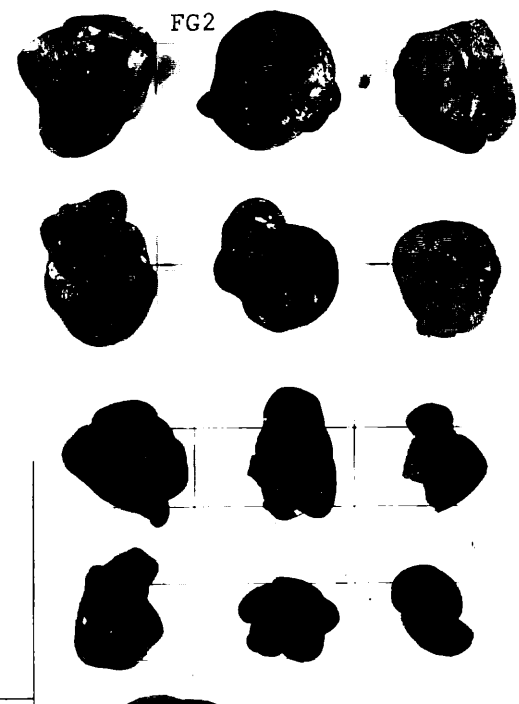

FG1

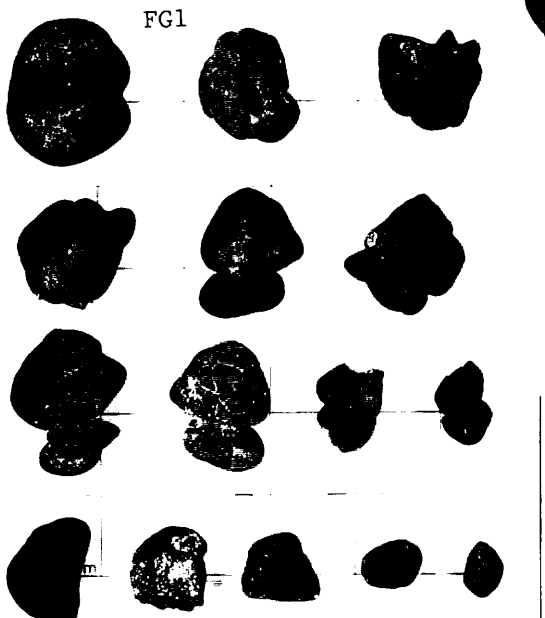

FG2

(53)

1644	P179	0 kg/m^2	-	-	Z mud
	FG248-1	0	10%	-	Z mud
	FG248-2	0.2	8	SPs+r	-

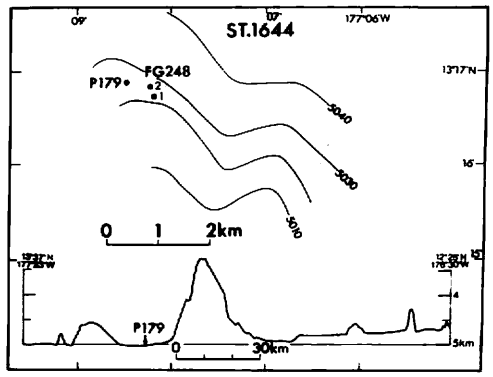

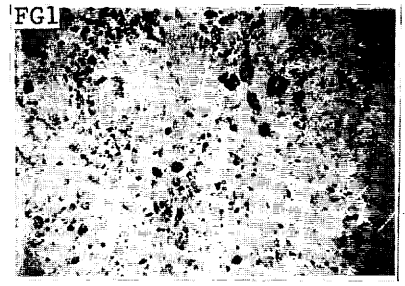

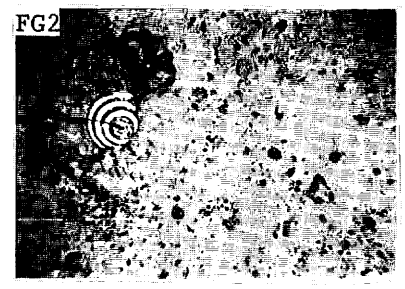

1645	B30	20.2kg/m^2	80%	Ds, DPs	Z rich clay
	FG249-1	23.4	80	Ds, IDPs	Z rich clay
	FG249-2	21.8	80	DPs, IDPs	Z rich clay

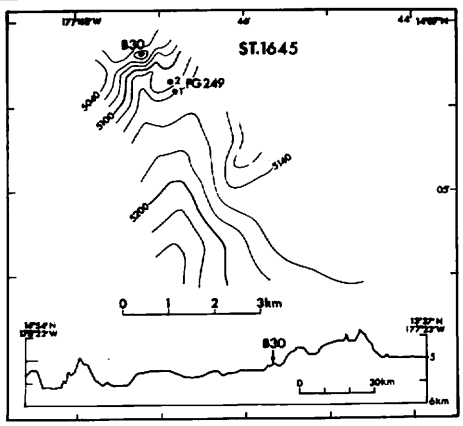

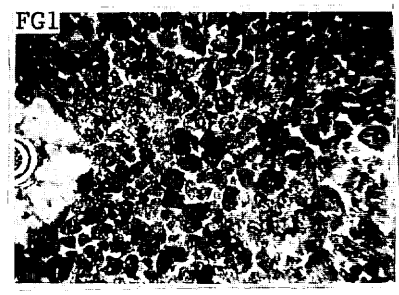

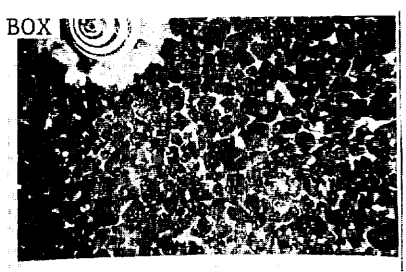

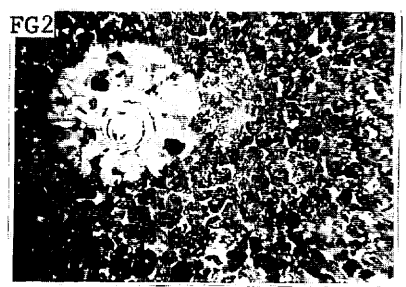

(54)

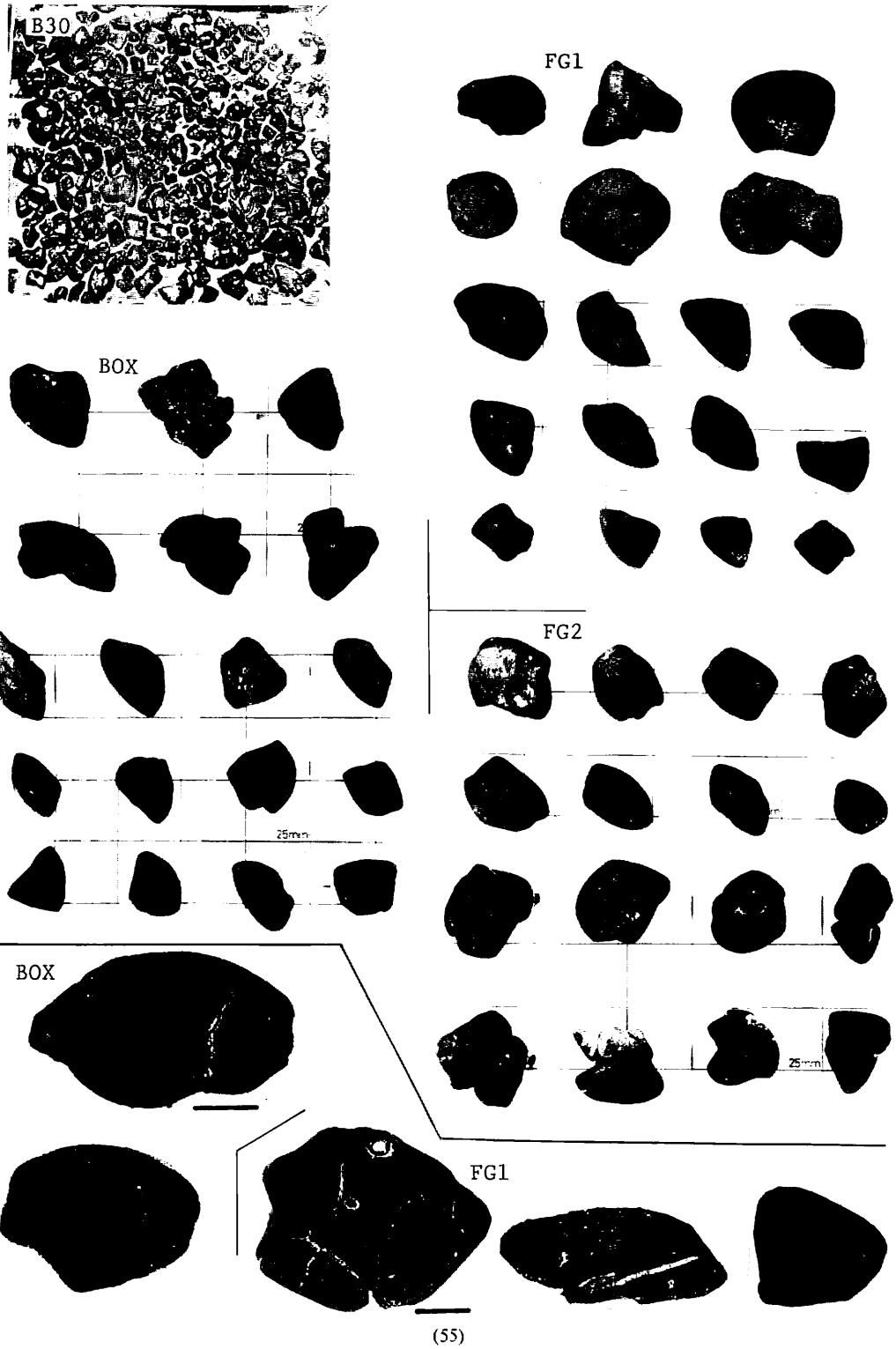

(55)

1646	B31	2.1kg/m^2	30%	Ds, DPs, Ts	Z rich clay
	FG250-1	7.2	40	Ts, Ds	Z mud
	FG250-2	5.5	30	DPs, Ts	Z mud

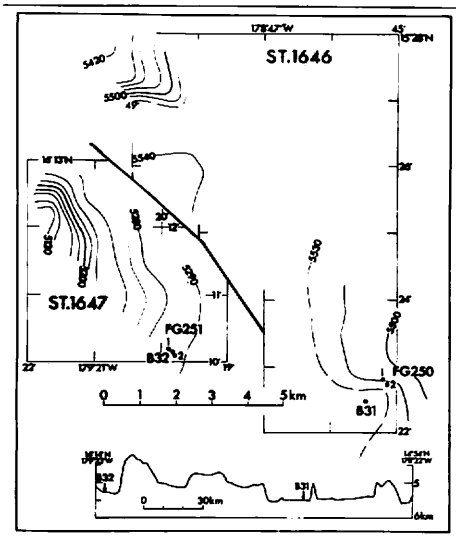

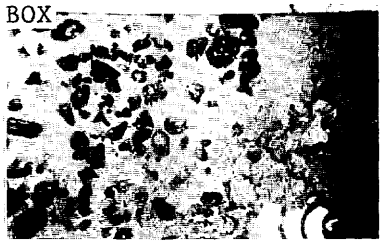

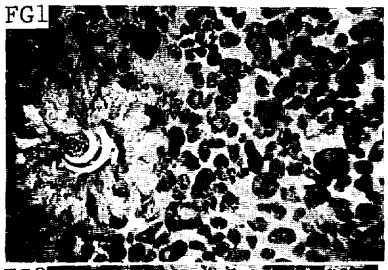

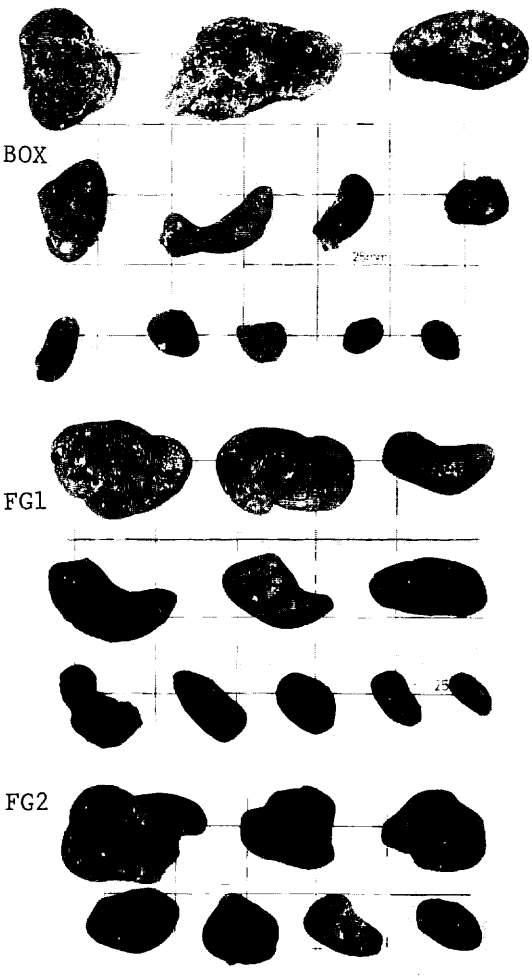

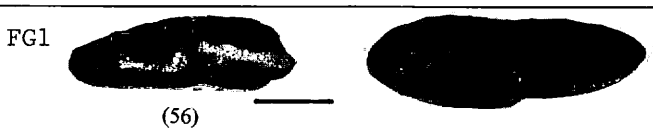

(56)

1647	B32	15.4kg/m^2	80%	Ds	Z mud
	FG251-1	6.2	50	Fs	Z mud
	FG251-2	13.5	70	Ds, Ss	Z mud

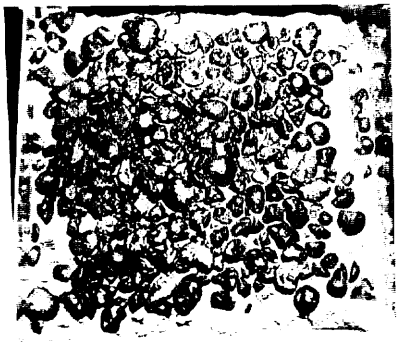

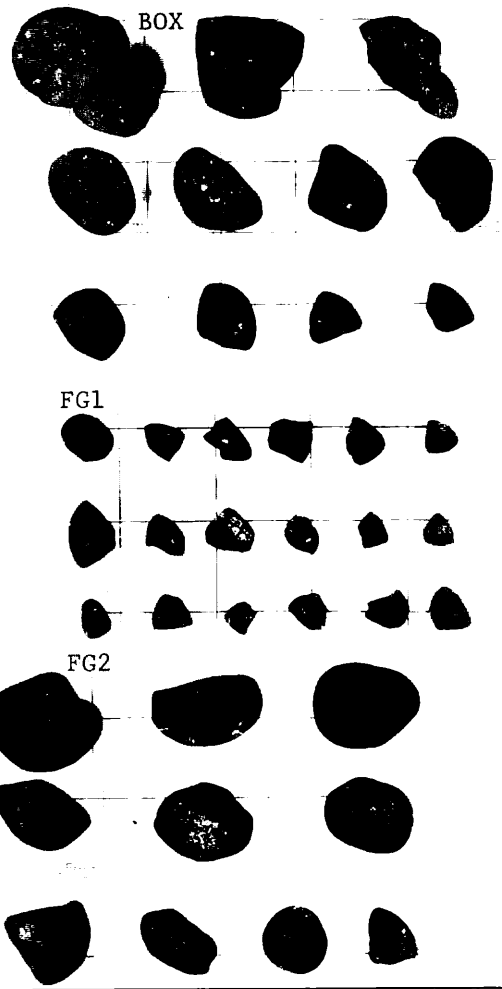

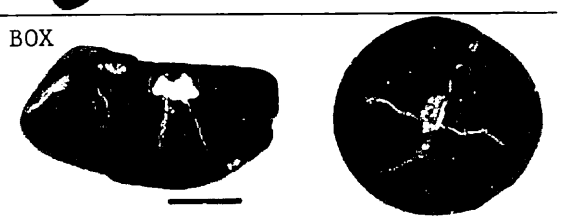

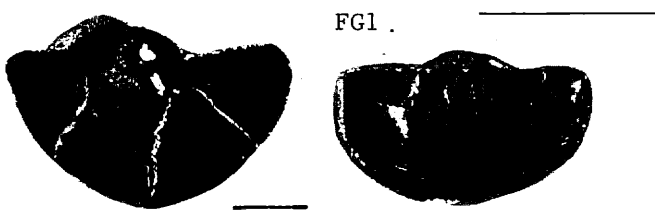

(57)

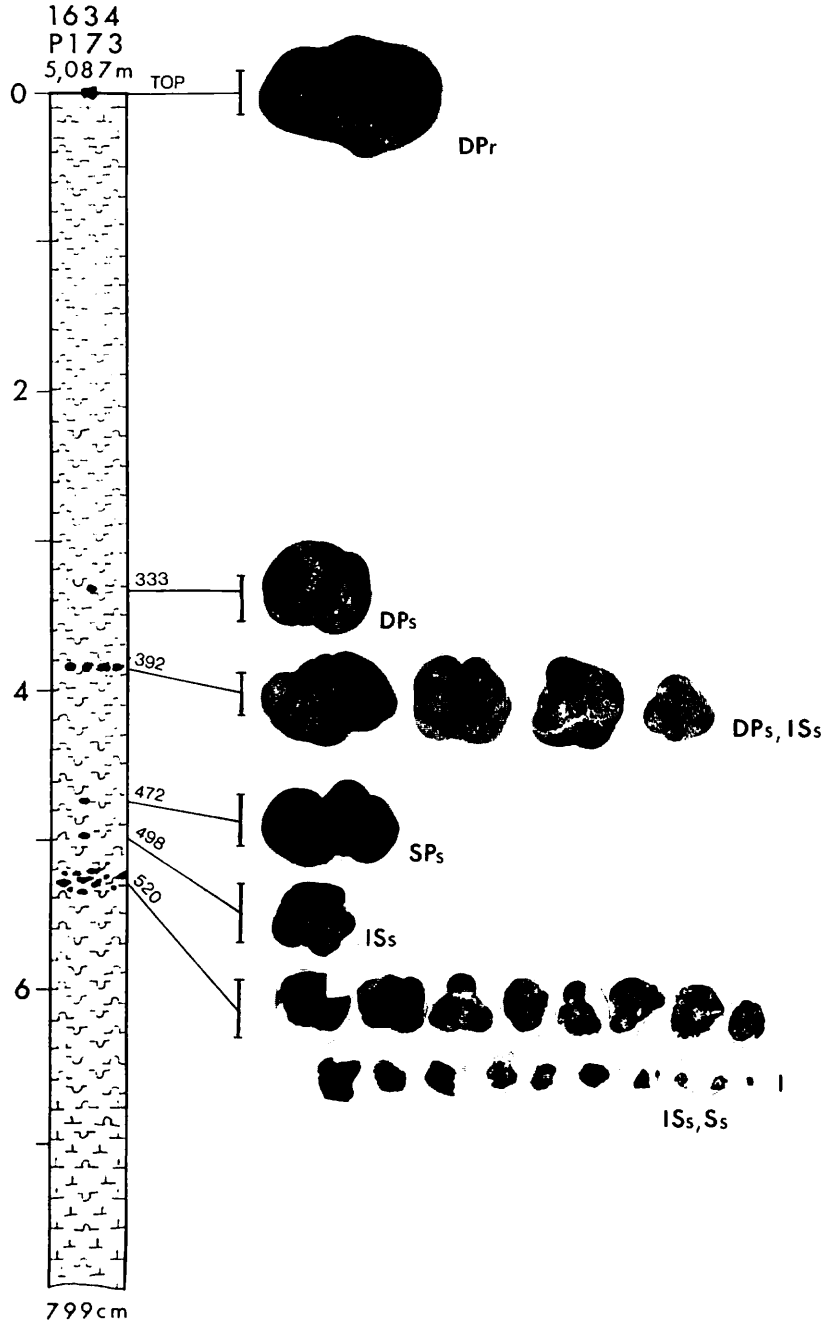

(1)

Appendix VII-3 Maganese nodules buried deep in the sediment columns of the piston cores (1–3). Depth from the sea floor is shown in meters (left side) and in centimeters (right side). The vertical scale bar is 1 cm. See Fig. V-4 for the legends of lithologic description of cores.

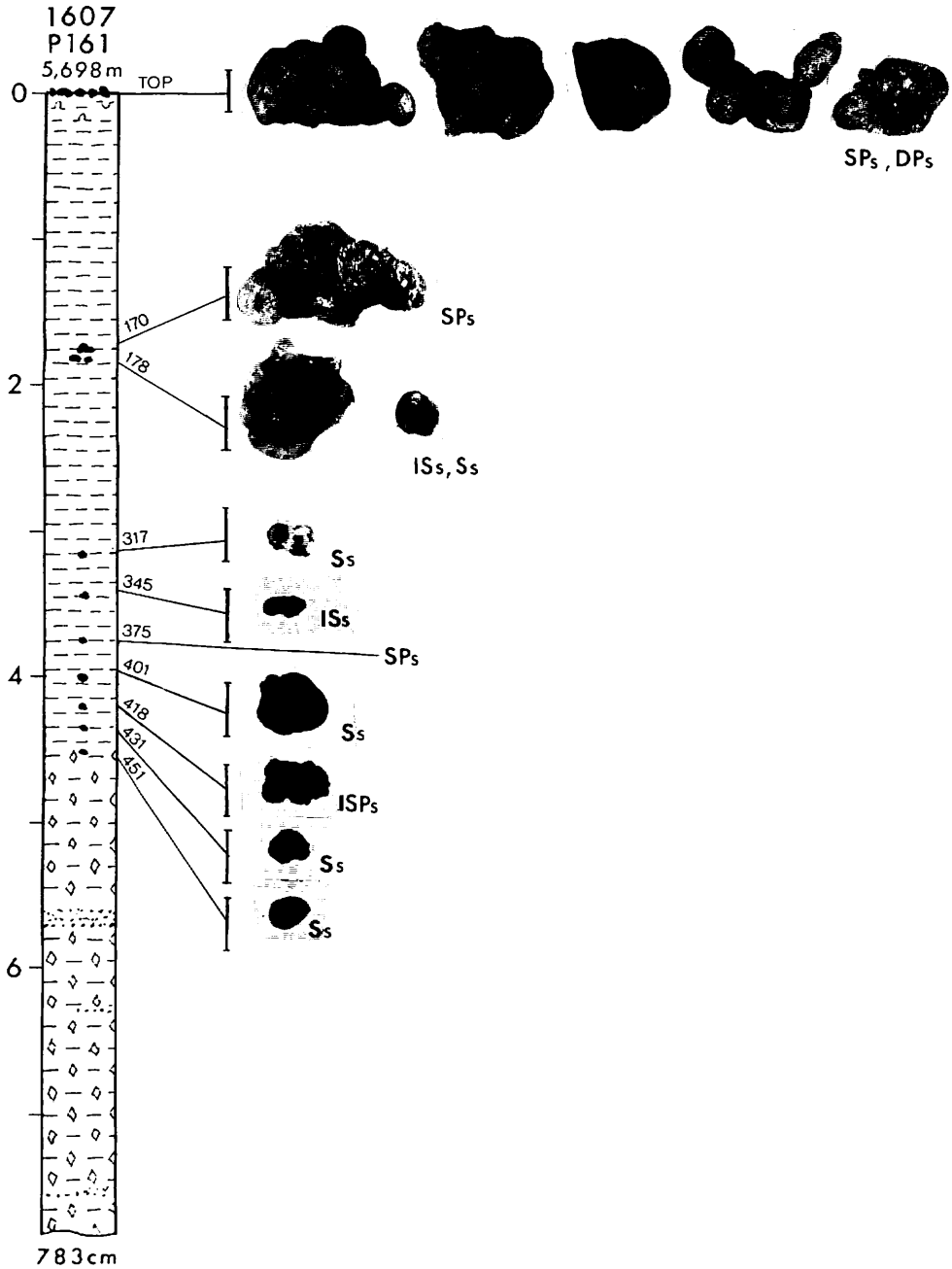
1607
P161
5,698m
TOP
0
2
4
6
SPs , DPs
170
178
SPs
ISs, Ss
317
Ss
345
ISs
375
SPs
401
Ss
418
431
451
ISPs
Ss
Ss
783cm

(2)

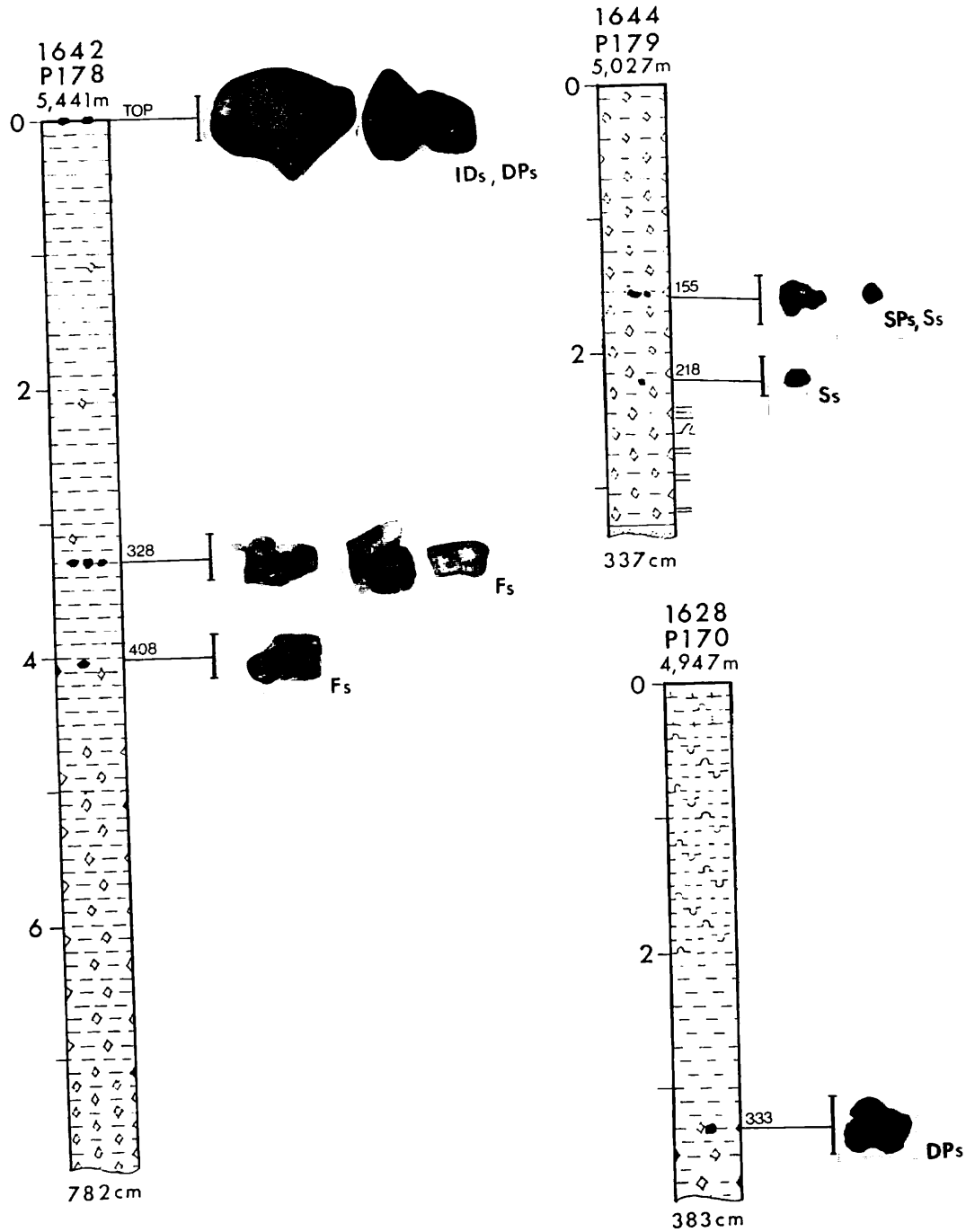
1642
P178
5,441m
TOP
IDs, DPs
328
Fs
408
Fs
782cm
1644
P179
5,027m
155
SPs, Ss
218
Ss
337cm
1628
P170
4,947m
333
DPs
383cm

(3)